Understanding the Barriers to Retinal Ganglion Cell Replacement Therapy

By

MIKAELA JAYE LOUIE
DISSERTATION

Submitted in partial satisfaction of the requirements for the degree of

DOCTOR OF PHILOSOPHY

in

Biochemistry, Molecular, Cellular, and Developmental Biology

in the

OFFICE OF GRADUATE STUDIES

of the

UNIVERSITY OF CALIFORNIA

DAVIS

Approved:

Anna La Torre, Chair

Marie Burns

Nicholas Marsh-Armstrong

Ian Korf

Committee in Charge

2023

Abstract

Mammalian vision begins in the retina, the layer of light sensitive neural tissue that lines the back of the eye, that is comprised of six main neuronal cell types: photoreceptors, bipolar cells, horizontal cells, amacrine, and retinal ganglion cells (RGCs). When light enters the eye and contacts the photoreceptors, a cascade of signals is sent through the highly organized structure of the retina until it reaches the RGCs, the output neurons of the retina. RGCs play a critical role by projecting the only axons that leave the retina, making the resulting nerve, called the optic nerve, the only connection between the eye and the brain. The optic nerve and the RGC population is the target of many retinal degenerative diseases, including glaucoma, which affects more than 70 million people worldwide. However, there are few treatments for glaucoma, and none can restore any vision loss. Therefore, development of alternative methods like retinal ganglion cell replacement therapy is an urgent need.

In this dissertation, I investigate the barriers to successful RGC replacement, specifically the establishment of a reliable source of donor cells, the survival of donor cells, and the physical barriers within the host eye. Using two transgenic RGC reporter mice, the Isl2-GFP and Brn3b-mCherry lines, I found that MAP4K4 inhibition can increase the survival of RGCs during the *in vitro* production of RGCs, as well as post intravitreal transplantation. I also show that the ocular immune system actively targets donor RGCs and that intravitreal RGC transplantation causes transient retinal inflammation. Additionally, I show that mechanical disruption of the inner limiting membrane causes transient activation of immune cells to the disruption site. Lastly, this dissertation details the contributing factors to a successful RGC transplantation, including evidence of protein material transfer between donor and host RGCs. Together, I find that there is great promise to the development of RGC transplantation, but a complex system of barriers must be addressed before a reproducible method can be developed for clinical applications.

For Daniel
You left early so I couldn't show you this,
but it's ok, I'll do that when I see you again.

Acknowledgements

I would first like to thank my mentor, Anna La Torre. I'm sure you would agree that this was not the easiest graduate school experience, but I am so thankful to have been your student. You continued to support me through some of the most difficult times in my life and ultimately never gave up on me– for that I am so grateful to you. I will take all that I have learned from you, both professionally and personally, and bring that into the next chapter of my scientific career. Next, I'd like to thank the members of my dissertation committee: Nick Marsh-Armstrong, Marie Burns, and Ian Korf for your support and encouragement, especially during the final milestones before graduation. Thank you as well to the members of the retinal development group for your generous feedback and insight: Ala Moshiri, Nadean Brown, Sergi Simó, and Tom Glaser.

I'd like to thank all the members of the Simó and La Torre labs that I have worked with these last five years: Adam Miltner, Corinne Fairchild, Elizabeth Fishman Williams, Jisoo Han, Keiko Hino, Miranda Kreuger, Raenier Reyes, Simran Cheema, Steven Decker. I have had so much fun and learned so much from you all. Thank you for accepting/participating in all my antics and stupid jokes, answering my many questions, and helping me find random reagents in places that I checked at least twice before but still couldn't find it. Thank you, Adam, for mentoring me when I first joined the lab, I could not have had a better person to teach me the techniques needed for this project. Thank you, Jisoo, for basically adopting me into your family and taking care of Panya. Thank you also to the undergraduate students I worked with, Amanda Tang and Ericka Morales.

Thank you to the Eyepod Core, especially Robert Zawadzki and Ratheesh Meleppat. I am appreciative of how generous you have been to train me on the SLO and OCT and to teach me the engineering behind it. Thank you to the lunch crew from the Burns/Pugh Labs: Emily Davis, Eric Miller, Kaity Ronning, Gabe Peinado. I will miss all the fun we had. Thank you to my

BMCDB cohort, especially Sam and AJ. We made it! Thank you to those bay area queers, I am so grateful for all the times you drove up to see me. Thank you to my friends from home, 10+ years is a long time to know someone and I'm glad that it is you all. Thank you, Kylie, I could not have made it through the pandemic without visiting your Animal Crossing island.

Finally, thank you to my family. Thank you for feeding me, for supporting me, for guiding me and helping me grow. I love you all so much. To my mom and dad: thank you for providing me with so many opportunities to succeed in life. I have only been able to reach this point due to your hard work. Thank you to my brother Kyle for being one of my biggest role models growing up– I'm glad we can be so silly together still. Thank you to Panya, my silly little blueberry muffin. You've brought more light into my life than you will ever understand, because you're a dog.

Camilla, who knew that all these years you were just walking down the halls of Tupper. I am forever grateful for your love and support; I would not have made it to this point without you. You are my best friend, my favorite person, and I cannot wait to see what our future together holds.

Table of Contents

ABSTRACT II

ACKNOWLEDGEMENTS III

CHAPTER 1: INTRODUCTION 1

The history of vision science 1
The retina 3
RGC degenerative diseases 7
Strategies to restore vision 10
Retinal development 12
In vivo imaging techniques 16
Pluripotent stem cells 19
Retinal organoids 21
Figures 23
Literature Review: Barriers to retinal ganglion cell replacement therapy 29
Abstract *29*
Introduction *29*
The ocular immune response *32*
The inner limiting membrane *36*
Reactive gliosis: bridging physical and molecular barriers *37*
Conclusion *39*
Figures *40*

CHAPTER 2: INHIBITION OF DLK TO IMPROVE THE SURVIVAL OF STEM CELL DERIVED RGCS 42

Introduction 42
Results 46
The expression pattern of Isl2-GFP recapitulates endogenous Isl2 expression during retinal development *46*
Generation and analysis of an Isl2-GFP iPSC line *47*
GCK-IV kinase inhibition improves RGC survival in retinal organoids *48*
Discussion 50
Isl2-GFP iPSCs produce GFP labeled RGCs after differentiation *50*
Inhibition of MAP4K4 increases in vitro RGC survival *51*
Materials and Methods 53
Figures 57

CHAPTER 3: MAP4K4 INHIBITION AND RGC SURVIVAL AFTER INTRAVITREAL INJECTION 66

Introduction 66
Results 68
MAP4K4 inhibition may impact the survival of donor cells 48hours post-transplantation *68*
MAP4K4 inhibition does not increase the long-term survival of transplanted RGCs post-injection *69*
Intravitreal injections of RGCs can cause retinal inflammation *70*
Discussion 71
MAP4K4 may only affect the initial survival and have no effect on long-term survival *72*
RGC transplantation activates the ocular immune system *72*
Materials and Methods 73
Figures 77

CHAPTER 4: THE OCULAR IMMUNE RESPONSE TO INTRAVITREAL INJECTION OF RGCS 83

Introduction 83
Results 86
The immediate immune response to intravitreal injection 86
Phagocytosis of exogenous cells by microglia 87
Discussion 88
Materials and Methods 89
Figures 93

CHAPTER 5: DISRUPTION OF THE INNER LIMITING MEMBRANE ACTIVATES THE OCULAR IMMUNE SYSTEM 97

Introduction 97
Results 100
The immune response after 24 hours post ILM disruption is localized 100
Effect of ILM disruptions on the ocular immune response over time 101
Discussion 102
Methods 104
Figures 107

CHAPTER 6: OPTIMIZATION OF RGC TRANSPLANTATIONS 110

Immunopurification of RGCs 110
Intravitreal injection 111
In vivo imaging 112
Optimization of injection technique 113
Material Transfer 115

CHAPTER 7: CONCLUDING REMARKS 120

References 126

Table of figures

Figure 1.1: Retinal anatomy. 23
Figure 1.2: Types of primary glaucoma 24
Figure 1.3: Retinal development and RGC genesis 25
Figure 1.4: Simplified SLO system. 27
Figure 1.5: Simplified OCT system 28
Figure 1.6: RGC transplantation pipeline. 40
Figure 1.7: The inner limiting membrane. 41

Figure 2.1: Isl2-GFP expression in the developing and adult retina 57
Figure 2.2 Isl2-GFP iPSC production and gene expression 58
Figure 2.3: Isl2-GFP organoid differentiation and gene expression 59
Figure 2.4: Histological analysis of retinal organoids 60
Figure 2.5: Isl2-GFP organoids express RPC and RGC genes by qPCR 61
Figure 2.6: GCK-IV kinase inhibition increases RGC survival and promotes neurite outgrowth in mouse retinal organoids 62

Figure 3.1: In vivo imaging after 48 hours post 77
Figure 3.2: MAP4K4 inhibition does not increase long term cell survival 78
Figure 3.3: MAP4K4 inhibition does not affect transplanted cell morphology or location 80
Figure 3.4: In vivo imaging and histological evidence of retinal inflammation following RGC transplantation 81

Figure 4.1: Microglia response to injected cells 93
Figure 4. 2: Phagocytosis of mCh cells injected intravitreally 95

Figure 5.1: Immune response 24hours after ILM disruption 107
Figure 5.2: Immune response to ILM disruption over time 109

Figure 6.1: Optimization of immunopurification technique 116
Figure 6.2: Artifacts of intravitreal injection 117
Figure 6.3: Material transfer between donor and host RGCs. 119

Table of tables

Table 2.1: qPCR primers 63
Table 2.2: Antibodies used in this study 64
Table 6.1: Antibodies used in chapters 3-5 12120
Table 6.2: RGC transplantation outcomes 127

Sucking at something is the first step towards being sort of good at something.

— Jake the Dog, Adventure Time

Chapter 1

Introduction

The history of vision science

From the Latin word *visio*, the action noun for *visus* meaning “that which is seen”, vision is arguably one of the most impactful senses in our human experience. Fascination with and study of the eye most likely predates any written history, but references to the eye date back to Ancient Babylon within the Code of Hammurabi that delivers the famous line “an eye for an eye…”[1]. Most of the world’s civilizations studied the function and anatomy of the eye since antiquity, yet few written accounts from areas like Ancient Egypt, Greece, and India remain[2–6].

The first accounts of the retina as a layer of the eye date back to the Alexandrian physician Herophilus (325-280 BCE), who documented his dissections of cadaver eyes. Here he described a cobweb-like, or *arachnoeides,* layer that he also likened to a net drawn up around the back of the eye. This layer was eventually named the retina, most likely translated from the Latin word *rete* meaning net[7,8]. Continuing Herophilus’s work, in 200 AD physician and philosopher Galen managed to describe the anatomy of the eye in surprisingly accurate detail, including the cornea, lens, vitreous cavity, optic muscles, and the retina with the optic nerve. However, he declared the lens the primary source of vision[9].

For the next 1400 years, philosophers continued to debate the mechanics of vision asking, “what structure is the primary source of vision?”. Is the eye active, emanating light to seize the image of an object? Or does light pour into the eye, which is transported throughout the body to create sight?[10,3] Finally, in 1604 Johannes Kepler presented the first theory of sight starting with the retina in his manuscript *Astronomiae Pars Optica* (The Optical Part of Astronomy). From here on, the study of vision transformed from philosophical debates on the origin of vision to an understanding of the of light refraction[11,12]. While the gross anatomy of the eye continued to be discovered, it was not until the widespread use of the microscope that we could fully appreciate the intricacy of vision. In 1894, Santiago Ramón y Cajal published the first characterization of the different retinal neurons in *Die Retina der Wirbelthiere* (The retina of vertebrates). As a testament to the artistry of science, Ramón y Cajal recreated the organization and complexity of the mammalian retina with hand drawn figures[13].

In tandem with understanding the functionality and structure of the eye is understanding the pathology of the eye. Early eye procedures could only target anterior eye diseases, with brutal methods like couching, a precursor to modern cataract surgery, that forcefully dislodges the clouded lens using a sharp object like a needle[14]. Ophthalmology as the practice we know today took shape in the early 19th century, with the founding of the first university ophthalmology department in the general hospital of Vienna by Austrian ophthalmologist Georg Joseph Beer[15]. Here physicians could receive standardized training for ophthalmology by a state sanctioned organization. The field was further revolutionized with the invention of the ophthalmoscope by Hermann Von Helmholtz in 1851 and then the slit lamp in 1911 by Allvar Gullstrand, the only ophthalmologist to receive a Nobel Prize, with Carl Zeiss. Together, these instruments allowed for unprecedented diagnostics of ophthalmic diseases[16,17]. Most notably, the inner eye could finally be examined, and the structure and diseases of the retina revealed.

The retina

Vision is the ability to take light stimuli and transform it into signals that the brain uses to construct an image of the world around it. This complex process begins in the retina, the neural tissue lining the back of the eye. The retina is divided into ten general layers. Starting from the outermost layer, closest to the sclera, and working our way towards the vitreous cavity the layers are as follows: retinal pigment epithelium (RPE), photoreceptor outer segments, photoreceptor inner segments, external limiting membrane, the outer nuclear layer (ONL), outer plexiform layer (OPL), inner nuclear layer (INL), inner plexiform layer (IPL), and the ganglion cell layer (GCL). Each nuclear layer contains a distinct population of retinal neuron somas that synapse with their respective targets in the plexiform layers (fig. 1). As a photon enters the eye through the cornea, it is focused by the lens onto the retina. In the mammalian eye, this photon first interacts with most posterior layer containing the photoreceptors (PR)[18]. There are two types of PRs: rods and cones that react to light stimuli through a cascade known as phototransduction[19]. PRs synapse with bipolar cells (BC) that pass their signal to retinal ganglion cells (RGCs), the output neurons of the retina[18]. RGCs project long axons that bundle together to form the optic nerve (ON) at the central retina. The ON leaves the eye socket and mainly terminates at the lateral geniculate nucleus in the thalamus. The circuitry continues by synapsing with the primary visual cortex located in the posterior occipital lobe. It is here that specialized neurons form the visual image synthesizing all of the information from the retina[20].

Photoreceptors

Photoreceptors (PR) are the primary light sensitive neurons in the retina, located in the ONL. They are split into two main groups: rods and cones that have slightly different morphology and function. The structure of the PR is separated into the apical outer segment (OS) and the basal inner segment (IS). The OS is made up of membranous discs and contains all the enzymatic

machinery for phototransduction, the process of transforming light stimuli into neural signals[21,22]. This structure of the PR is what gives rods and cones their respective names; rod OS are slim and straight, whereas cone OS are stockier and conical in morphology. The IS of PRs consists of the soma and the synaptic terminal that synapses with second order neurons in the OPL[21,22]. PR axon terminals contain specialized structures called ribbons that regulate the release of the neurotransmitter glutamate. In the primate retina, rods only contain one ribbon, whereas cones contain more than 50[21]. Integral to PR function is the photosensitive protein opsin contained within the OS discs. Opsins exist in different forms depending on the PR subtype. There are three cone subtypes that express either a short, medium, or long-wave opsin (S-, M-, L-opsin) that are sensitive to 420nm, 530nm, and 560nm light wavelengths, respectively. This diverse population of cones allows us to perceive a wide range of colors in high light conditions (the visible spectrum). There is only one known type of rod, which contains rhodopsin that is sensitive to 500nm wavelengths usually found in to low light conditions[23].

Horizontal cells

Horizontal cells (HC) are laterally connecting cells in the INL that synapse with PRs at the OPL and modulate the information flow from PRs to bipolar cells. HCs facilitate both long- and short-range interactions between PRs and through inhibitory feedback mechanisms they aid in contrast enhancement and color opponency[24]. HCs are electrically coupled to each other by gap junctions, receive glutamatergic input from PRs and provide feedback and feedforward signals to PRs and BCs, respectively. There is evidence for several feedback mechanisms, the most well-studied involves signaling via GABA, but a role for hemichannel-dependent coupling and has also been proposed[25]. Classical studies have identified three different subtypes of horizontal cells (H1, H2, and H3) based on their morphologies and synaptic terminal organization[26], and two of these subtypes have been recently validated by single-cell RNA-sequencing approaches and molecular markers[27,28].

Bipolar cells

Bipolar cells (BC) are interneurons that continue the phototransduction cascade once a PR is hyperpolarized. Tartuferi, a student of Golgi, coined the term “bipolar cell” for neurons that exhibit two protrusions, one “going up” and one “going down”. This distinct morphology is an indicator of their function, as bipolar cells link the outer and the inner retina, and in mammals this connection is largely feedforward[29]. BCs are divided into ON and OFF subtypes based on their response to light- ON BCs are depolarized to light and OFF BCs are hyperpolarized to light. In the mouse retina, they can further be classified into 13 subtypes based on the retinal circuitry they are a part of, such as the rod pathway or the ON/OFF pathways (Types: 1a, 1b, 2, 3a, 3b, 4, 5a, 5b, 5c, 5d, 6, 7, 8, 9, Rod Bipolar cell). The shape and stratification of a bipolar cell’s synaptic terminal is usually a good indication of their subtype identity, but recently different molecular markers have also been identified[29].

Amacrine cells

Amacrine cells (AC) are the most diverse group of neurons in the retina, with as many as 60 subtypes[30]. They are mostly located in the INL, but some are found in the GCL, called displaced ACs. ACs regulate retinal circuits through GABA or glycine mediated synaptic inhibition of BCs and retinal ganglion cells (RGCs). These feedback loops shape both temporal and spatial aspects of the BC and RGC receptive fields, creating more complex visual signals in the inner retina[31,32]. ACs also participate in lateral inhibition between other ACs, but this function is not fully characterized.

Retinal glia

Glia are the support cells throughout the central nervous system (CNS). While initially considered to function solely as “nerve glue”, or the cells that physically held the CNS together,

glial cells have been shown to play a much larger role in maintaining the function of the CNS. Müller glia (MG) are the primary glia of the retina, and they are the only retinal cell type to span all retinal layers[1,2]. Thus, MG are important in the maintenance of the microenvironment and structure of the retina. In a homeostatic eye, MG support the rest of the tissue by transferring molecules between cells, removing cell debris, and secreting trophic factors.

Astrocyte cells are another glia located mainly in the retinal inner nuclear layer and the nerve fiber layer. Like MG, ACs provide neurotrophic factors to and structural support for the surrounding neurons[33,34].

Retinal ganglion cells

RGCs are the output neuron of the retina, meaning they are the last neurons to receive information before signals are sent to the brain. Like ACs, RGCs are diverse with 45 subtypes in the mouse retina and 17 in the primate. Each subtype is distinguished by physiological, anatomical, and molecular characteristics- some have far-reaching dendritic arbor, synapsing with several BCs, while others have condensed arbors with a smaller receptive field[35]. RGC axons project to nearly 40 brain regions, including the Lateral Geniculate Nucleus (LGN) and Superior Colliculus [35,36]. Interestingly, RGCs not only pass light and color information to the visual cortex, RGCs often function to detect visual features in addition to light stimuli. For example, some RGCs are directionally sensitive, responding only to increases in light stimuli from a specific direction (ON-directionally sensitive ganglion cells), while other RGCs respond only when the light stimuli falls directly within the center of the cell's receptive field (W3-RGC)[35,36]. Another distinct RGC subtype is the alpha RGCs (αRGCs). First described in studies of cat retina, αRGCs have large soma and wide branching dendrites that have SMI-32 positive neurofilaments. However, in mice, the term refers to any large RGC that is SMI-32 positive, regardless of physiological properties or morphology. A less prevalent mammalian RGC subtype is the melanopsin (Opn4) expressing RGCs (intrinsically-photosensitive or ipRGCs). Initially found to play a role in circadian rhythm

entrainment[37], ipRGCs project to several brain regions, including the Suprachiasmatic Nucleus (SCN), which is primarily responsible for generating circadian rhythms in mice and humans[38]. Additionally, mice lacking Opn4 have contrast sensitivity defects, demonstrating how ipRGCs also contribute to image forming processes[39]. However, of all the subtypes, the W3-RGC is the most numerous type of RGC, comprising 13% of the RGCs in the center of the mouse retina[40]. The variety of RGC types is unsurprising when considering the diversity of horizontal, bipolar, and amacrine cells that process information prior to RGCs receiving any input.

Retinal pigment epithelium

Although distinct from the neural retina, the retinal pigment epithelium (RPE) is a critical component for proper retinal health and function[41,42]. The RPE is a monolayer of pigmented, epithelial cells that interface with the PR OS and is responsible for OS phagocytoses as well as other functions vital to retinal health[43,44]. Phototransduction and light exposure both contribute to the buildup of toxic photooxidative products in PRs. Thus, PRs may shed up to 10% of their volume daily that must be efficiently phagocytosed by RPE cells to prevent accumulation of toxic metabolites and other molecules in the ONL[43]. The RPE also plays a critical role in phototransduction by converting all-*trans*-retinol, released by PRs shortly after receiving a photon, into 11-*cis*-retinal that is necessary for PR opsin function[45,46].

RGC degenerative diseases

RGC degenerative diseases are devastating conditions can often lead to complete vision loss. One of the most common examples of an RGC-specific degenerative disease is glaucoma. Estimated to affect around 76 million people worldwide today[47], glaucoma defines a family of diseases that result in progressive degeneration of the RGCs and visual loss[48,49]. Glaucoma can

remain asymptomatic until it is severe, resulting in a high likelihood that the number of affected individuals is much higher than the number known to have it, and population-wide studies suggest that only 10-50% of people with glaucoma are aware they have it. While the molecular mechanisms that initiate RGC death in glaucoma are poorly understood, physicians have characterized several warning signs/early symptoms of the disease. ON cupping is a common first sign of developing glaucoma and is defined as the enlargement of the optic cup to optic disk ratio[50]. Increased intraocular pressure (IOP) is another presenting symptom, and is currently the only treatable clinical aspect of glaucoma[48]. Therapies to reduce intraocular pressure include topical medicine to increase aqueous humor outflow, surgery, or laser treatments, but these therapies can only slow disease progression and cannot reverse vision loss from RGC death[48,51]. However, several studies have shown that only ~50% of glaucoma patients present with high IOP and that increased IOP does not necessarily lead to neurodegeneration[52,53,51].

Primary glaucoma can be classified into two main categories: open-angle glaucoma and angle-closure glaucoma, also referred to as closed-angle glaucoma. In both cases there are issues with the drainage of the aqueous humor within the anterior chamber that cause mechanical and physiological stress within the eye that eventually leads to RGC death[51]. In a healthy eye, the aqueous humor is secreted by the ciliary body that then flows into the anterior chamber to help give form to this structure (fig. 2). The aqueous humor also acts as a surrogate to blood within the avascular anterior chamber by providing nutrients to the ocular tissue and removing cell excrement and debris. The aqueous humor mainly drains from the anterior chamber via the trabecular meshwork and is absorbed by the episcleral veins, although other pathways that drain into the uveal meshwork and eventually the ciliary muscle interstitium have been proposed[54,55].

About 80% of glaucoma cases are categorized as primary open-angle glaucoma (POAG), defined by an increased resistance to the drainage pathways of the aqueous humor through the trabecular meshwork[51,56] (fig. 2). Studies have found that this increased resistance is due to an increase in extracellular matrix (ECM) and structural remodeling of the trabecular meshwork. A

reduction in aqueous humor outflow often results in an increase in IOP that puts mechanical stress on posterior eye structures, the most vulnerable being the lamina cribrosa where the ON exits the eye. Studies suggest that lamina cribrosa compression/deformation may cause RGC death, but the exact mechanisms behind glaucoma induced RGC death are still unknown[51]. There are several genes associated with the development of POAG, but these only account for a minority of glaucoma cases. For example, mutations in the myocilin gene, one of the most common causes of inherited retinal diseases, account for only 3-5% of POAG cases[51,57]. Less common than POAG is primary angle-closure glaucoma (PACG), which is typically caused by pupillary block that physically blocks the aqueous humor outflow[51,58] (fig. 2). PACG also has an increased probability of developing bilateral blindness compared to POAG, although this difference has yet to be fully understood. There are also many conditions that cause secondary glaucoma, such as trauma, tumors, and sides effects of some corticosteroids, demonstrating the complexity of the physiological and molecular mechanisms behind glaucoma[48].

Leber's Hereditary Optic Neuropathy (LHON) is another blinding condition that causes RGC death. However, unlike glaucoma, mitochondrial defects are the root cause of RGC death in LHON[59]. These mitochondrial DNA mutations are further divided into the more common primary and the less prevalent secondary mutations. There are five known primary mutations, each of which is a point mutation in the protein coding gene for subunits of the electron transport complex I or complex IV[60]. The secondary mutations are thought to act synergistically with other mitochondrial DNA mutations to increase the probability of blindness[60]. Recently, the NADH:ubiquinone oxidoreductase subunit S4-null ($Ndufs4^{-/-}$) mouse has been shown to be a promising model of LHON. The Ndufs4 subunit is an 18 kDa subunit of the N module within complex I and is thought to be involved in complex I assembly and/or stabilization[61]. Originally created to study Leigh syndrome, an encephalomyopathic disease caused by complex I mutationss[62], the $Ndufs4^{-/-}$ mouse was shown to have a targeted loss of RGCs within the retina,

like LHON[63,64]. These mice had cell loss in the GCL by postnatal day 31 (P31) and RGC functional defects by P32[63,64]. Additionally, optomotor reflex measurements showed that by 5 weeks, Ndufs4$^{-/-}$ mice had a significant decrease in visual function compared to their wild type littermate controls[64]. However, since this the Ndufs4 gene is fully inactivated within this mouse, it has a very short life span and does not survive past 7 weeks. Thus, retinal specific CRE-driver mouse lines would be an invaluable tool to study the effects of complex I disorders in the context of RGC degenerative diseases like LHON.

Regardless of the genesis of RGC degeneration, major challenges still exist to restore vision after RGC death. One strategy several labs have investigated is creation of visual prosthetic devices that interface with appropriate thalamic and cortical structures to relay visual information in lieu of an ON. However, this method is less ideal in that it requires a high-risk surgery on the patient's brain that must also be healthy enough to accept the prothesis and extremely complicated image processing by the implant[65]. Another strategy, and the focus of my thesis, is to replace lost RGCs with exogenously produced RGCs, since the human retina possesses little to no intrinsic regeneration capability. However, this strategy must overcome the challenging task of not only physically integrating the exogenous cells into the host tissue, but recapitulating RGC dendritic arborization and axon pathfinding that occurs in development- all within an adult brain.

Strategies to restore vision

The adult mammalian retina cannot regenerate retinal neurons or their axons after injury; therefore, the cells lost to retinal degenerative diseases, like glaucoma and LHON, can never be recovered endogenously. This is in opposition to other vertebrates like *Xenopus laevis* and *Danio rerio* that after traumatic loss of RGC axons, possess the ability to regenerate axons and reinnervate the correct brain regions to functionally restore vision[66–68]. It is unclear why adult mammalian retinal neurons evolved to choose apoptosis over regeneration, when early postnatal

rodent RGCs have been shown to exhibit robust axon growth in vitro[69–72]. However, over the last 10 years it has been shown that inhibition of regulators the mammalian target of rapamycin (mTOR) and Janus kinase/signal transducers and activators of transcription (JAK/STAT) pathways, implicated in cell proliferation and differentiation, can increase axon regeneration in the adult CNS[73–76]. However, these measures cannot restore lost RGCs and thus, different methods, like RGC replacement therapy, must be considered for later/more severe cases of the disease.

Engrafting RGCs into a host retina is the first challenge towards developing a clinically relevant RGC transplant therapy. PR transplant studies have taken advantage of the apical location of the PR layer to deliver exogenous cells into the space between the PR and RPE called the subretinal space[77–81]. However, the delivery of RGCs is not as simple, considering that the GCL is located within the eye, on the basal/vitreal side of the retina. Thus, to transplant RGCs directly adjacent to the GCL, the injection apparatus must pass through all the layers of the retina. The only structure separating the GCL from the vitreous is the nerve fiber layer (NFL), which is comprised of RGC axons, astrocytes, MC end feet, and extracellular matrix proteins that form the basal basement membrane (inner limiting membrane, ILM)[82–85]. Therefore, the first step to achieve exogenous RGC engraftment, one must pierce through the eye into the posterior chamber, place the cells near the surface of the retina, and have the cells survive in the correct layer.

The next challenge for RGC transplantation is to grow the engrafted cells' axons to the proper brain targets millimeters away from the retina. Previous studies from Hankin and Lund demonstrated that embryonic retina could project RGC axons specifically to the superior colliculus, and no others, after transplantation into various brain regions of neonatal mice and rats[86–88]. Importantly, Hankin and Lund reported that RGC axon guidance was dependent on the distance from the exogenous tissue to the desired brain target. They found that placing the engraftment too far away would result in axons growing across the surface of the brain and not targeting the superior colliculus[88]. These studies shed light on the potential requirements for

successful RGC engraftment; a patient may need to have some amount of ON left to serve as a scaffold that guides the exogenous RGC axons to their specific brain regions. Although these challenges may seem daunting, lessons from retinal development, where similar processes like RGC genesis and axon guidance occur, may help determine the possible strategies to establish methodologies for successful RGC transplantation.

More details about the current challenges for RGC replacement therapies are discussed in the next Chapter.

Retinal development

The mechanisms that lead to the development the vertebrate retina are highly conserved across species, with the general retinal structure conserved throughout the breadth of vertebrates[89]. The vertebrate eye originates from interactions between the neuroepithielium of the neural tube, surface ectoderm, and extraocular mesenchyme. In early mouse embryogenesis, the eye field is specified in the medial anterior neural plate shortly after gastrulation by a gene regulatory network known as the eye field transcription factors (EFTF) [41,42,90–92]. The EFTFs include *Rax, Pax6, Six3, Lhx2* [41,42,90,91,93]. Once the eye field is specified, it is bifurcated along the midline in a Sonic Hedgehog (*Shh*) dependent process. Soon after, the ventral diencephalon evaginates to form the optic vesicles (OVs) (fig. 3A)[42,91,93]. The OV then contacts the surface ectoderm to form the lens placode that subsequently invaginates, while the OV folds in on itself to form the optic cup (OC), containing the two principal layers of the early eye—the RPE and the neural retina. At this stage, from embryonic day 9 (E9) to E9.5 in the mouse, different structures of the OC are delimited by the expression of specific transcription factors: *Mitf* labels the RPE, *Vsx2* (*Chx10*) labels the neural retina, and *Pax2* labels the optic stalk (fig. 3B)[41,42,93–95]. Simultaneously, the lens is formed by the invagination of the lens placode that eventually separates from the surface ectoderm and develops into the adult lens (fig. 3C)[41,91]. The surface

ectoderm then proliferates to repair the exterior OC, resulting in cornea formation (fig. 3D)[42]. The precise patterning of these early eye developmental factors is critical for proper eye formation, and although extensively studied, the full scope of these interactions has yet to be revealed[42].

Now the developing eye resembles the adult eye with all the general structures (neural retina, optic stalk, lens, cornea) present, marking the beginning of neurogenesis[42,93,96]. Retinal neurons are all derived from a single population of retinal progenitor cells (RPCs), that are specified by regulatory networks including *Pax6, Rax,* and *Otx2*. It has been widely established that retinal neurons are also born in a highly conserved and specific order[96–99]. Consequentially, retinal neurons are split into two general categories: early born neurons, including RGCs, HCs, cones, and GABAergic ACs, and late born neurons, including rods, BCs, and MGs[95,96,100]. It is still unclear how this specific birth order is maintained, but two general theories have been established in the field[95,100]. The competence model suggests that the developmental age determines the capability, or competence, of an RPC to produce specific types of retinal neurons, and extrinsic and intrinsic cues cause the RPCs to change that competence to produce a different set of neurons over time[101–103]. For example, expression of microRNAs (miRNAs) let-7, miR-9, and miR125b have been shown to regulate RPC competence in mice; when these miRNA are inhibited, there is an overproduction of early born neurons at the expense of late born retinal neurons[104]. An additional theory adds that stochastic gene expression also influences the competence of a population of RPCs[105,106]. Live imaging of the zebra fish retina revealed that progeny from a population of RPC clones are variable in size and cell fate, even at a single developmental time[105]. This data among others suggest that there is stochasticity to retinogensis, where RPCs undergo cycles and fluctuations of gene expression that changes the probability of producing certain retinal neurons[100,102,105,106]. Regardless of the mechanisms behind retinal cell fate determination, the RGCs are the first retinal neurons to be born[95,107].

RGC genesis

RGCs are the first neurons born in the mouse retina, beginning at E11.5[107]. This is evidenced by several reports showing *Brn3b*- and *Isl1*-expressing cells, both found to be necessary and sufficient to specify RGC fate[108–110], by E11.5 in the mouse retina[107,111–113]. Similarly, our lab has shown *Brn3b* driven mCherry reporter expression is detected as early as E11.5[114]. First, RPCs undergo mitosis at the apical side of the retina and produce postmitotic cells that express *Brn3b*[113,114]. Studies In zebrafish have shown that the newly born RGCs then migrate their somas to the basal layer while remaining attached to both apical and basal surfaces (bipolar somal translocation). This migration occurs in two stages: first the soma moves rapidly to the basal surface, and second, the apical attachment is lost causing slower, yet random, movements to within the GCL (fig. 3E**)**. Interestingly, RGCs were also found to have multipolar migration, although this was less frequent and efficient than the canonical bipolar translocation[115]. Fixed samples of mouse retina suggest that mammalian RGCs also migrate by somal translocation, although this has yet to be confirmed through live imaging[116]. RGC neurogenesis continues throughout mouse development, peaking between E13.5 and E16.5, and ending by P1-2 in the peripheral retina[117]. Even though RPC competence is cell-autonomous, extrinsic factors can also regulate RGC differentiation. Factors such as *Notch*, *Shh* and Fibroblast growth factors (*Fgf*s) have been shown to regulate cell fate decisions[103]. For instance, activation of *Notch* induces RPC proliferation and inhibits RGC differentiation. Similarly, *Shh* is expressed in newly generated RGCs and acts as a negative feedback controller of RGC genesis[118].

Although the complete gene regulatory network driving progenitor cells to an RGC fate is not completely understood, critical transcription factors for RGC genesis and survival have been identified. *Atoh7* is transiently expressed in the mouse retina starting at E11 and is necessary for the generation of RGCs, but not sufficient. Loss of *Atoh7* leads to an 80% reduction in RGCs and an increase in ACs and cone PRs[119–121]. First, several transcription factors regulate the expression of *Atoh7* in neurogenic RPCs. For instance, *Pax6* positively regulates the expression of *Atoh7*, while high levels of *Vsx2*, normally present in proliferative RPCs, inhibit *Atoh7*. Additionally, *Vsx2*

is downregulated while *Atoh7* is upregulated in neurogenic progenitors[122,123]. The spatiotemporal expression of *Atoh7* is also regulated by different bHLH genes such as *Ngn2* and *Hes1*[124,125].

Brn3b is a class 4 POU domain transcription factor expressed in RGCs as well as other neurons of the central nervous system[114,126]. *Brn3b* is expressed in 70% of mouse RGCs, and homozygous germline *Brn3b* knockout mice lack 60-70% of RGCs, demonstrating an essential role for *Brn3b* in RGC development and survival[109,127]. Like the Brn3 transcription factor family, the LIM homeodomain transcription factors Islet-1 and Islet-2 (*Isl1* and *Isl2*) are expressed in postmitotic RGCs[110,128]. Inactivation of *Isl1* causes mouse embryonic lethality by E11.5, possibly due to defects in vascular development[129]. *Isl1* expression is also found in ACs in the INL and GCL[130]. *Isl2* was discovered several years after *Isl1*, sharing a large portion of its sequence with *Isl1* and is even recognized by antibodies raised against *Isl1*[131]. The first study of *Isl2* expression in the retina used *in situ* hybridization to show that *Isl2* is expressed in ~50% of mouse RGCs in a seemingly equal temporal to nasal gradient[132]. *Isl2* mRNA is expressed in the retina from E13.5 through adulthood and is only present in postmitotic RGCs[128]. However, *Isl2* expression also plays a role in other mechanisms during postmitotic RGC development.

Isl2 plays a role in RGC axon guidance by regulating the decision between contralateral and ipsilateral RGC projections. In a key study, Pak and colleagues used an *Isl2*-null mouse in combination with an *Isl2*-lacZ reporter mouse to study the location of *Isl2*+ cells in the retina and its role in mouse RGC development. The authors found that in the ventral-temporal crescent (VTC), a region in the periphery of the ventral-temporal retina, the number of *Isl2*+ RGCs is significantly lower than the rest of the retina, and that *Isl2*+ RGCs only project contralaterally. Indeed, in the *Isl2*-null mice, number of ipsilaterally projecting RGCs was increased compared to their wildtype counterparts. Furthermore, this data suggests that *Isl2* acts as a repressor another transcription factor, *Zic2*, which is restricted to the VTC and may activate the ipsilateral axon pathfinding[133]. Thus, the authors conclude that *Isl2* directs RGC axons to project contralaterally rather than ipsilaterally, however the reason behind this specificity is still unknown[128].

To develop RGC replacement therapies to restore lost vision, RGCs will need to be generated *in vitro* and survive when transplanted *in vivo* long enough to integrate into the host GCL and connect with the retina and, eventually, the brain. Understanding how RGCs migrate and project axons during development will reveal the methods to connect transplanted RGCs to the brain.

In vivo imaging techniques

The ability to study the eye has only been as good as the technology available to physicians. Key to the progression of ophthalmology is the invention of tools to image the back of the eye. Initial methods used an external light source to illuminate the eye but could not penetrate the pupil to see clearly into the eye. It is not until the ophthalmoscope, invented in 1851 by Hermann Von Helmholtz, that oculists/ophthalmologists were able to view into the eye and see the retina[16]. The ophthalmoscope has three elements: a light source, a reflecting surface to direct the light to the eye, and a way to focus the light. The initial design needed to be mounted on a table, using oil/paraffin lamps as a light source, with mounted plates of glass that could be adjusted in angle and distance to the patient's eye. With the invention of the camera in the 1810's, the ophthalmoscope was soon adapted to record fundus images on film. While revolutionary in its creation, the ophthalmoscope lacked the image resolution to visualize individual retinal neurons for almost 150 years[134]. The first demonstration of imaging the individual neurons was in 1995 by Miller and colleagues who obtained fundus images of the cone mosaic in a healthy human eye[135].

Scanning laser ophthalmoscopy

The scanning laser ophthalmoscope (SLO) was invented in 1980 by Webb, Hughes, and Pomerantzeff. This system diverged from the conventional fundus camera by raster scanning a single laser point across the retinal surface that reflected through several spatial filters to the

beam detector. By scanning across the retina point by point and using a detector with higher sensitivity than film, SLO images had greater axial resolution than fundus cameras. Eventually, confocal microscopy was applied to this system to send the back reflectance from the retina through a pinhole before reaching the detector. This allowed for a reduction in imaging artifacts from out of focus light[136,137]. Modern SLO systems begin with emission from a laser diode that is collimated by a lens. The now parallel rays pass through a beam splitter to separate the backscattered signal from the incident path before entering the XY-scanning unit. Light is reflected by a lens moving in two dimensions to create a series of scans sweeping across the retina. The signal light, now a series of separate scans, follows the same path back to the scanning unit where it is "descanned" into a single beam. The signal light is separated from the incident beam by the beam splitter and deflected into the detector, originally a photomultiplier tube, after passing through a pinhole to exclude out of plane reflectance[137] (Figure 4).

While originally designed for clinical use, SLO systems built to image rodents have become invaluable to the field of retinal biology[138–142]. The main challenge faced when converting a system designed for the human eye to a rodent is the difference in size- a mouse eye is 10x smaller than that of a human. Perhaps due to its nocturnality, the mouse eye has a numerical aperture of about 0.5 when the pupil is fully dilated, a ~2-fold increase compared to the human eye[143–145]. Thus, several labs have taken advantage of the mouse eye's intrinsic resolution capacity to create systems that can have a lateral (xy) resolution of ~3μm[140]. Combined with adaptive optics (AO) to compensate for optical aberrations that can blur an image, AO-SLO can have an xy resolution of ~1μm in a system built to image mice retina[139]. Finally, SLO can be used to detect fluorescence, allowing cells of specific lineages or treatments to be imaged over time, reducing the reliance on only histology to create longitudinal studies of the mouse retina[138,140,142].

Optical coherence tomography

In addition to imaging the surface of the retina, non-invasive imaging techniques that can penetrate through the tissue and create a cross sectional view have been a vital tool in the advancement of modern ophthalmology and vision science. Optical coherence tomography (OCT) was first coined in 1991 in a study by Huang and colleagues that described a system that can create cross-sectional images of a tissue by measuring the light reflected by the tissue's structures from a low-coherence light source that have a confined travel range[146,147]. Although OCT can technically be used to image any tissue type, the authors specifically chose the retina to demonstrate the practicality of OCT because the retina is a transparent, laminated tissue that had established morphological features. The features of the OCT retinal images acquired in this study directly corresponded to those found through histological analysis, establishing OCT as a powerful tool to image the retina[146]. Indeed, the most common usage of OCT in modern medicine is in ophthalmology[147].

The main principle behind OCT is tissue structures can reflect (back reflectance or back scattering) a beam of light directed towards. Using this property, the system measures the various light "echoes" that are dependent on the distance from the light source and the composition of the structure to create a cross-sectional image (fig. 5)[148]. To briefly summarize the general OCT system, light is directed towards a beam splitter where one beam is incident to the sample and the other follows the reference path towards the reference arm containing a flat optical mirror at a predetermined distance. Next, the back scattered light, or echo, from the sample travels along the incident path and meets with the light reflected from the reference arm at the beam splitter and continues towards the photodetector. Interference of the two reflected light can only occur if the length of the incident path and reference path are equal, and it is this beam that is demodulated into the echo time delay and light intensity called the amplitude scan (A-scan). A cross-sectional image (B-scan) of the entire tissue is formed by laterally scanning the sample[146–148]. Current iterations of OCT systems have built upon this initial design to forego the measurements of echo time delay in favor of spectral interference measurements, which resulted

in a significant increase the acquisition speed and tissue contrast[147]. Additionally, several labs have combined OCT with other live imaging techniques like SLO, and have developed OCT angiography to visualize the retinal vasculature without dyes[139,141,149–152]. Live imaging techniques such as SLO and OCT are a boon to vision science and will continue to be as they become more common in research facilities.

Pluripotent stem cells

Differentiation was first established as a one-way street, famously visualized by Waddington's landscape model of marbles rolling down a mountain[153]. As developmental time continues, stem cells, which are defined by their ability to self-renew and differentiate into other cell types, slowly lose their developmental capacity, and become specified and later committed towards one cell type. Thus, embryonic stem cells (ESCs) – the cells found in the inner cell mass of the blastocyst at early stages of development- are pluripotent as they can produce all cell types in the embryo, including the three embryonic tissue layers (ectoderm, mesoderm, and endoderm). In humans, ESCs disappear after the 7th day and begin to form the embryonic tissues. ESCs extracted from the inner cell mass can be cultured in vitro, and under the right conditions, they can proliferate indefinitely. In contrast, hematopoietic stem cells (HSC) for example are multipotent and only differentiate into blood cell fates[154,155].

However, in 2006, Takahashi and Yamanaka reported the groundbreaking discovery of four genes that can induce pluripotency in differentiated somatic cells[156]. Using retroviral transduction, Takahashi and Yamanaka demonstrated that mouse embryonic fibroblasts could be reprogrammed into a pluripotent state when transduced with vectors expressing *Oct3/4*, *Nanog*, *Klf4*, and *c-Myc***.** This study was built on a half-century's worth of work, evidenced by the 2012 Nobel Prize in Physiology or Medicine awarded to both Dr. Shinya Yamanaka and Sir John

Gurdon, that tried to answer the fundamental question: how do embryonic cells lose the ability to generate all cell types as the cell differentiates?

Early experiments aimed at understanding how the genetic content of cell nuclei change over developmental time involved transplanting nuclei from various *Xenopus laevis* donor cells into *Xenopus* oocytes. Briggs and King first showed that a complete embryo can form when nuclei from blastula cells are transplanted into enucleated oocytes[157]. However, within this study and one that followed shortly, it was shown that the further differentiated a cell is, the less chance of survival the resulting embryo has when the cell's nucleus is transplanted into an egg[157,158]. This story came to a head with Gurdon's study that awarded him his Nobel Prize. Here he used tadpole intestinal epithelial cells to source nuclei for transplantation into oocytes in the first test of whether fully differentiated cell nuclei still retain the genetic information to form tadpoles. The results followed the general trend of the other transplantation studies in that only 1.5% of the epithelial nuclei produced tadpoles[159]. Thus, it was concluded that differentiated cells retain the genetic content to produce all cell types but are restricted in the capacity of when and where differentiation into new cell types takes place. However, these studies helped build the foundation for the concept of differential gene expression, which is the basis for reprogramming cells into a pluripotent state as shown by Takahashi and Yamanaka[156].

Many may argue that the breadth of stem cell applications is the future of modern medicine. This is in part due to the discovery of induced pluripotent stem cells (iPSCs) that can theoretically be used to produce any tissue type from a patient's own cells. For example, pre-clinical trials could create iPSCs from patients with the target indication to test a drug candidate. This is especially useful in cases where the prevalence of the disease is low or requires specific tissue types to test that are not easily acquired. Additionally, iPSCs can be used to validate results from animal trials before entering human trials. Finally, stem cell-based therapies could help fill the global deficit in donor tissue. Some tissues, like the retina, are incredibly hard to source due to the size of the tissue and the technical difficulty of harvesting it. However, iPSCs derived from

a patient's own tissue could be differentiated into the tissue of interest to use for transplantation, reducing the risk of rejection[160].

Retinal organoids

Numerous protocols have been published describing mouse and human ESC or iPSC culture differentiation into retinal neurons. These methods were designed to reproduce the normal embryonic environment by the addition of signals like *Igf-1*, *Dkk1* and *Noggin*[161,162]. However, stem cells differentiated into retinal neurons in 2D cultures are often criticized on the basis that they fail to recapitulate the 3D structure of an actual retina. Therefore, the emergence of 3D culture changed the landscape of retinal organoid production[163]. This method, first reported by Eiraku and colleagues produced tissue structures that mimicked the optic cup in composition and organization[163]. Many labs have adopted this technique for differentiating stem cells into retinal neurons *in vitro,* including adapting protocols to produce human retinal organoids[164], and developing custom bioreactor systems to improve the survival of organoids in culture[165]. Other protocols use a combination of 2D and 3D techniques, this method was first introduced by Meyer and Gamm, and although it may be more laborious that other protocols, it generates high yields of all the different cell types, organized in well-defined layers.

Efforts to improve the reproducibility and quantitative nature of retinal organoids have also shown success, as in Vergara and colleagues approach that uses a microplate reader to quantify reporter fluorescence and compensate for difference in organoid size[166]. Although retinal organoids lack the rest of the organism, specifically vasculature, the immune system, and brain connectivity, organoids remain useful for investigating retinal development and disease. For example, Eldred and colleagues used human retinal organoids to show that thyroid hormone signaling is critical to specify cone subtypes[167]. Several other studies have analyzed cell-autonomous defects in neurons generated in human retinal organoids made from stem cells

harboring human disease gene mutations[168,169]. Additionally, our lab has validated that MG can promote neuron survival by co-culture of stem cell-derived RGCs with retina-derived Müller glia[34,170].

Figures

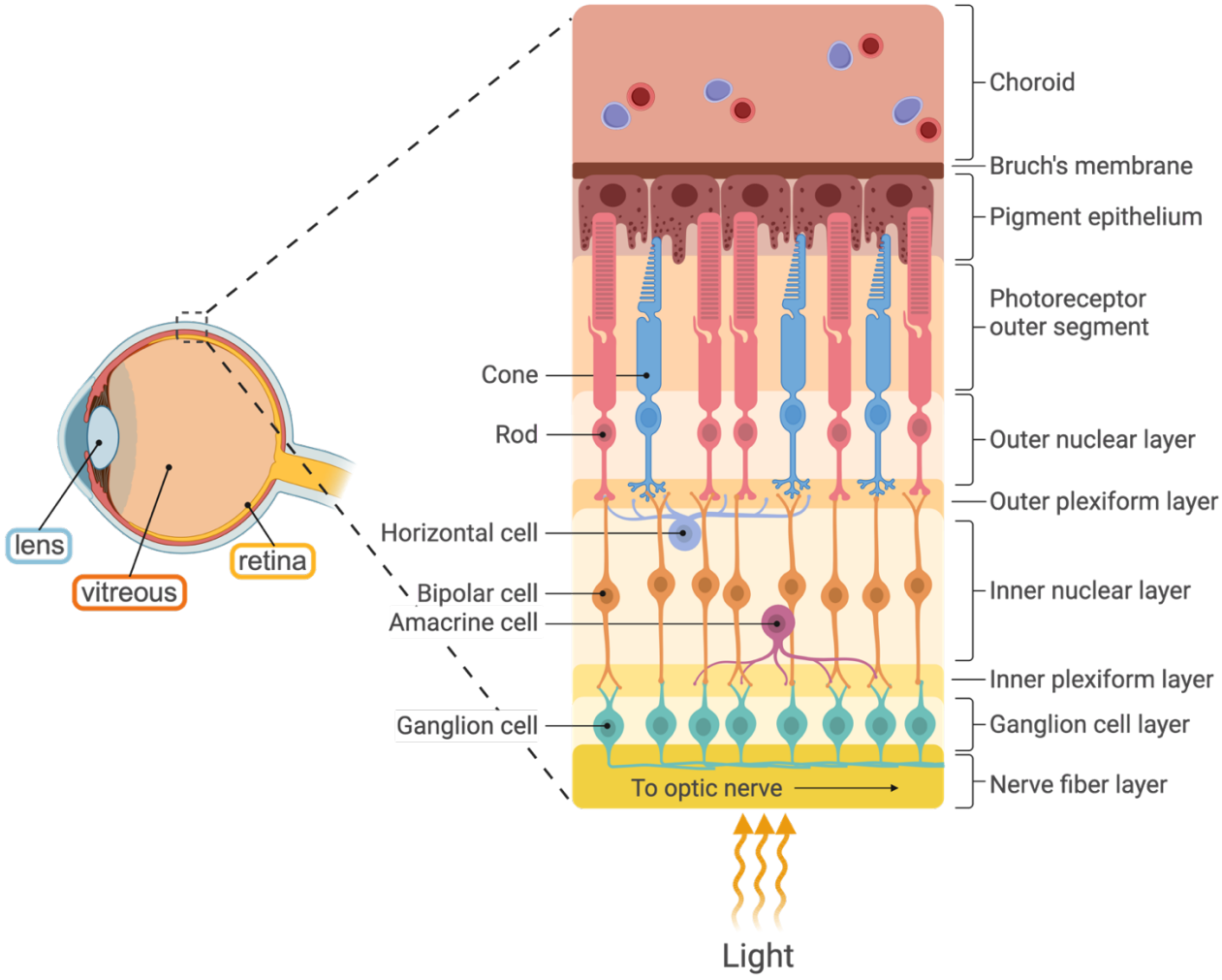

Figure 1.1: Retinal anatomy. A cross section of a human eye with inset is blown up in to show detailed histology of the retina. As light enters the eye, it is focused by the lens onto the retina. Photons are absorbed by rod and cone photoreceptors to begin a signaling cascade that eventually reaches the ganglion cells that transmit this information to the brain for further processing. The vitreous is a jelly-like substance that fills the inner eye. The choroid is highly vascularized to provide nutrients to the retina.

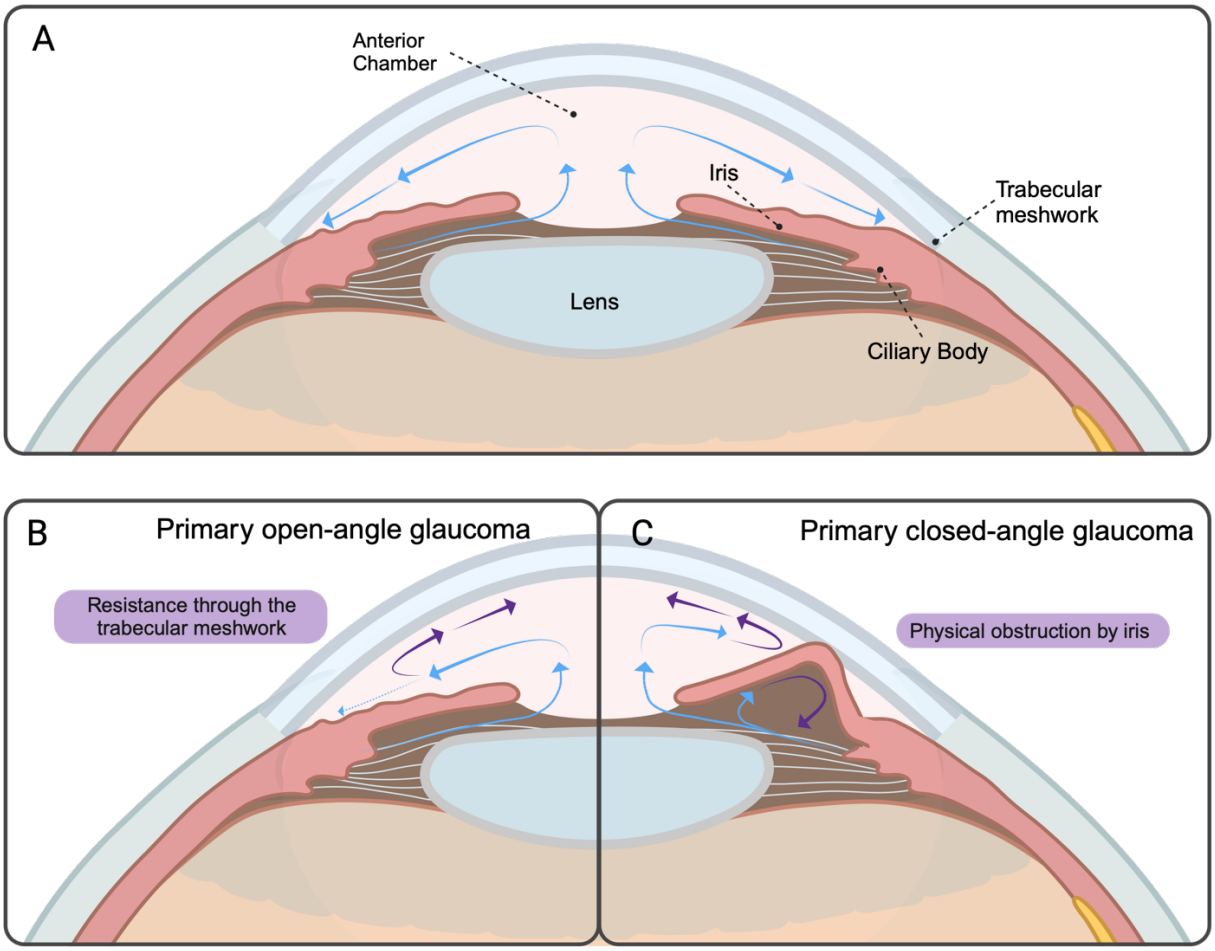

Figure 1.2: Types of primary glaucoma. Cross sectional views of the anterior eye in either A) normal B) open-angle glaucoma or C) closed-angle glaucoma conditions. A) The aqueous humor, represented by blue arrows, flows from the ciliary bodies, into the anterior chamber and out through the trabecular meshwork. B) Primary open-angle glaucoma occurs when resistance to aqueous humor outflow increases within the trabecular meshwork, causing backflow into the anterior chamber and often increases intraocular pressure. C) Primary closed-angle glaucoma occurs when the iris or another eye tissue physically blocks the outflow of the aqueous humor through the trabecular meshwork.

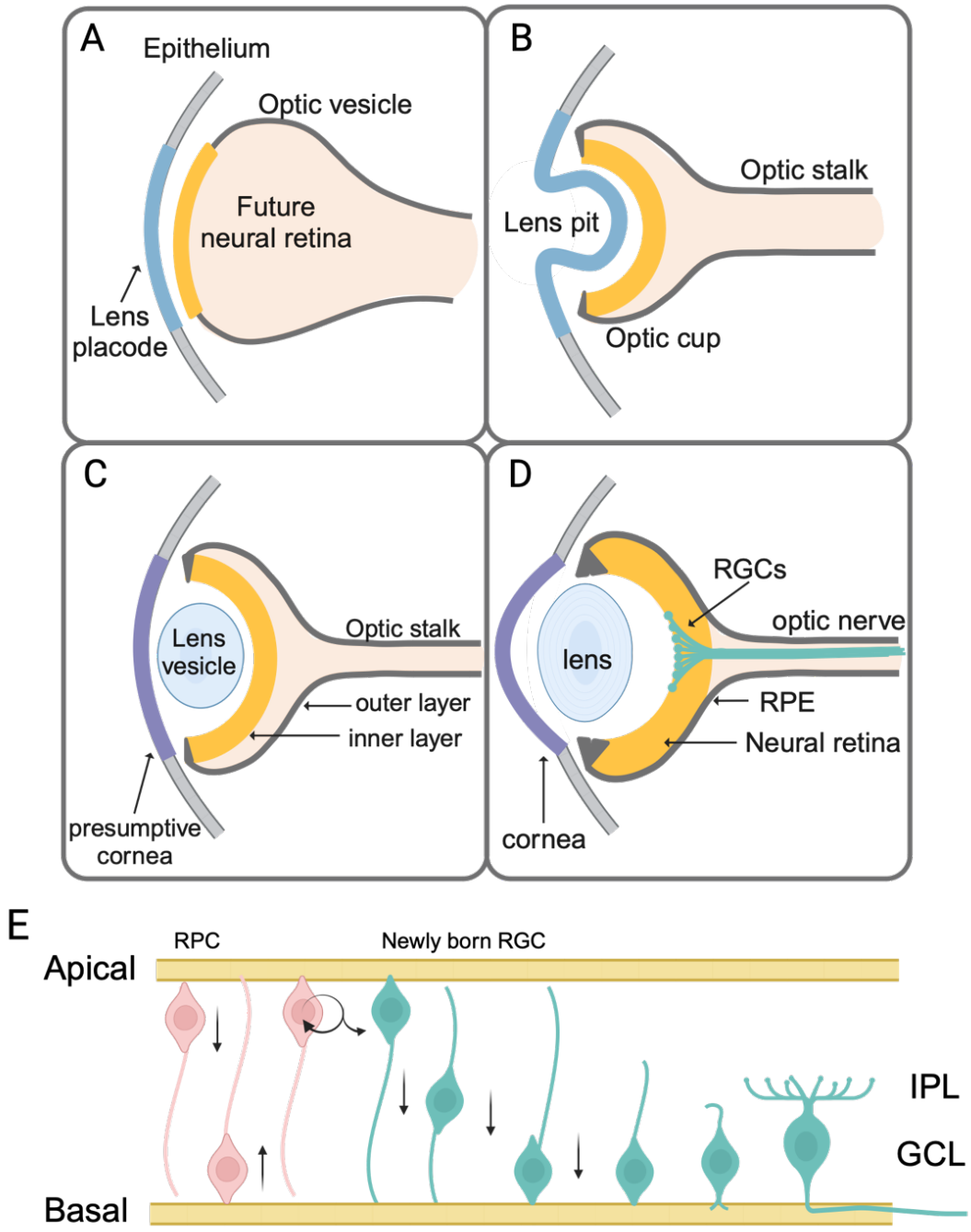

Figure 1.3: Retinal development and RGC genesis. A-D) Early vertebrate eye development. A) The optic vesicle, originating from the ventral diencephalon, contacts the surface ectoderm (epithelium) to form the lens placode. B) Invagination of the optic vesicle and the lens placode forms the optic cup and lens pit, respectively. C) The inner (neural retina) and outer (retinal

pigment epithelium) layers of the optic cup are specified. The lens vesicle (future lens) is formed after separating from the lens placode. The surface ectoderm proliferates to repair the exterior surface to form the presumptive cornea D) General structures of the adult eye are seen by embryonic day 11.5. E) RPCs use somal translocation to continuously migrate from the apical to basal surfaces of the retina. RGCs are born at the apical surface after asymmetric division of RPCs. Newly born RGCs migrate to the basal surface where they retract apical processes and form the GCL. RGCs then begin to project axons towards the optic nerve head and develop dendritic arbors in the IPL. Abbreviations) RPC: retinal progenitor cell, RGC: retinal ganglion cell, IPL: inner plexiform layer, GCL: ganglion cell layer

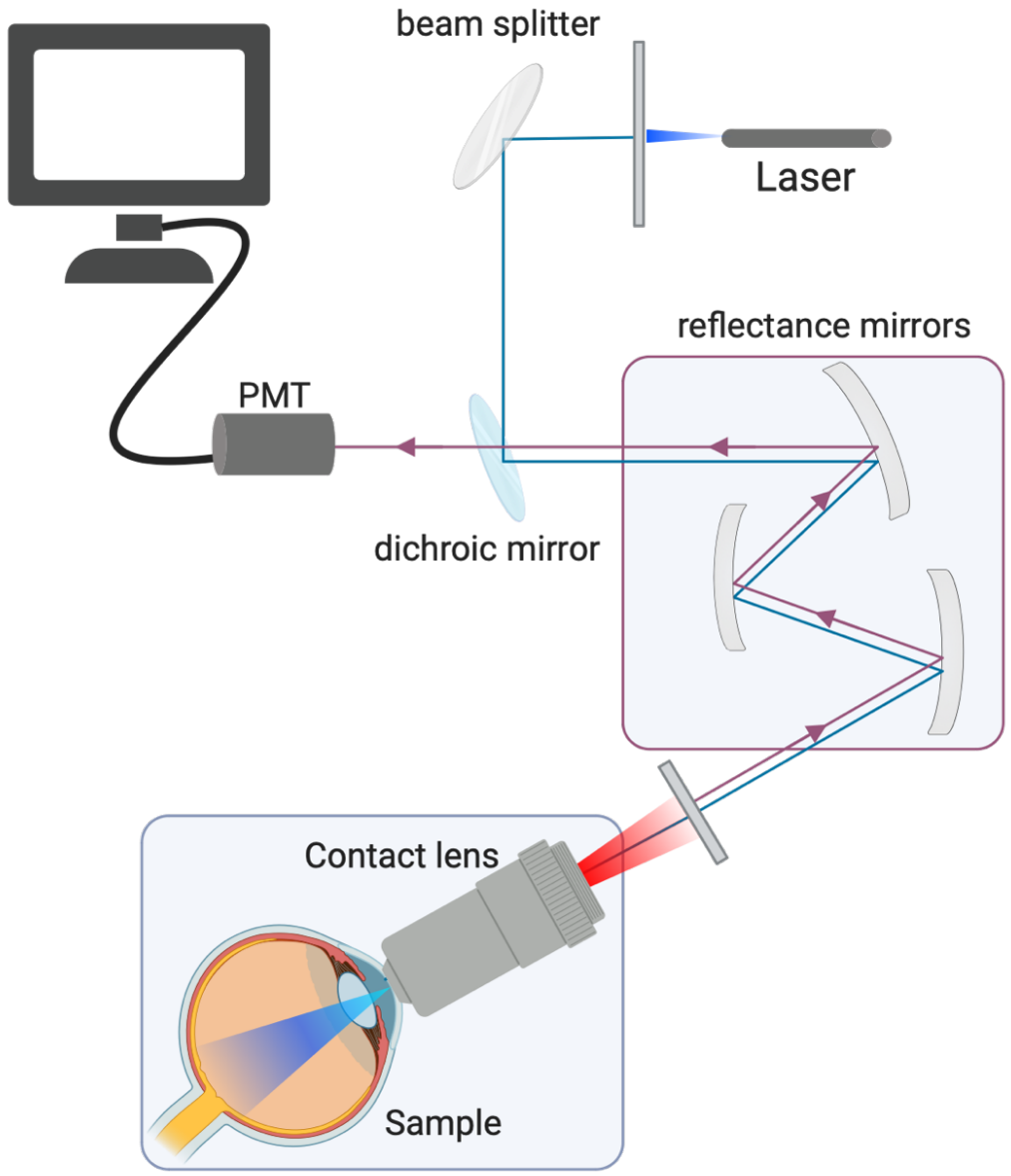

Figure 1.4: Simplified SLO system. Light from a laser diode travels through a series of mirrors to reach the XY-scanning unit (blue line). This sweeps across the sample (retina). The reflections are descanned to form a single beam that follows the same path as the incident beam (red line). The reflection passes through a dichroic mirror and is received by the PMTs that send information to a computer software to create a fundus image of the eye. Abreviations) PMT: photomultiplier tube.

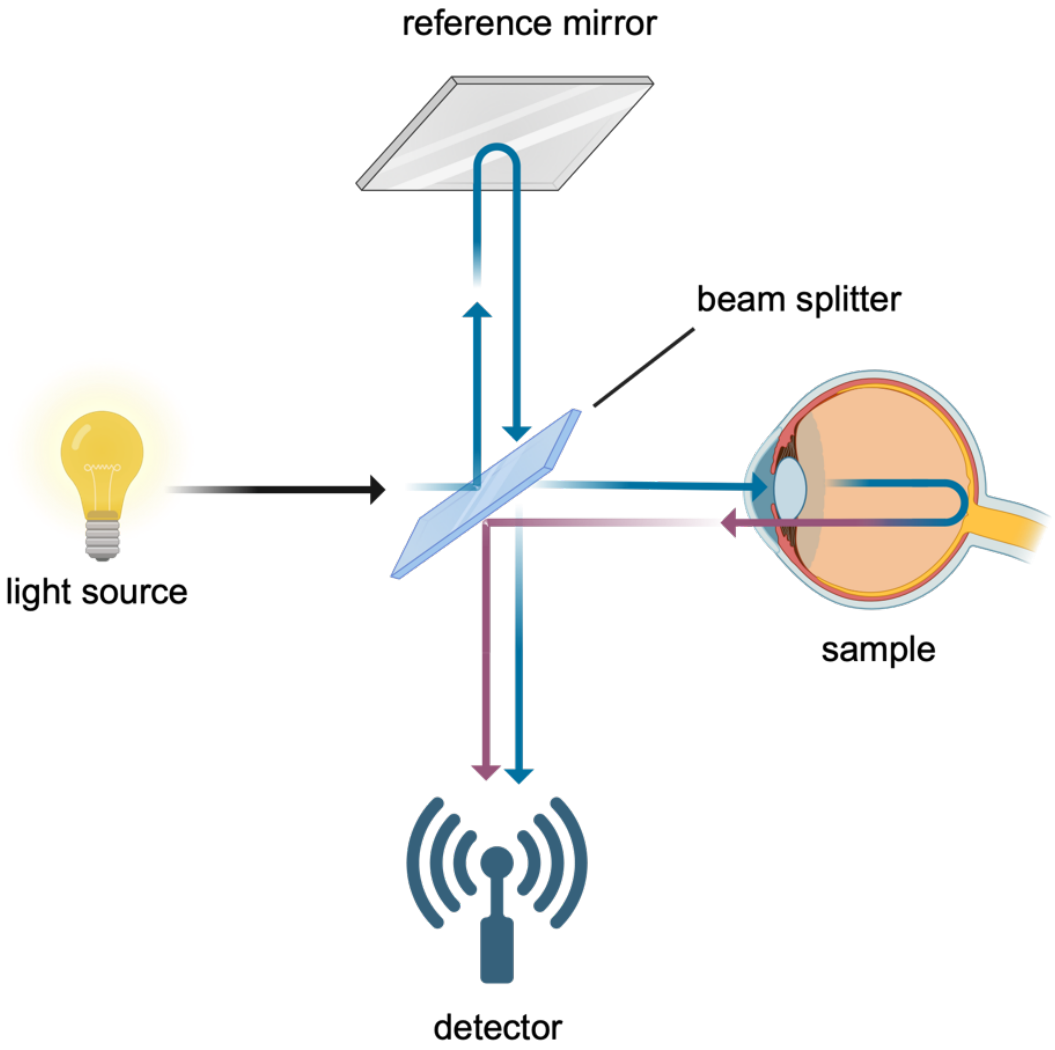

Figure 1.5: Simplified OCT system. Light emissions pass through a beam splitter that is either reflected (to reference mirror) or transmitted (to sample). The reflections of these two pathways are received by the detector that uses time and distance traveled of the two beams to produce a cross sectional image.

Literature Review: Barriers to retinal ganglion cell replacement therapy

Abstract

Glaucoma is one of the leading causes of blindness worldwide. The hallmark of glaucoma is the progressive degeneration of the retinal ganglion cells (RGCs), the cells that form the optic nerve (ON) and the only output of the retina. Currently, treatments for vision loss due to glaucoma only aim at preventing the progression of the disease and there are no methods available to restore sight after the RGCs have degenerated. RGC replacement therapy offers novel opportunities to treat vision loss by reestablishing the lost RGC population with healthy donor cells. Past attempts have analyzed the integration of purified donor RGCs into the host mouse retina. While many of these studies demonstrated long-term survival of donor RGCs into the host eye, many of these studies also reported that the engraftment rate of transplanted cells is incredibly low. Physical barriers within the eye, retinal glia reactivity, and the retinal immune response are all hypothesized factors contributing to the low success of RGC engraftment. In this review, we discuss how these factors may prevent successful RGC engraftment and the recent progress to overcome these limitations and develop effective clinical therapies to treat RGC degenerative diseases.

Introduction

Mammalian vision is the result of a complex network of highly specialized neurons within the eye and the brain. When light enters the front of the eye, it is focused by the lens onto the retina, the light sensitive neural tissue lining the back of the eye. Photoreceptors cells detect light and initiate a process called phototransduction that begins the cascade of signals through the

retina that eventually reach the retinal ganglion cells (RGCs), whose axons bundle together to form the optic nerve (ON), the only connection between the eye and the brain[171,18].

RGCs have been classified based on their functional properties and morphology, and more recently, based on their transcriptional signatures. Functionally, RGCs can be divided into different types, such as ON and OFF cells, which respond to increases or decreases of light, respectively. Morphologically, RGCs have been classified based on the size, shape, and distribution of their dendritic arbors. More recently, single cell-sequencing technologies have been applied to understand the diversity of RGC subtypes. At least 45 different subtypes have been identified in mice[172–174]. Similarly, 12-18 types of RGCs have been identified in primates[27,175]. Interestingly, the number of RGCs is drastically smaller than the pre-processing neurons, with the ratio of rods to RGCs being about 100:1 and cones about 6:1[35,176]. Therefore, maintaining this population of cells is vital to vision as it integrates and outputs all the information from the retina. Many diseases cause the degeneration of the ON and apoptosis of the RGC population, resulting in vision loss and eventual blindness; this includes glaucoma, ischemic optic neuropathy, Leber's hereditary optic neuropathy, and dominant optic atrophy, among others[177].

Glaucoma is one of the leading causes of blindness in the world, affecting more than 70 million people globally. One of the primary risk factors that contributes to glaucoma is age, and the projected incidence of glaucoma will see an increase to 111.8 million people in 2040 as the population ages[47,178]. However, unlike vertebrates such as *Xenopus laevis* and *Danio rerio*, the adult mammalian retina cannot regenerate retinal neurons or their axons after injury; any RGC lost to this disease is gone forever. Several strategies are being trialed to avoid neural cell death and to promote axonal regeneration. For example, several studies have shown that the Dual Leucine Zipper kinase (DLK) is a key mediator of the injury response after RGC damage and a target for potential neuroprotective strategies [179–184]. Indeed, when DLK and/or its mediators in the germinal cell kinase IV (GCK-IV) family are inhibited, there is an increase in RGC survival following optic nerve crush[181,185,186]. Similarly, many studies have investigated mechanisms to

promote axonal regeneration. Over the last decade, it has been shown that of regulators the mammalian target of rapamycin (mTOR) and Janus kinase/signal transducers and activators of transcription (JAK/STAT) pathways can increase axon regeneration in the adult CNS[73–76,187]. However, neither of these strategies will be useful to restore vision at the later stages of the disease when the RGC somas are no longer present.

While the mechanisms behind RGC degeneration due to glaucoma are not yet understood[188], it has been shown that RGC death correlates with sensitivity to elevated intraocular pressure (IOP), the only known modifiable risk factor for glaucoma. Consequently, to date, the only available treatment for glaucoma is reduction of the IOP, including topical medications that reduce the production of or increase the outflow of the aqueous humor. However, several studies have shown that only ~50% of glaucoma patients present with high IOP and that increased IOP does not necessarily lead to neurodegeneration[52,53,51]. While studies have shown that lowering the IOP can slow the progression of the disease in both elevated and normal-tension glaucoma patients, the current treatments only slow RGC degeneration and do not regenerate the lost RGC population[189,69,190]. Therefore, to restore vision, it is necessary to explore different treatment methods that can promote the survival and regeneration of RGCs.

RGC replacement therapy is a promising method to treat vision loss due to glaucoma. In the past decade, several groups have developed methods to transplant RGCs into host eyes. In most of these protocols, first, a population of donor RGCs are purified from whole retinas or generated *in vitro*. Then, the donor cells are intravitreally injected into the host eye and are further tracked with either *in vivo* imaging techniques such as scanning laser ophthalmoscopy (SLO) or using histological techniques (fig. 1).[191] Past studies have analyzed the survival and integration of purified donor RGCs into the ganglion cell layer (GCL) of a host retina. While donor RCG long-term survival has been observed, the technique currently utilized is inefficient to promote engraftment. At best, approximately 45% of injection attempts yield no living cells[192] and the injected population depletes rapidly within the first 24 hours, resulting in a loss of roughly 93% of

living cells[192–194]. Moreover, successful integration of transplanted RGCs remains in question. There has only been one published study that observed transplanted RGC axon projection into the brain, with this result seen in 1 in 80 samples[194]. Additionally, multiple studies have shown that the integration rate of donor living cells is low. These studies suggest that while successful transplantation relies heavily on the viability of the donor RGCs, the integration rate may be determined by the mechanisms against foreign bodies within the host eye itself[192–195]. One hypothesis is that the inner limiting membrane (ILM), the layer between the retina and the vitreous body, physically blocks exogenous RGCs from migrating into the host GCL[191,196]. Another is that the ocular immune system plays a role in the acute loss of injected RGCs by eliciting phagocytosis of the donor RGCs[197,198]. The reality is likely a combination of these and other factors.

In this review, we discuss the barriers within the eye that prevent successful RGC replacement therapy. This includes the inner limiting membrane (ILM), the barrier between the retina and the vitreous, and the retinal immune system. Although the observed cell survival is promising, understanding how the host eye prevents integration is necessary to achieve clinically applicable results.

The ocular immune response

RGC replacement therapy is an invasive technique; it requires the insertion of a needle through all layers of the retina, a delicate tissue, to inject a suspension of foreign cells into the vitreous cavity. While the intravitreal (IVT) injection technique itself may seem like a barrier to successful transplantation due to the tissue damage it causes, it is, in reality, a low-risk procedure used in clinics to deliver treatments for various ocular conditions. This includes the delivery of antiviral agents to treat cytomegalovirus retinitis, deliver gas as a treatment for retinal detachments, and, although not an injection, aspiration of the vitreous for biopsy[199,200]. IVT injection also provides a higher local concentration of a molecule and reduces the risk of systemic administration of drugs that can be associated with toxicity[199]. Although this may seem

counterintuitive due to the link found between neuroinflammation and neurodegenerative diseases, the key difference is that in neurodegenerative diseases, the tightly regulated CNS immune response is often compromised and the organ is in a state of chronic inflammation[201–203]. Thus, the homeostatic state of the CNS is to keep the immune system heavily regulated which has aided researchers in deeming the CNS, including the retina, as immune privileged[204].

Immune privilege was initially used to describe areas in the body where exogenous tissue grafts survive for extended periods of time, compared to rest of the body that acutely rejects exogenous grafts[204–206]. In early studies showed that skin grafts into the anterior chamber of rabbit eyes could survive at least 10 days, which researchers at the time attributed to an immunological isolation of these sites that prohibited entry from immune cells[204,205]. However, it is more widely accepted that instead of exclusion of immune cells, immune privileged tissues have built-in systems that regulate immune responses to ultimately reduce the chances of inflammation-induced damage, and in the case of the retina, vision loss[204,207,208]. Ocular immunity is generally maintained by microglia, the resident immune cells of the retina. Known as the “immunological watchdogs”, microglia cells surveil the retinal microenvironment for any changes. Their resting morphology is a small cell body with many long projections that span the nuclear layers. In a healthy adult retina, microglia reside in the plexiform layers and form a network of evenly tiled non-overlapping cells[209–212]. Microglia are generally maintained in their surveying phenotype through their interactions with retinal neurons to prevent them from becoming pathologically reactive[213]. For example, fractalkine (CX3CL1), expressed by retinal neurons, binds to its receptor found on microglia, CX3CR1, to keep retinal microglia in their “guard duty” state[214,215]. Consequentially, the immunomodulation via the CX3CR1-CX3CL1 axis is also considered neuroprotective[212]; deletion of *Cx3cr1* in a rd10 retinal degeneration mouse model resulted in increased microglial reactivity, infiltration into the outer nuclear layer (ONL), and photoreceptor death[216]. Similarly, one study found that subretinal transplantation of cells engineered to secrete CX3CR1 inhibited microglial reactivity in rats with light-induced photoreceptor degeneration[217].

However, microglia do not exist just to be modulated, they perform crucial mechanisms to help resolve and heal an injury[212].

In a damaged retina, microglia are the first to converge on the injury site after detecting changes in the microenvironment, such as increases in cytokines and chemokines, release of damage associated-molecular patterns (DAMPs), or a decrease in “calming” signals like CX3CR1. Once at the insult, microglia responding to pro-inflammatory signals transform into ameboid phagocytes to clear apoptotic cells while also beginning the inflammatory signaling cascade by secreting proinflammatory cytokines, interleukins, and interferons[210,212,218,219]. However, microglia responding to Th2 cytokines like interleukin-4 (IL-4) to induce a neuroprotective phenotype that secretes anti-inflammatory and neurotrophic factors to help with tissue repair and reestablishing homeostasis[219–221]. In a significant injury, the microglia response becomes more severe, and several studies have shown that circulating monocytes can be recruited to the retina, most commonly after damage to the retinal blood brain barrier (BRB). The BRB refers to two barriers, one is formed by the retinal endothelial cells and the inner microvasculature spanning the inner retinal layers (iBRB), the other consists of the RPE and the innermost layer of the choroid (oBRB)[222]. Recruitment of circulating monocytes to the retina can occur through C-C motif chemokine ligand 2 (CCL2) release by microglia and retinal endothelial cells, depending on how soon after the injury occurred[221,223,224]. The infiltrating monocytes then differentiate into microglia-like macrophages and can establish residence within the plexiform layers to seemingly replace the lost resident microglia population and reestablish homeostasis, but the full capacity of their role in retinal inflammation has yet to be defined[211,224–228].

As mentioned previously, clinical IVT injection is low-risk, however it is unclear if ocular inflammatory responses targeting the injected material are completely non-existent[84,229–231]. The most common clinical application of IVT injection worldwide is the intraocular delivery of anti-vascular endothelial growth factor (VEGF) agents[232]. Thus, the sides effects of this age-related macular degeneration treatment have been heavily studied[231,233,234]. Pertinent to RGC

replacement therapy is the observed phenomenon of delayed onset inflammatory vasculitis, occurring in 3.3% of patients as far out as 12-18 months post-brolucizumab, a VEGF inhibitor, treatment[233]. Such delay suggests that the inflammatory response is not due to the surgical trauma, but possibly the drug itself, although factors like patient history and condition may be more important[231]. Similarly, C. Bouguet and colleagues performed a clinical study of patients with Leber hereditary optic neuropathy (LHON) to investigate the immune responses to IVT injection of a recombinant adeno-associated virus 2 (rAAV2) carrying the NADH dehydrogenase 4 (*ND4*) gene, commonly mutated in LHON patients[235]. After the 3-year study, the authors found no associations between the ocular inflammation and the AAV2 dosage or neutralizing antibodies titers.[235] Thus, it seems that inflammation due to IVT injection of small molecules or viruses is patient specific. However, IVT injection of cells have a host of different factors compared to small molecule inhibitors, such as the cells undergoing apoptosis and expressing pro-inflammatory factors, most likely soon after delivery into the eye.

In one of the earliest studies of retinal cell replacement, Jiang and colleagues demonstrated that allogeneic retinal grafts from newborn mice placed in the vitreous cavity can survive for up to 12 days. Interestingly, they observed differentiation of the retinal grafts into mature cell retinal tissue with no signs of immunological rejection[236]. However, this study is not entirely comparable to RGC injection in that the whole retina were grafted instead of single cells. Currently, only bone marrow mesenchymal stromal cells (BM-MSCs) have been used to specifically study the inflammatory response to intravitreal cell transplantation[198,237]. A study by Norte-Muñoz and colleagues showed that, although the eye holds an immune privilege status, allogeneic and xenogeneic (human) transplantation of BM-MSCs into mouse host causes activation of microglia and recruitment of cluster of differentiation 45 (CD45)+ cells, a surface protein expressed by leukocytes. In contrast, syngeneic transplantation resulted in no significant microglia activation or recruitment of CD45+ cells. Additionally, immunosuppression with cyclosporine did not dampen the microglia activation after allogeneic transplantation of BM-MSCs,

which the authors hypothesize may be due to cyclosporine only affecting the adaptive immune response[238]. Therefore, intravitreal injection of genetically dissimilar cells, even with immunosuppression, activates the ocular immune system and causes the loss of the transplanted cell population, something that must be considered when attempting to transplant cells from an exogenous source.

The inner limiting membrane

The inner limiting membrane (ILM) is the basement membrane that separates the vitreous from the neural retina. Like other basement membranes of the body, the ILM structure is mainly formed by self-polymerizing laminin IV and collagen scaffolds, whose linkage is facilitated by nidogen. The retinal side of the ILM interfaces with the end processes (endfeet) of Müller Glia (MG), the radial glia that spans the entire retina. Here, laminin binds to the high concentrations of dystroglycans found within the MG endfeet, which is suggested to be a necessary interaction for proper retinal development[239]. Data suggests that one of the main roles of the ILM for proper retinal development is to help establish the eye's apical/basal polarity by promoting directional microtubule assembly within RGC axons through laminin activated integrin signaling[240]. Disruption of this signaling cascade results in RGC aggregation that bulges through the ILM, in addition to general disorganization of the ILM's structure[240]. Interestingly, the extracellular matrix proteins that form the ILM during development originate from lens and ciliary body, not the retina, and these structures do not seem to continue producing proteins for the ILM in adults, as sections of the ILM surgically removed does not regenerate itself. In mice, the ILM is a consistent thickness (~70nm), whereas the human ILM differs in thickness depending on the retinal region. For example, the ILM in the human fovea is thickest at ~400nm, whereas the periphery is closer to 70nm[240–242]. Furthermore, the ILM increases in thickness and rigidity with age, something that may be relevant to ocular therapies targeting age related diseases[240]. High resolution transmission electron microscopy shows that the ILM is separated into three layers: a layer of

electron lucent lamina lucida followed by electron-dense lamina densa, and ending with another lamina lucida layer[82] (fig. 2). However, these distinct layers found in basement membranes may be an artifact of tissue processing and the membrane actually a cohesive layer[243,244].

The ILM is a critical obstacle to successful intravitreal cell transplantation. While the ILM does allow selective diffusion of small molecules like glucose, lactate, and ascorbate, most studies in RGC replacement show that intravitreally transplanted cells are localized just outside of the ILM, suggesting that the ILM is physically blocking cells from integrating into the host tissue[193,194,191,192,195]. Indeed, when the ILM is disrupted, transplanted cells can integrate into the tissue at a higher rate. This was first demonstrated in a series of *in vitro* experiments using rat retina, wherein the ILM of rat retinal explant culture was physically removed and then cocultured with mesenchymal stem cells (MSC). In areas where the ILM was mechanically removed, there was an increase in MSCs found beyond the ILM compared to non-disrupted areas[196]. These observations were reproduced using human embryonic stem cell derived RGCs (hES-RGCs) in a later study by the same group. hES-RGCs cocultured on retinal explants only integrated at areas where the ILM was disrupted, such as the incisions made to flatten the retina. Additionally, ILM digestion with low concentrations of Pronase-E targeting collagens and laminins resulted in a nearly 40-fold increase of hES-RGC neurites extending into the inner plexiform layer[245]. This is in opposition to previous studies using collagenase that showed no increase in donor cell retinal integration. It is unclear why only one of these enzymatic approaches increases cell integration, thus further investigation into the structure of the ILM and its potential permeability is necessary.

Reactive gliosis: bridging physical and molecular barriers

The factors listed above obviously do not exist in a vacuum; physical damage to the ILM does cause inflammation and glia within the retinal nerve fiber layer are most likely the facilitators of this reaction[246]. Glia are the support cells throughout the central nervous system (CNS). While initially considered to function solely as “nerve glue”, or the cells that physically held the CNS

together, glial cells have been shown to play a much larger role in maintaining the function of the CNS. As previously noted, MG are the primary glia of the retina, and they are the only retinal cell type to span all retinal layers[18]. Thus, MG are important in the maintenance of the microenvironment and structure of the retina. In a homeostatic eye, MG support the rest of the tissue by transferring molecules between cells, removing cell debris, and secreting trophic factors. Astrocyte cells (AC) are another glia that exist mainly in the retinal inner nuclear layer and the nerve fiber layer. Like MG, ACs provide neurotrophic factors to and structural support for the surrounding neurons[33,34]. In response to injury, retinal glia undergo process also known as reactive gliosis that can change their morphology, biochemistry, and physiology to reduce the severity of tissue damage. In short, reactive glia support the surrounding uninjured tissue, regulate inflammation at the damage site, and create a scar to protect the neural tissue from further injury[33,247,248]. One of the hallmarks of reactive gliosis is rapid synthesis of the intermediate filament proteins glial fibrillary acidic protein (GFAP) and vimentin (Vim) in glia[249–251]. While the initial gliotic activity is beneficial, prolonged gliosis can be detrimental to the tissue and often implicated in neurodegenerative diseases[33,252,253].

Studies suggest that the molecular mechanisms during reactive gliosis may be key in understanding how to regenerate the mammalian CNS. Several studies have shown that mice lacking GFAP and Vim have abnormal responses to CNS injury[254–259]. When both intermediate filament proteins are absent, evidence shows that mice do not form astrocytic scars correctly and seem to be prone to reinjury after direct brain trauma[254]. Interestingly, these double mutant mice have also been shown to exhibit axon regeneration and locomotive recovery after hemisection of the spinal cord[255]. It seems that there is a tradeoff between glial scar formation, and therefore neuroprotection, and neural regeneration in the mammalian CNS. In the context of transplantations, *Gfap*$^{-/-}$ *Vim*$^{-/-}$ double mutants seem to allow CNS transplantations to integrate in a higher abundance compared to wild type animals. This has been demonstrated in hippocampal injections, IVT injections, and subretinal grafts[237,260,261]. These experiments also show that the

transplanted cells have increased axonogenesis and remain in the *Gfap*$^{-/-}$ *Vim*$^{-/-}$host tissue for several weeks. Mechanical removal of the ILM also seems to suppress gliosis by damaging the basal processes of the Müller glia. After disruption, areas with less glia reactivity, usually corresponding to ILM removal, saw an increase in integration of donor cells. However, suppressing glial reactivity with *α*-aminoadipidic acid (AAA) resulted in increased integration even with a fully intact ILM[196]. In the context of RGC cell replacement, gliosis seems to be an active barrier to transplanted cells surviving and integrating.

Conclusion

The mammalian retina is a complex tissue that is the source of vision. However, due to the non-regenerative nature of the mammalian CNS, retinal degenerative diseases can be devastating to a patient's quality of life. Additionally, as modern medicine extends the average lifespan, age-related retinal degenerative diseases will become more common, yet curative treatments remain scarce[47,51,190]. However, the advancement of modern medicine has also allowed for the development of novel therapies, like RGC replacement[191]. Unsurprisingly, there are many reasons why RGC replacement therapy is difficult. First, one must acquire a large enough population of donor cells that also survive the injection process. Next, these cells must move past the ILM and into the host tissue. Finally, the cells are faced with the endogenous immune response that includes reactive gliosis, all designed to protect the body from foreign invaders. While this is a daunting task for a 10-micron cell, recent efforts into removing these barriers have helped us gain insight into improving conditions for this perilous journey and eventually bringing this technique to the clinic[196,237,245].

Figures

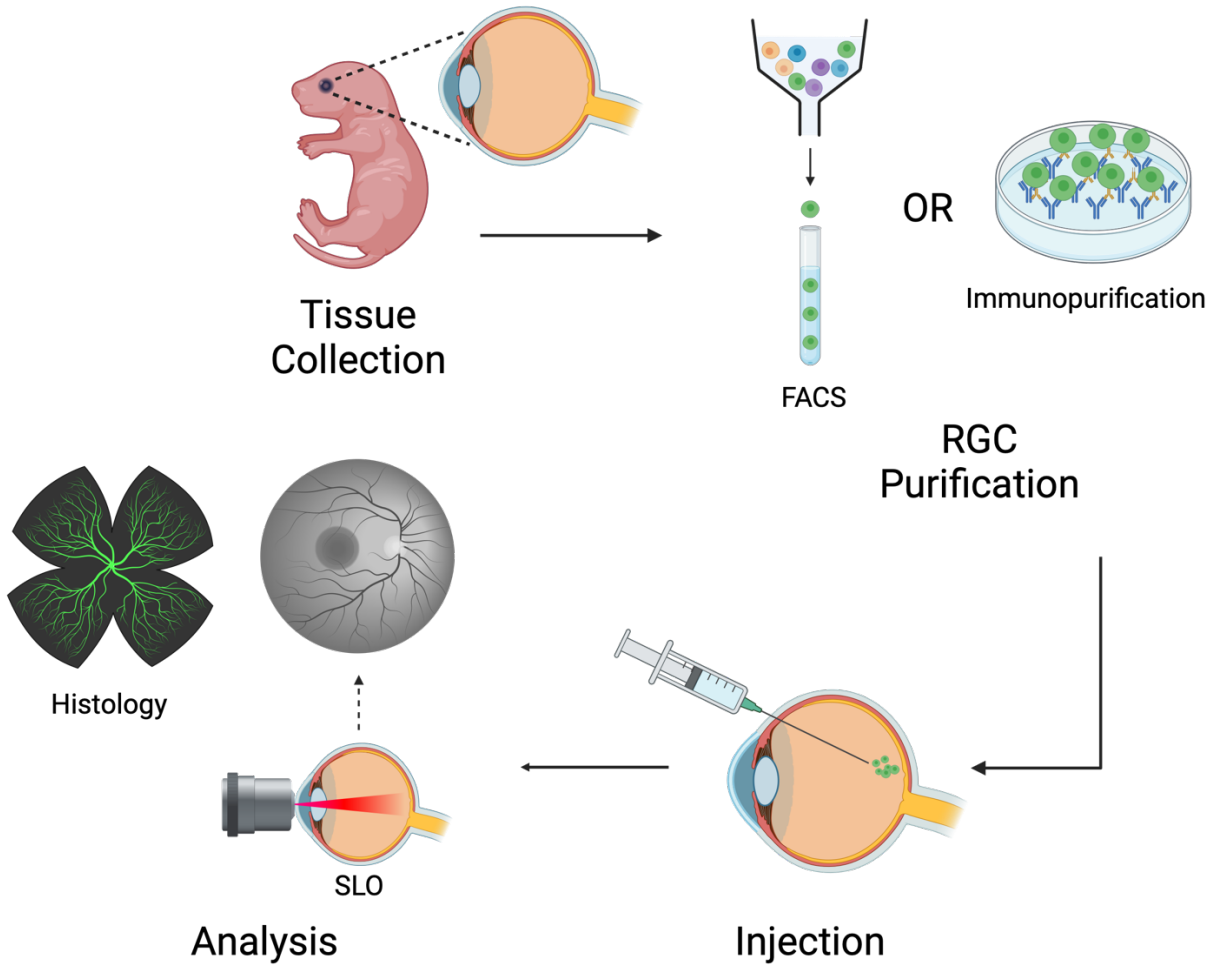

Figure 1.6: RGC transplantation pipeline. A schematic of the general pipeline for retinal ganglion cell (RGC) transplantation in mice. 1) retinae are collected from P0-P2 pups then 2) the RGC population is purified via fluorescence activated cell sorting (FACS) or immunopurification. 3) The purified population is injected intravitreally into the host eye. 4) Host eyes are analyzed by live imaging, histology, or a combination of both. Abbreviations) FACS: fluorescence activated cell sorting, RGC: retinal ganglion cell, SLO: scanning laser ophthalmoscopy.

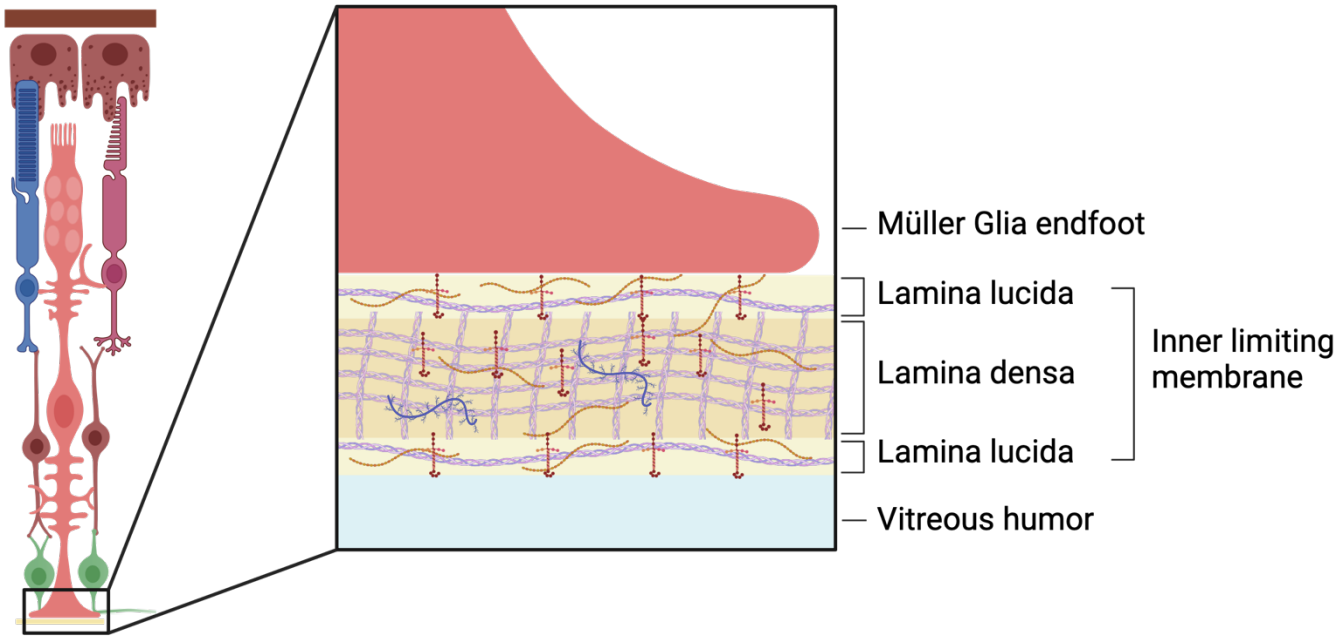

Figure 1.7: The inner limiting membrane. A truncated diagram of a retinal cross section with the four of the main retinal neurons: photoreceptors, bipolar cells, retinal ganglion cells, and Müller glia. The enlarged section demonstrates the structure of the inner limiting membrane and its general components. This includes laminins, collagens, hyaluronic acid, dystroglycan.

Chapter 2

Inhibition of DLK to improve the survival of stem cell derived RGCs

Mikaela Louie[1], Adam M. Miltner[1], Simranjeet K. Cheema[1], Yesica Mercado-Ayon[1], Stephen Kwong[1], and Anna La Torre[1].

[1]Department of Cell Biology and Human Anatomy, University of California - Davis, Davis CA, US.

Introduction

Retinal ganglion cells (RGCs) are the only output neurons that connect the retina circuitry to the visual centers of the brain[19]. Thus, RGC degeneration is one of the main causes of blindness, affecting more than 70 million people worldwide[47]. Several diseases lead to irreversible RGC damage including glaucoma, hereditary optic neuropathies, and ischemic optic neuropathies[177,262]. The current treatments are unable to restore vision and consequently, the potential to replace lost RGCs is of great interest[48,51]. Previous studies have shown some success

in transplanting RGCs *in vivo* using rodent models, but a clear method to produce a large quantity of donor RGCs for transplant purposes has remained elusive[192–195,263–265]. Thus, even when the challenges surrounding RGC transplantation are overcome, it will not be clinically relevant if there is no consistent source of donor cells.

Sourcing donor tissue for RGC transplants is uniquely challenging— human RGCs cannot be isolated without damaging their axons and RGCs make up only ~3% of the entire retina[266,267]. Additionally, there is in general a deficit of donor tissue, with a 6:1 ratio of patients on the transplantation waiting list for organs that can currently be transplanted, like lung and kidney, to transplantations performed[268]. With these challenges in mind, producing donor RGCs *in vitro* is the most plausible strategy to pursue. The derivation of the first mouse embryonic stem cell (ESC) lines and the isolation of the first human ESC line introduced the prospect of producing limitless donor tissue without the need of human donors[269,270]. Additionally, successful generation of human induced-Pluripotent Stem Cell (iPSC) lines opened the possibility to produce tissue from a patient's own cells[156,271,272]. Consequentially, two-dimensional (2D) and 3D stem cell differentiation techniques to produce tissue specific cell types *in vitro*, like retinal neurons, have evolved rapidly[163,273,274]. While these technical achievements have solved the problem of a lack of donor tissue, current retinal organoid culturing methods still have limitations. For example, 2D culture can more realistically replicate the microenvironment within a single retinal layer but lacks the overall laminated structure of the retinal and do not survive well when lifted off the culture plate, while 3D cultures recapitulate the retinal lamination but see an eventual decline of the RGC population as the organoids are kept in vitro[164,275–277]. It is currently unclear what factors contribute to RGC attrition, but methods from neuroprotective strategies could provide useful approaches to scale up RGC production for clinical applications.

In neurodegenerative diseases such as Alzheimer's disease and glaucoma, dual leucine zipper kinase (DLK) and its co-mediator leucine zipper kinase (LZK) are key mediators of the injury response[68,179–183,278–281]. For example, axonal injury causes the retrograde transport of

DLK/LZK from the injury site to the soma. Here, the c-Jun N-terminal kinase (JNK) cascade is triggered that ultimately results in the phosphorylation of JUN, a regulator of cellular injury response pathways[68,185,281–283]. In the peripheral nervous system (PNS), the resulting gene expression changes promote axon regeneration and, in some cases, restore function. In contrast, within the central nervous system (CNS), DLK dependent changes in gene expression often result in cell death[284]. Although other axon injury response pathways exist, most axotomy induced gene expression changes are dependent on DLK signaling[185,285]. Therefore, inhibition of DLK and LZK has a robust effect on survival, making DLK/LZK targeting a leading neuroprotective strategy. In the context of RGC degenerative diseases, the goal for these strategies is to ultimately regenerate the optic nerve, requiring both the the survival of RGCs and regeneration of their axons. However, the relationship between neuron survival and axonogenesis has yet to be fully understood.

DLK inhibition is an antagonist to axon regeneration strategies. For example, knockdown of phosphatase and tensin homolog (PTEN) typically results in axonogenesis, but when crossed with $DLK^{-/-}$ animals, this phenotype is no longer observed[73,76,181,187]. Similarly, DLK has been shown to mediate the retrograde transport of signal transducer and activator of transcription three (STAT3). STAT3 is involved in axon regeneration via mechanisms that rely on the accumulation of its phosphorylated state within cell bodies, and STAT3 inhibition practically abolishes any neurite growth caused by known retinal neuron axon regenerative strategies, like inflammatory stimulation of the inner eye[185,286]. Unsurprisingly, DLK deletion causes the loss of phosphorylated STAT3 accumulation typically seen in a wildtype animal[185]. Although the role of DLK in PTEN and STAT3 mediated axon regeneration is still unknown, DLK is important for axon regeneration. This poses a challenge for some neurodegenerative diseases, like traumatic optic neuropathy, where axotomized yet surviving RGCs require methods to promote both survival and axon regeneration. In this context, DLK/LZK inhibition is unlikely to be a viable neuroprotective strategy, and thus, identification of novel targets is needed.

Manipulation of downstream targets of DLK/LZK is a strategy that has been explored to uncouple the effects of regeneration and survival. However, this approach has yet to show success. For example, targeted disruption of JUN can increase survival but impairs regeneration, like DLK inhibition[283]. Curiously, the most robust axon promoting disruptions, such as knockout of Krüppel-like transcription factors (KLFs), PTEN, suppressor of cytokine signaling three (SOCS3), or STAT3, do not promote lasting or substantial increases to neuronal survival[73,187,287,288]. Recently, we conducted a genetic screen using human stem cell-derived RGCs to identify the germinal cell kinases IV (GCK-IV) kinases as a suitable target for both axon regeneration and neuron survival[186]. Previous studies have shown that the GCK-IV kinases regulate the DLK/JNK pathway, although the exact mechanism is currently unknown[289]. In our previous study, we demonstrated that GCK-IV kinase inhibition is robustly protective to RGC survival after optic nerve crush (ONC) and synergizes, rather than antagonizes, the axon regeneration triggered by knockout of the canonical repressor, PTEN[186]. Here, we demonstrate that inhibition of GCK-IV kinases can address the attrition of RGCs over time and promote the survival and neurite outgrowth of RGCs in mouse retinal organoids using a novel line of reporter iPSCs derived from a Bacterial Artificial Chromosome (BAC) transgenic reporter mouse created as part of the GENSAT (Gene Expression Nervous System Atlas) project, insulin related protein 2 (Isl2)-GFP. This data demonstrates the potential for GCK-IV inhibition as a neuroprotective/axon regenerative strategy for neurodegenerative diseases, as well as a strategy to improve organoid differentiation protocols.

Results

The expression pattern of Isl2-GFP recapitulates endogenous Isl2 expression during retinal development

The Isl2-GFP reporter mouse was originally created by the GENSAT project and first characterized by Triplett et al.[290]. We recovered from cryogenic storage from the Mutant Mouse Resource and Research Center (MMRC) at UC Davis. Previous reports indicated that GFP was highly expressed in a subpopulation of contralateral-projecting RGCs in adult Isl2-GFP mice, but the developmental expression pattern was unknown[128]. Isl2 mRNA and protein have been reported at embryonic ages, so we sought to ensure the BAC reporter accurately recapitulated Isl2 expression in the developing embryonic retina during RGC genesis. We collected Isl2-GFP mice at embryonic day (E) 13.5, 15.5, and Postnatal day (P) 0 to analyze the pattern of GFP expression in the developing mouse retina. Isl2-GFP fluorescence in the retina is present from E13.5 (fig. 1G-J), persists through adulthood (fig. 1A-F), and is expressed in RGCs as well as in many peripheral sensory neurons, such as the trigeminal ganglion neurons (fig. 1H, L).

To determine the dynamics of Isl2-GFP expression, we performed co-localization experiments using established markers for different stages of RGC development. Previous reports show that Brn3b, a master regulator of RGC development[109,126], is detected before Isl2 expression, and that Brn3b, but not Isl2, is expressed in nascent RGCs migrating to the ganglion cell layer (GCL)[114,128]. As expected, we did not observe Isl2-GFP expression at E11.5, despite nascent RGCs being present as visualized with pan-Brn3 staining (fig. 1G). Isl2-GFP and a pan-Brn3 antibody colocalize at E13.5 (fig. 1K) with colocalization persisting through P0. However, the Isl2 and Brn3 expressing RGC populations are not entirely the same, with Brn3 labeling more RGCs than Isl2 throughout development into adulthood. It is more obvious that the Isl2-GFP+/Brn3- and Isl2-GFP-/Brn3+ RGC population is larger than the Isl2-GFP+/Brn3- population

at P0 than in embryonic ages (fig. 1K and 1N). Additionally, we rarely observed Atonal homologue 7 (Atoh7)+, which is expressed by a subset of retinal progenitor cells in their terminal cell cycle and is required for RGC genesis[108,291,292] , and Isl2-GFP+ cells in E16.5 Isl2-GFP histological sections (fig. 1L). This agrees with Pak et al.'s findings that Isl2 is only expressed in postmitotic RGCs[128]. Thus, the temporal aspects of Isl2 expression appear to be preserved in the regulatory elements within the BAC used to make the Isl2-GFP animal.

Interestingly, Isl2-GFP is expressed in ON-bipolar cells in adult cryosections, although much weaker than in RGCs as noted by Triplett et al.[290]. Isl2-GFP+ cells in the GCL are always Pax6+ and RBPMS+, indicating the Isl2-GFP transgene is not expressed in displaced amacrine cells (fig. 1A-D). Other reports have shown Isl1 expression in bipolar cells in early postnatal retina samples as well as mature ON-bipolar cells[293]. Taken together, these data show that the Isl2-GFP transgene accurately recapitulates Isl2 expression during development and in the adult animal. Thus, we chose the Isl2-GFP reporter mouse to derive an iPSC line because it labels ~40% of RGCs starting early in development and remains into adulthood.

Generation and analysis of an Isl2-GFP iPSC line

To create a reporter iPSC line from the Isl2-GFP mouse, mouse embryonic fibroblasts (MEFs) were isolated from E13.5 Isl2-GFP mice by passing embryos through successive 20-gauge and 30-gauge needles after removal of the heads and internal organs. The resulting dissociated tissue was plated and cultured in media supplemented with 10% fetal bovine serum. After two passages, the cultures were transduced with two reprogramming lentiviral plasmids—one expressing Oct4 and Sox2, and one expressing Lin28 and Nanog. After 28 days, we observed iPSC colonies in the MEF cultures that were picked and expanded in a feeder-free culture system (fig. 2A).

Isl2-GFP iPSCs are morphologically indistinguishable from ESCs and express known stem cell markers, including the genes used for reprogramming and others such as SSEA[273] (fig.

2A). Importantly, the expression of pluripotency genes decreased after iPSCs were differentiated into retinal organoids (fig. 2B). In contrast, we observed an increase in expression of retinal progenitor cell markers during organoid differentiation. By differentiation day 6 (D6) genes normally expressed in RGCs significantly increased compared to undifferentiated iPSCs (fig. 5A).

D7.5 was the earliest we observed GFP+ neurons in Isl2-GFP organoid cultures that was followed by a rapid production of GFP+ neurons between D8-D10. Isl2-GFP neurons purified by Fluorescence Activated Cell Sorting (FACS) had higher Brn3b expression compared to the GFP- population, suggesting that GFP+ neurons are RGCs (fig. 3C, n=3). Immunohistochemical analyses of Isl2-GFP organoids show a strict colocalization of GFP+ neurons with RGC markers pan-Isl1/2 and pan-Brn3, axon marker Tuj1, and the pan-RGC marker RBPMS. Additionally, we did not observe GFP+/Otx2+ cells in Isl2-GFP organoids at the latest timepoint analyzed, D15, suggesting that there were no ON-BCs present in the organoid culture because all bipolar cells are Otx2+[294,295] (fig. 4A-C). Additionally, we observed the formation of optic cup-like structures by D10 that contained a distinct layer of GFP+ cells closer to the center of the organoid, as well as GFP+ cells seeming to migrate from the outermost/basal side towards this layer (fig. 3B and 4D). Further examination of these areas revealed that the GFP+ cells both within and migrating towards this layer co-localize with Brn3 and RBPMS, suggesting that Isl2-GFP RGC genesis can recapitulate the endogenous apical to basal migration (fig. 4D). Together, these observations suggest that the Isl2-GFP+ neurons are indeed RGCs that express RGC markers: Isl2, RBPMS, and Brn3, but do not express the ON-BC marker Otx2, and that they recapitulate the physical mechanisms of RGC genesis (fig. 4)

GCK-IV kinase inhibition improves RGC survival in retinal organoids

Multiple groups have reported that neurons produced in retinal organoid culture have a significant decrease in RGC survival as time in culture increases. In our Isl2-GFP organoid cultures, we observed that the majority of the RGC population has died by D25. However, we

have recently demonstrated that GCK-IV kinase knockouts promote RGC survival *in vivo* without inhibiting axon regeneration. In our previous study, we tested PF-06260933 (PF), a GCK-IV inhibitor that is highly selective against the kinome, and showed that we can improve the survival of cultured mouse and human RGCs with this molecule[186,296]. To determine if this strategy can improve RGC survival within our organoid model, on D13 we added either PF-06260933 (PF) or vehicle control (DMSO) to the culture media. In a pilot experiment, we tested concentrations of 100 nM, 200 nM, 500nM, and 1□M of PF-06260933. After 7 days, we observed toxicity in the cultures with 1□M and 500nM, so we used 200 nM for all the subsequent experiments (fig. 6C).

Retinal organoids were collected after 30 days of culture and assessed for the number of RGCs and axon density. To determine differences in RGC survival, organoids were immunolabled for GFP and RBPMS to obtain the total number of RGCs. Organoids cultured in PF resulted in a 3.7-fold increase in the number of RGCs compared to their vehicle control ($p<0.01$, n=6-7/group, fig. 6A-B). This increase was seen in quantification of both GFP and RBPMS, suggesting that PF culture improves the survival of all RGCs, not just a subpopulation. This is an important distinction because it has been shown that some RGC subtypes are more resilient to retinal disease and injury[75,297,298]. However, this data suggests that GCK-IV inhibition is not merely enhancing this intrinsic robustness but targeting a shared mechanism within all RGCs. Additionally, there was a 3.5-fold difference in fluorescence intensity between PF and vehicle cultures, suggesting that PF culture helps to maintain the overall health of cells in addition to increasing survivability ($p<0.05$).

To determine neurite outgrowth, retinal organoids were immunostained for Tuj1, a marker for neuron cytoskeletons. We observed a 2.3-fold increase in neurite density of organoids cultured in PF compared to organoids cultured with vehicle only (, $p<0.05$, n=6-7/ group, 6A-B). Additionally, Tuj1 expression was more homogenous throughout the entire organoid after PF culture, opposed to the more clumped densities found in the control organoids (fig. 6A). This suggests PF culture results in less degeneration within the center of the organoid, an observation commonly made for all organoid culture[277,299]. Thus, these results demonstrate that GCK-IV

kinase inhibition is a promising strategy to improve RGC survivability and neurite outgrowth in retinal organoid culture.

Discussion

Glaucoma is a family of optic neuropathies that occur due to the degeneration of the optic nerve and RGCs. While treatment for these blinding diseases has advanced, they are only designed to reduce intraocular pressure (IOP) to slow the progression of the disease and can only be used for a subset of the patient population[48]. Thus, efforts to establish new treatment methods that are applicable to the wider patient population and can address vision loss have gained traction within the last 10 years. One method is to replace the dying RGC population with healthy donor cells from an outside source. However, traditional donor tissue harvesting is not a feasible method to obtain enough cells for RGC cell replacement therapy, especially given the prevalence of diseases like glaucoma[47]. Alternative methods for cell production, like *in vitro* differentiation of stem cells, is now widely studied to fill the deficit of donor tissue, although current protocols can only produce a modest number of cells that have limited survival[191]. Therefore, to develop a more efficient method to source donor RGCs*,* we characterize the *in vitro* production of RGCs using an RGC reporter iPSC line and show that inhibition of the GCK-IV kinase MAP4K4 can increase the survivability of these cells.

Isl2-GFP iPSCs produce GFP labeled RGCs after differentiation

Previous work has established 3D culturing methods to differentiate stem cells into retinal cell fates. These cultures self-organize into laminated retinal cup-like structures that express markers for all six main retinal neurons: photoreceptors rods and cones, bipolar cells, horizontal cells, amacrine cells, Müller glia and retinal ganglion cells[163,273,274]. Here, we characterize an iPSC line made from the Isl2-GFP reporter mouse to use as a source of RGCs for *in vivo*

transplantation. When cultured in retinal degeneration media, the iPSCs differentiate into retinal neurons and self-organize into laminated retina-like structures[163,273,274]. We also show that, within the context of the retina, GFP seems to exclusively label RGCs *in vitro* contrary to what is shown within the mouse model. ON-BCs express GFP in Isl2-GFP mice, albeit weaker than the expression in RGCs. However, it is unclear if there are simply no ON-BCs by D15 or if the GFP expression is significantly weaker when BCs are produced *in vitro*. It should be noted that Isl2-GFP is found throughout the mouse CNS, specifically in developing spinal motor neurons and the trigeminal nerve, and the possible *in vitro* production of these neuron subtypes should not be discounted[290].

Since our long-term goal of this study is to use these cells as a source of donor tissue for RGC replacement therapy, we must consider the variation in developmental time scale to isolate fully mature RGCs. After exiting the cell cycle, newborn RGCs must migrate from the apical to the basal layers of the retina[100]. Here, we show that stem cell derived Isl2-GFP RGCs express GFP while migrating and that this coincides with the peak of the RGC population ~D11 (data not shown). However, this poses slight issues in the context of RGC transplantation due to the immunopurification methods commonly used to isolate the donor cell population[300]. There is an established method of using the membrane protein Thy1.2 to isolate RGCs from dissociated retina, but Thy1.2 is only expressed postnatally, and it is unclear if stem cell derived RGCs express Thy1.2 at the time when there is the most RGCs present within the organoid. Thus, more experiments should be performed to determine if this standard practice can be used.

Inhibition of MAP4K4 increases in vitro RGC survival

Several groups have reported the limited survival of RGCs within both mouse and human retinal organoid culture- by D25 in mouse culture and D160 in human culture there is a significant attrition of RGCs, and structural disorganization of the inner organoid layers followed by degeneration of the organoid[164,275,276]. Here we show that inhibition of the GCK-IV kinase MAP4K4

increases the survival of RGCs *in vitro*. It has been reported that the DLK pathway a key regulator of neuronal cell death and injury response and that GCK-IV kinases are involved in the activation of DLK[179–183,278–280]. However, the exact mechanism by which GCK-IV kinases like MAP4K4 regulate DLK is unclear– DLK can be activated through dimerization-induced autophosphorylation in the absence of upstream kinases. Additionally, GCK-IV inhibition behaves differently than DLK inhibition regarding axon regeneration, whereas DLK knockdown in models of axon regeneration (PTEN-/- mice) inhibits axon regeneration, GCK-IV inhibition results in a synergistic effect on axon regeneration[181,186,187]. While it is unclear how MAP4K4 inhibition improves axon regeneration, previous work has shown that MAP4K4 facilitates focal adhesion turnover in microtubules that is involved in axon pathfinding and outgrowth[301,302]. Similarly, we observed an increase in axon density within retinal organoids cultured with a MAP4K4 inhibitor compared to those with only vehicle added.

The lack of nutrients and oxygen in the center of 3D cultures most likely contributes to the degeneration of RGCs due to central position of the GCL. Thus, vascularization of retinal organoid cultures may improve RGC survival via co-culture with vascular cells or a microfluidics system. However, these methods have yet to demonstrate true vascularization due to limitations of 3D printing technology, and the *in vitro* formation of blood vessels often disrupts the self-organization of organoid structures[299]. To date, the only method that results in angiogenesis comparable to a living organism is to transplant organoids *in vivo* and use the host microenvironment to establish a functional vascular system. However, this method poses issues for retinal organoids because the retinal vasculature exists in two separate systems, one formed in the inner retina and the other formed by outer retina that requires retinal pigmented epithelium[222]. Thus, the organoid tissue would need to be transplanted in a way to span the length of the entire retina of the host animal. Therefore, thinking of retinal organoids as a model of degeneration from D25 onwards may be the most feasible if we are to use them as a source of cells for transplantation.

Materials and Methods

Animals

Adult mice (*Mus musculus*, CD-1 IGS) were obtained from Charles River Laboratories (Wilmington, MA). Isl2-GFP mice were cryogenically revived by the UC Davis Mutant Mouse Resource and Research Center (MMRC) on the CD-1 IGS background. All the animals had *ad libitum* access to food and water and were kept at a constant temperature of 21°C on a 12h light/ 12h dark cycle. All mouse husbandry and handling were performed in accordance with protocols approved by the University of California Davis Animal Care and Use Committee (IACUC protocol #22032), which strictly adheres to all NIH guidelines and satisfies the Association for Research in Vision and Ophthalmology guidelines for animal use.

Generating Isl2-GFP iPSCs

E13.5 Isl2-GFP transgenic embryos were collected from pregnant Isl2-GFP females. Embryos were confirmed transgenic through phenotypic screening. Isl2-GFP+ embryos were then decapitated, organs were removed, and the remaining tissue was passed through successive 20-gauge and 30-gauge needles in MEF medium into individual conical tubes (see “List of tissue culture media and components” section). After dissociation, embryos were centrifuged at 1000rpm for 2 minutes, resuspended in 5mL MEF media, then plated into six-well plates (one embryo/well).

After two passages, MEFs were transduced with lentiviral particles expressing Oct4-IRES-Sox2 and lentiviral particles expressing Nanog-IRES-Lin28 (generated by the UC Davis Viral Packaging Core Facility at >10^6 TU/ml, Addgene plasmids #21161 and #21163). 2 □g/ml of Polybrene solution was added to improve transduction efficiency. Two days after viral transduction, individual six-well cultures of MEFs were transferred to 10cm dishes at a dilution ratio of 1:1, and media was changed every 2-3 days. After 14-21 days of culture, iPSC colonies

were evident based on morphology. Individual colonies were then picked with a P20 pipet, expanded in feeder free conditions, and analyzed for embryonic stem cell markers and their ability to differentiate into retinal organoids.

Mouse iPSC culture

Undifferentiated cells were maintained in iPSC maintenance media (see "List of tissue culture media and components" section) on growth factor reduced Matrigel coated plates (Trevigen cat. #3432-001-01) in normoxic conditions (5% CO_2/ 20% O_2, 37°C). Only low-passage (< passage 30) cultures were used for these experiments.

Retinal differentiation of iPSCs

iPSCs were differentiated into retinal organoids as previously described by La Torre et al.. Briefly, undifferentiated cells were dissociated into single cells then plated into 96-well ultra-low attachment plates in retinal differentiation (RD) media (5,000 cells/well, Day 0). Cell aggregates, or embryoid bodies, (EBs) formed in less than 10 hours. 24 hours after plating, 2% growth factor-reduced Matrigel (Trevigen) was added to each well. On day 4, the EBs were transferred to 6-well low-attachment plates in RD media. From day 4 to day 7, the RD media was substituted by neural differentiation (ND) media in a stepwise fashion (1:1 RD:ND, 1:3 RD:ND, 100% ND). From here on, media was changed every other day for 7 days.

List of tissue culture media and components

Mouse Embryonic Fibroblast (MEF) media: DMEM (Corning, cat. #10-017-CV) supplemented with 10% Fetal Bovine Serum (FBS, Gibco cat. #16141-079) and 1% Pennicillin-Streptomycin (Penn-Strep) solution (Gibco cat. #15140-122).

iPSC maintenance media: DMEM (Corning, cat. #10-017-CV) supplemented with 20% FBS (Gibco cat. #16141-079), 1% Non-Essential Amino Acids (NEAA, Gibco cat. #11140-050),

1% Sodium pyruvate (NaPyr, Gibco cat. #11360-070), 100μM β-Mercapto Ethanol (BME, Sigma #M3148-250ML), 1x Leukemia Inhibitory Factor (LIF, Millipore cat. #ESG1106), 3μM Chir99021 (GSK3β inhibitor, Stemgent cat. #04-0004-02), 0.4μM PD0325901 (MAPK/ERK pathway inhibitor, Stemgent cat. #04-0006), and 1% Penn-Strep (Gibco cat. #15140-122).

Retinal differentiation (RD) media: GMEM (Gibco, cat. #11710-035), supplemented with 1.5% Knockout Serum Replacement (KSR, Gibco cat. #10828-010), 1% NEAA (Gibco cat. #11140-050), 1% NyPyr (Gibco cat. #11360-070), 100μM BME (Sigma #M3148-250ML), and 1% Penn-Strep (Gibco cat. #15140-122).

Neural differentiation (NM) media: Neurobasal (Gibco cat. #21103-049) supplemented with 1x N2 (Gemini Biosciences 400-163), 1x B27 (Gibco 17504-044), 1% NEAA (Gibco cat. #11140-050), 1% NyPyr (Gibco cat. #11360-070), 1% Bovine Serum Albumin (BSA, Sigma cat. #A1595-50ML), 1M HEPES (Sigma cat. #H0887), 0.075% Sodium Bicarbonate (Gibco cat. #25080094) and Penn-Strep (Gibco cat. #15140-122).

Tissue processing

Undifferentiated Isl2-GFP iPSCs, day 15, or day 30 organoids were fixed in 4% PFA for one hour and washed with PBS (pH 7.0). Organoids intended for cryosectioning were then embedded in successive sucrose solutions of 10%, 20%, and 30% with a final embedding step in 30% sucrose:OCT. Organoids were embedded in OCT for cryosectioning.

Immunohistochemistry

Whole-mount organoids were permeabilized in PBS supplemented with 1% Triton X-100; organoid cryosections were permabilized in 0.3% Triton X-100 in PBS. After blocking non-specific antigens with blocking buffer (10% Normal Donkey Serum and 0.1% Triton X-100 in PBS), the tissue was incubated with primary antibodies at a dilution indicated in Table 3 at 4ºC overnight. The next day, the tissue was extensively washed with PBS and incubated with Alexa Fluor

secondary antibodies as indicated in Table 3. Subsequently, the tissue was washed with PBS, the cell nuclei were labeled with 4',6-diamidino-2-phenyindole (DAPI) at a dilution of 1:10,000, and the slides, retinas, or organoids were then mounted with Fluoromount-G (Southern Biotech, Birmingham, AL).

qPCR

Total RNA was extracted from the whole organoids using Trizol (Invitrogen) and chloroform extraction, according to the manufacturer's instructions. The RNA was digested with DNase1 (Qiagen, Hilden, Germany), cleaned using the Qiagen RNA mini clean-up kit and reverse transcribed into cDNA using the iScript reverse transcription kit (BioRad) for mRNA qPCR following the manufacturer's instructions. qPCR was performed using the primers indicated in Table 1.

Statistics

All qPCR data were first analyzed using Rstudio with a two-way ANOVA to determine if significant variation was present in gene expression among different groups of samples (i.e. differentiation days). T-tests were then used to determine significance between specific differentiation days and undifferentiated stem cells. P values generated from ANOVA and T-test analysis are available in supplementary tables.

Figures

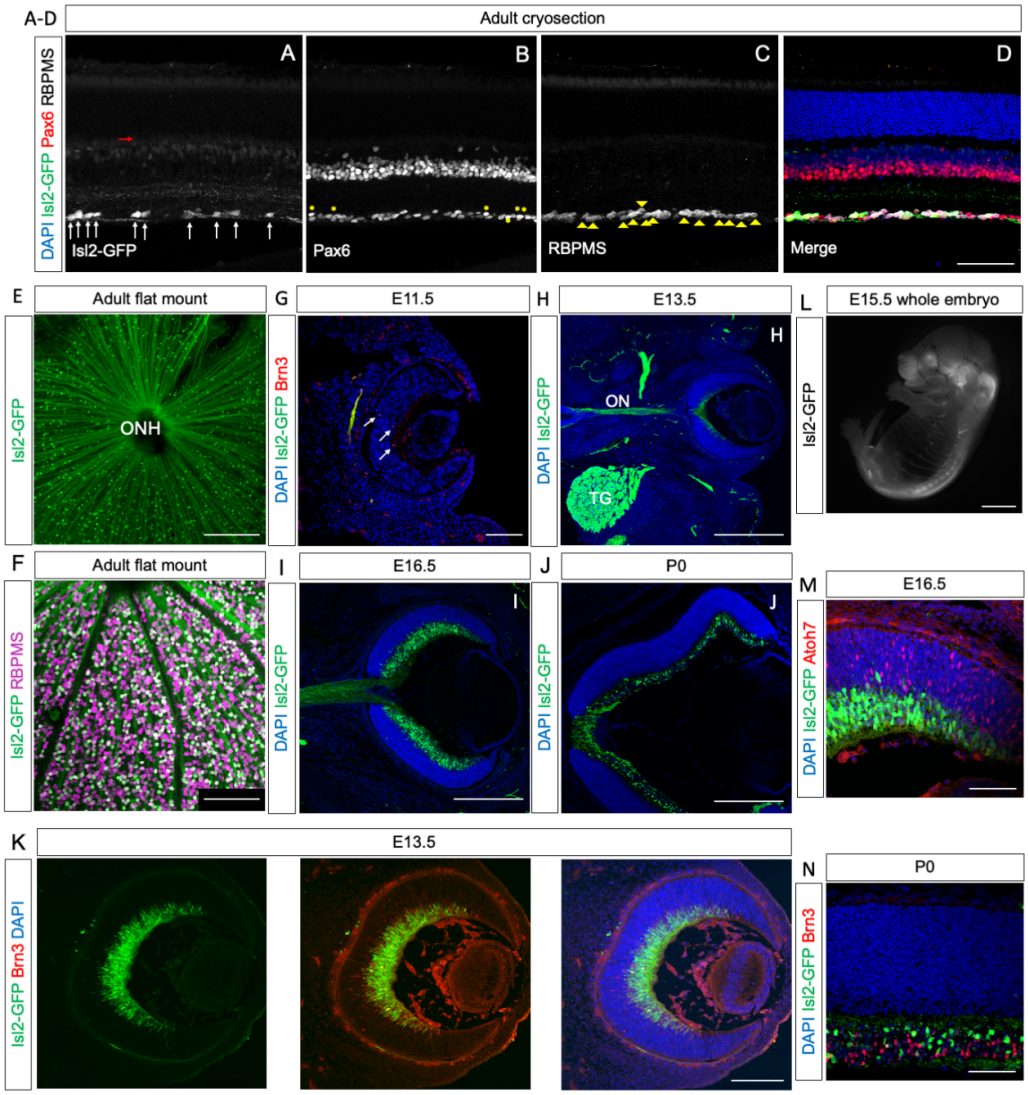

Figure 2.1: Isl2-GFP expression in the developing and adult retina. A-D) Cross section of adult Isl2-GFP retina showing A) GFP, B) Pax6, C) RBPMS, and D) A-C immunolabels merged with DAPI. White arrows: Isl2-GFP+ RGCs. Red arrow: Faint Isl2-GFP+ ON-bipolar cells. Yellow asterisks: Pax6+, Isl2-GFP- amacrine cells in GCL. Yellow arrowheads: RBPMS+, Isl2-GFP- RGCs in GCL. E) Adult Isl2-GFP flat mount showing only GFP expression. F) Adult Isl2-GFP flat mount showing GFP and RBPMS expression. G) E11.5 Isl2-GFP eye horizontal section. No Isl2-GFP+ RGCs are present yet, however sparce pan-Brn3 labeling is present (white arrows). H-J) Isl2-GFP expression in developing retina at H) E13.5, I) E16.5, and J) P0.

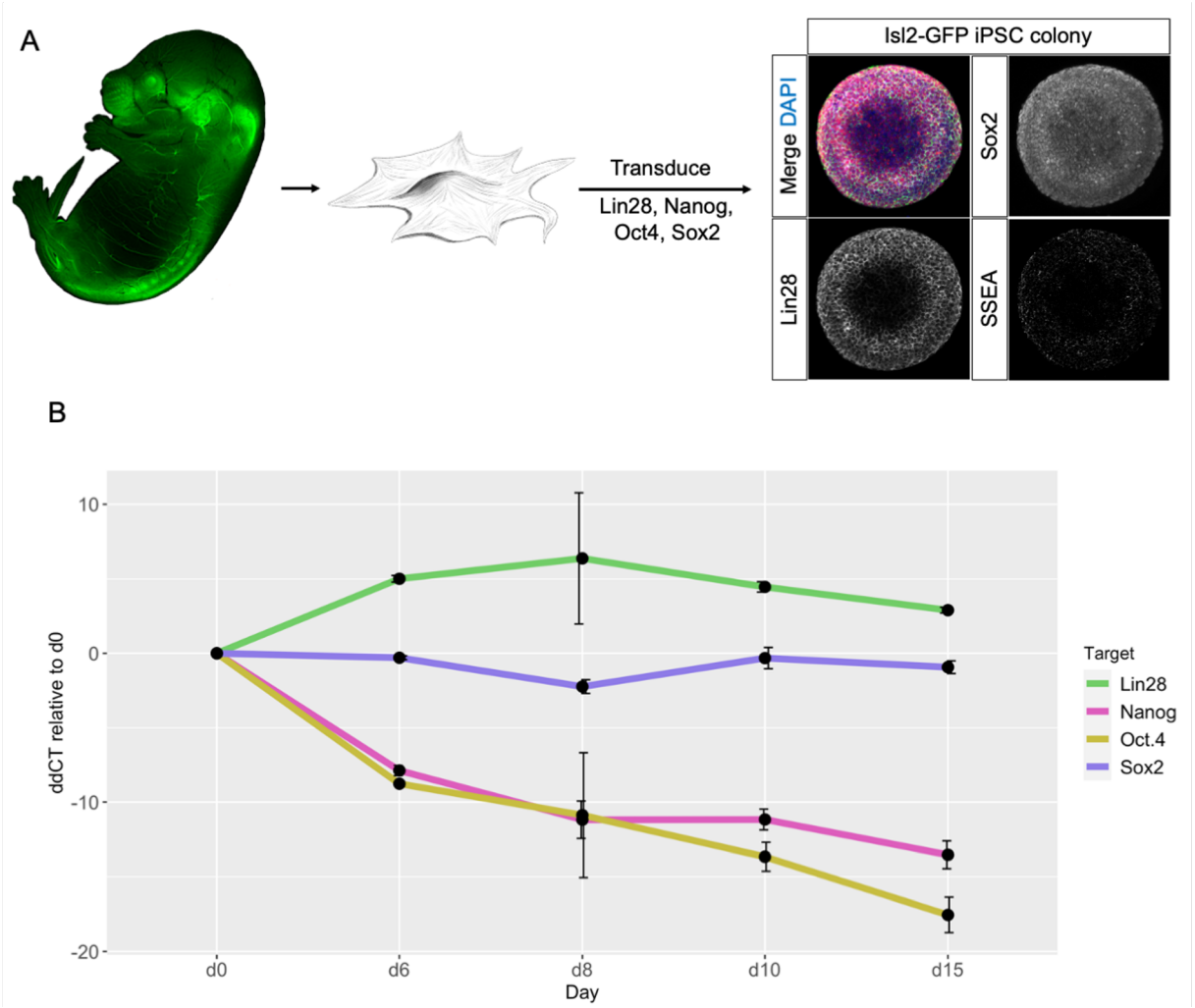

Figure 2.2 Isl2-GFP iPSC production and gene expression. A) E13.5 Isl2-GFP embryos were dissociated into MEF cultures, transduced with lentiviruses expressing reprogramming factors, and the resulting iPSCs express characteristic mouse embryonic stem cell genes. B) qPCR data showing that reprogramming genes are downregulated as Isl2-GFP iPSCs are differentiated into retinal organoids. Error bars: standard deviation. ANOVA significance and T-test P-values for each gene on each differentiation day relative to undifferentiated Isl2-GFP iPSCs are listed in supplementary tables 2.1 and 2.2.

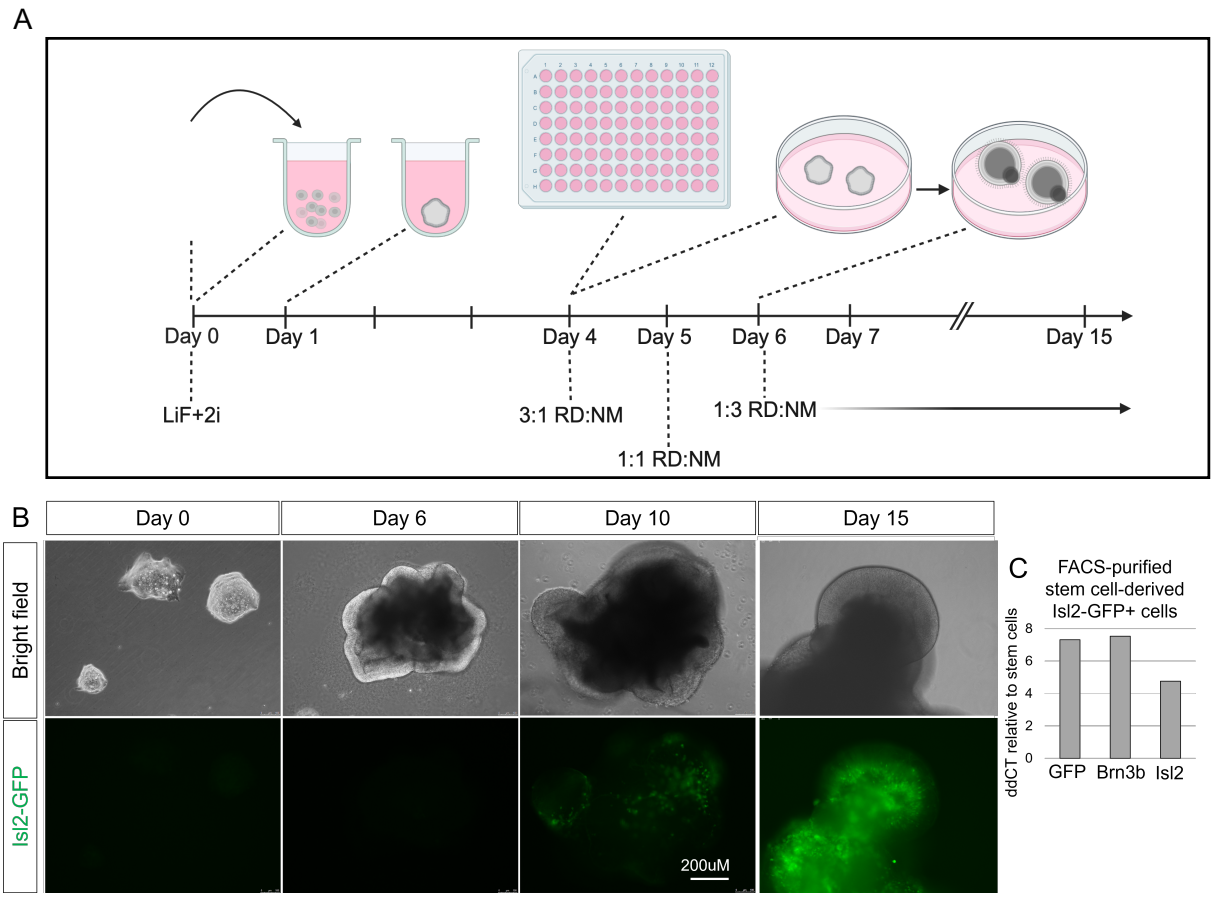

Figure 2.3: Isl2-GFP organoid differentiation and gene expression. A) Isl2-GFP organoid differentiation protocol diagram. Undifferentiated iPSCs are dissociated, plated at 5000 cells/well in a 96-well ultra-low-attachment plate, and Matrigel is added to a final concentration of 2% on day 1. Organoids are moved to low-attachment 6-well plates on day 4 and transitioned to neural maturation medium in a stepwise fashion from day 4 to day 6. B) Bright field and GFP fluorescence imaging of live Isl2-GFP organoids at indicated differentiation days. C) qPCR of FACS purified iPSC-derived Isl2-GFP+ cells showing GFP, Brn3b, and Isl2 expression relative to undifferentiated iPSCs.

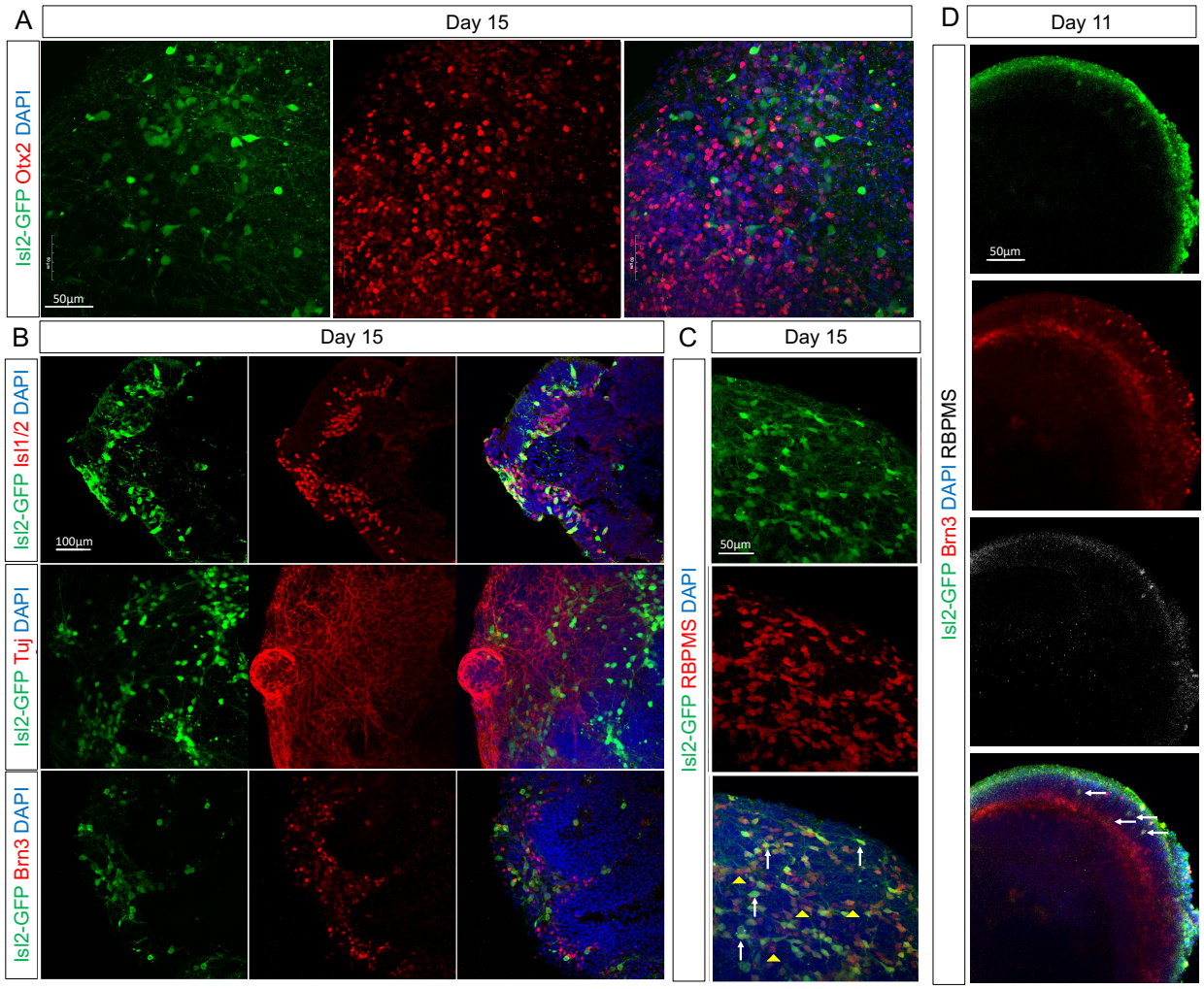

Figure 2.4: A-D) Immunofluorescene imaging of cryosectioned (A, B) or whole mount (C) day 15 and (D) day 11 Isl2-GFP organoids. A) Isl2-GFP organoid immunostained against GFP and Otx2. B) Isl2-GFP organoids immunostained against GFP (green, all rows), Isl1/2 (red, top row), Tuj1 (red, middle row), or Brn3 (red, bottom row). C) Isl2-GFP whole mount organoid immunostained against GFP (green), and RBPMS (red). D) Isl2-GFP organoid also immunostained against GFP (green), Brn3 (red), and RBPMS (gray) demonstrating lamination within optic cup-like structure. White arrows point to co-localization of GFP and Brn3 or GFP and RBPMS. Scales: B=200μm, A-D=50μm.

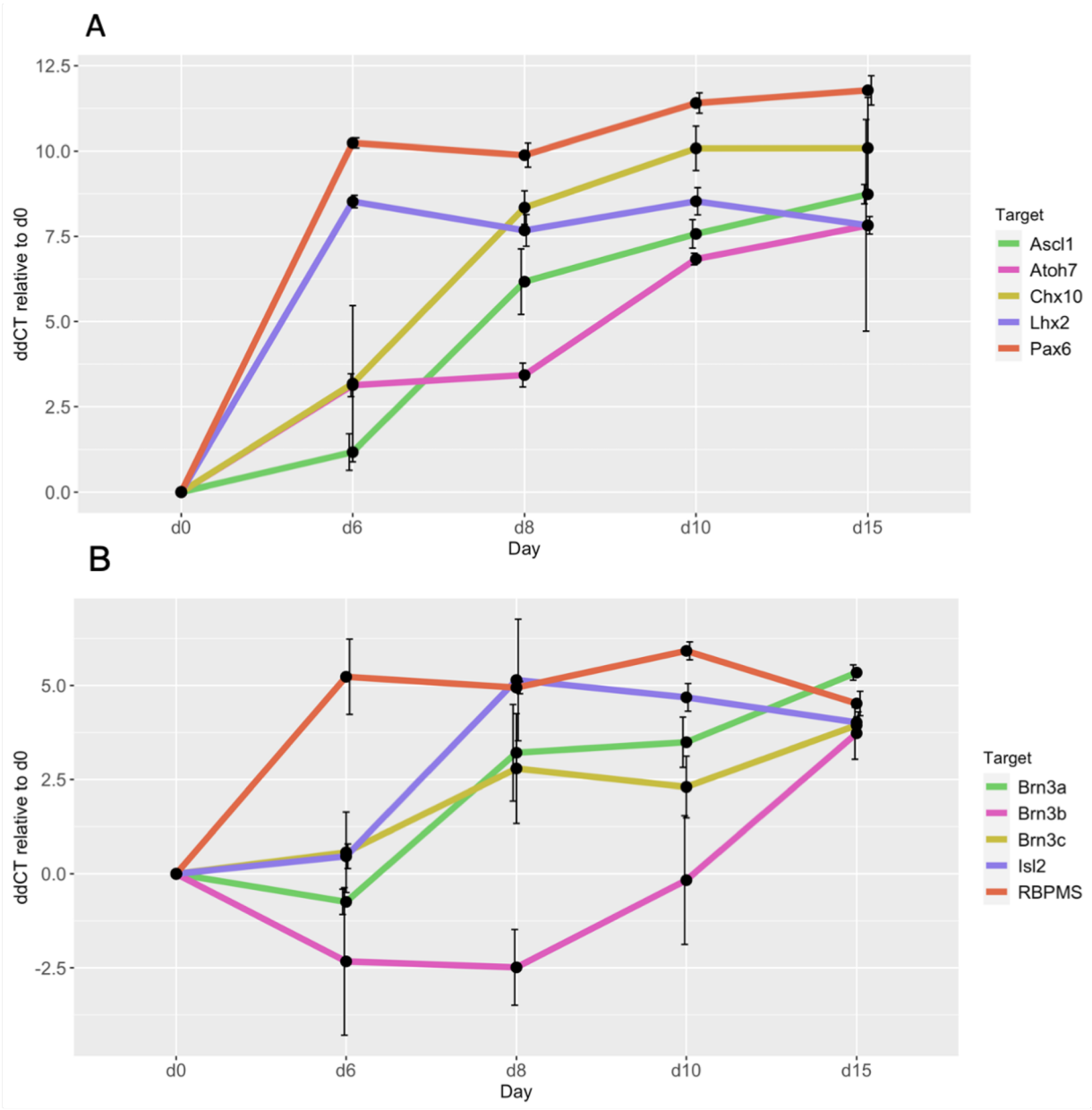

Figure 2.5: Isl2-GFP organoids express RPC and RGC genes by qPCR. A) Genes expressed in RPCs during retinal development are expressed in Isl2-GFP organoids. B) Genes expressed in RGCs during and after retinal development are expressed in Isl2-GFP organoids. Error bars: standard deviation.

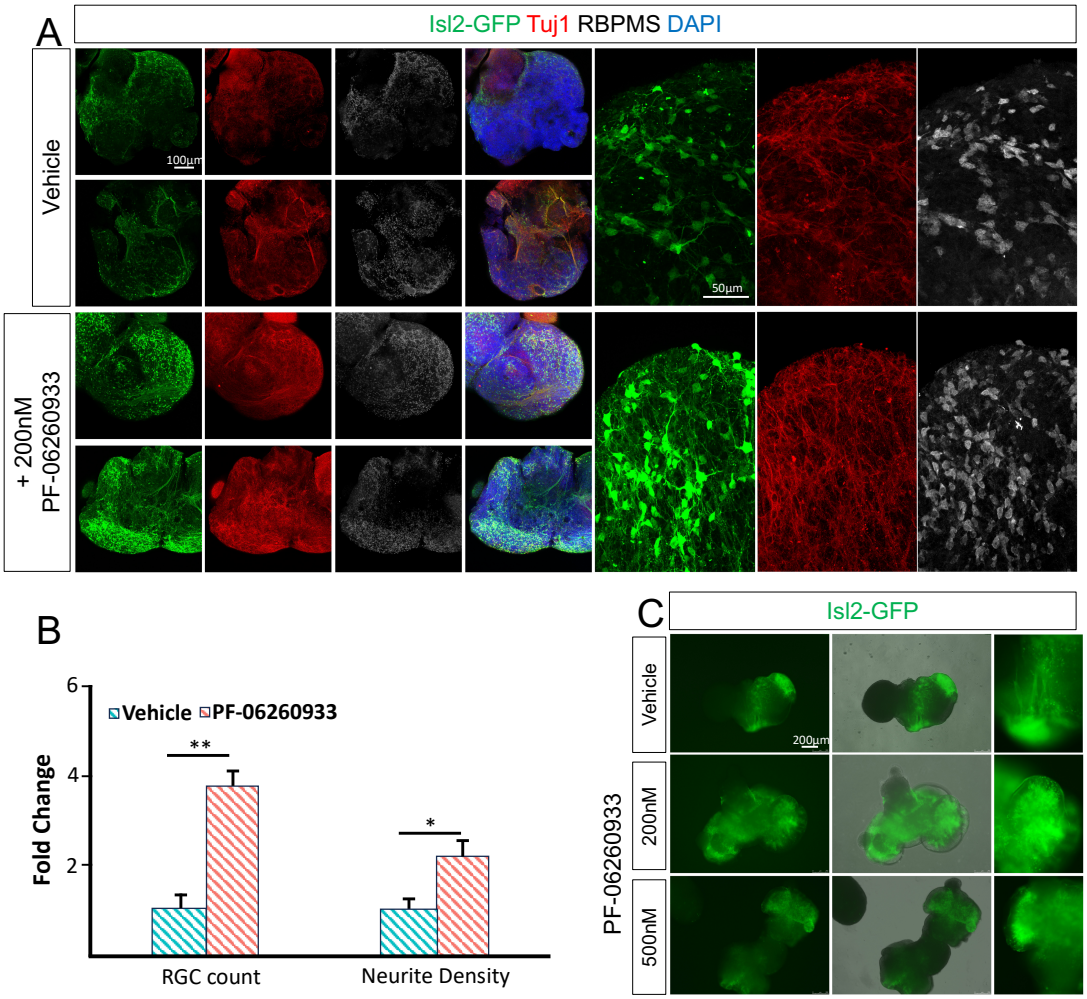

Figure 2.6: GCK-IV kinase inhibition increases RGC survival and promotes neurite outgrowth in mouse retinal organoids. miPSCs were differentiated into retinal organoids for 30 days in either vehicle (DMSO) or PF-06260933 (PF, 200 µM). Retinal organoids were fixed and immunolabeled for GFP and RBPMS to identify RGCs and Tuj1 to label neurites. A) Representative sections through organoids showing increased RGC survival and neurite elaboration. (Scale bar: 100 µm.) B) Quantification of RBPMS-positive cells for RGC counts and intensity using automated image analysis (n = 6–7 per group, *P < 0.05, **P < 0.01, Student's t test, error bars: SD) C) Live imaging of organoids cultured in 200nM or 500nM PF-06260933 for 7 days. Toxicity was observed in organoids cultured in concentrations greater than 200nM.

Table 2.1: qPCR primers

Oct4 FW	AGAGGATCACCTTGGGGTACA
Oct4 RV	CGAAGCGACAGATGGTGGTC
Sox2 FW	GCGGAGTGGAAACTTTTGTCC
Sox2 RV	CGGGAAGCGTGTACTTATCCTT
Nanog FW	TCTTCCTGGTCCCCACAGTTT
Nanog RV	GCAAGAATAGTTCTCGGGATGAA
Lin28 FW	TAGGTGGAGACGGCAGGATTT
Lin28 RV	ACCACAGTTGTAGCATCTTGGA
GFP FW	CCACATGAAGCAGCAGGACTT
GFP RV	GGTGCGCTCCTGGACGTA
Brn3a FW	CGCGCAGCGTGAGAAAATG
Brn3a RV	CGGGGTTGTACGGCAAAAT
Brn3b FW	TGGACATCGTCTCCCAGAGTA
Brn3b RV	GTGTTCATGGTGTGGTAAGTGG
Brn3c FW	CGACGCCACCTACCATACC
Brn3c RV	CCCTGATGTACCGCGTGAT
Isl2 FW	TGGGTGCTATGGGGGATCATT
Isl2 RV	GGCGACACGCGAAGGATAA
RBPMS FW	GTACCCAGCGGAGTTAGCG
RBPMS RV	AAGACAGGTGTGTTGGGCTTT
Chx10 FW	CTGAGCAAGCCCAAATCCGA
Chx10 RV	CGCAGCTAACAAATGCCCAG
Lhx2 FW	CTGTTCCAGAGTCTGTCGGG
Lhx2 RV	CAGCAGGTAGTAGCGGTCAG
Pax6 FW	CTGGAGAAAGAGTTTGAGAGG
Pax6 RV	TGATAGGAATGTGACTAGGAG

Ascl1 FW	GCAACCGGGTCAAGTTGGT
Ascl1 RV	GTCGTTGGAGTAGTTGGGGG

Table 2.2: Antibodies used in this study

Antibody	Specificity	Catalogue	Dilution	Source
Atoh7	RPCs	88639	1:200	Novus Biologicals
Pan-Brn3	RGCs	sc-6026	1:200	Santa Cruz
β-III-tubulin	RGCs	801201	1:1000	Biolegend
GFP		Ab13970	1:500	Abcam
Lin28	Pluripotent Stem cells/ early RPCs	Ab46020	1:200	Abcam
Otx2	RPCs, photoreceptors, bipolar cells	AF1979	1:250	R&D Systems
Isl1/2	RGCs, AC	39.4D5	1:200	Developmental Studies Hybridoma Bank
Pax6	RPCs, RGCs	901301	1:200	Biolegend
RBPMS	RGCs	1832-RBPMS	1:500	Phosphosolutions
Sox2	RPCs/ Müller glia	sc-17320	1:500	Santa Cruz
SSEA	Pluripotent stem cells	MAB2155	1:500	Biotechne
Alexa 488 anti-goat	Goat IgG	A11055	1:500	Thermo Fisher
Alexa 568 anti-mouse	Mouse IgG	A10037	1:500	Thermo Fisher
Alexa 488 anti-rabbit	Rabbit IgG	A21206	1:500	Thermo Fisher
Alexa 647 anti-Guinea Pig	Guinea Pig IgG	A21450	1:500	Thermo Fisher

Supplementary tables:

Supplementary table 2.1: Two-way ANOVA P-values for differentiation days 0, 6, 8, 10, and 15 for genes shown.

Gene target	P-value	Gene target	P-value	Gene target	P-value	Gene target	P-value
Nanog	0.000436	let-7a	9.93E-06	Pax6	5.09E-09	Brn3a	0.000133
Oct4	0.000124	miR-9	3.09E-05	Chx10	8.44E-06	Brn3b	0.00243
Sox2	0.148068	miR-125b	6.08E-08	Lhx2	3.52E-07	Brn3c	0.247883
Lin28	0.0265	let-7d	3.17E-05	Ascl1	1.01E-07	Isl2	0.000333
		Prtgn	2.42E-08	Atoh7	0.000416	RBPMS	6.98E-07

Supplementary table 2.2: T-test P-values for undifferentiated stem cell markers. All gene targets on specified differentiation days were compared to undifferentiated iPSCs.

Differentiation day	Nanog	Oct4	Sox2	Lin28
Day 6	0.119847628847695	0.0582476780750203	0.833736422032333	0.00742295960189496
Day 8	0.05852458322548	0.0298832577713998	0.210099037335408	0.1236742822165
Day 10	0.0633311622248932	0.0201505538598553	0.826154728026154	0.0065000478636633
Day 15	0.0424137680542634	0.0102693869060343	0.534134109586989	0.0255056851777118

Supplementary table 2.3: T-test P-values for RPC genes. All gene targets on specified differentiation days were compared to undifferentiated iPSCs.

Differentiation day	Pax6	Chx10	Lhx2	Ascl1	Atoh7
Day 6	0.00536417655322965	0.123849046125676	0.0106319551083925	0.195575314325394	0.0115599256890666
Day 8	0.00407858464239746	0.00100349420998517	0.00944572048369473	0.00192428113556873	0.00873007559178304
Day 10	0.00336516742311582	0.000279930285599572	0.00823972695775771	0.00293679255372633	0.00332561376792629
Day 15	0.00223387912131137	0.00118498989474588	0.0118527329637193	0.00325764274817304	0.0413910180306827

Supplementary table 2.4: T-test P-values for RGC genes. All gene targets on specified differentiation days were compared to undifferentiated iPSCs.

Differentiation day	Brn3a	Brn3b	Brn3c	Isl2	RBPMS
Day 6	0.540656452848462	0.18380082376212	0.323672723267375	0.693940084614168	0.00423932590137531
Day 8	0.0681917283045213	0.0867989010611863	0.929591398909891	0.0205587122037395	0.00156301860753981
Day 10	0.0602899985415529	0.904783301003379	0.751635536378217	0.0390659092461192	0.000446548366868122
Day 15	0.0326186450894921	0.0344674907948793	0.660925949275626	0.0550740484594082	0.000471860591748883

Chapter 3

MAP4k4 inhibition and RGC survival after intravitreal injection

Introduction

Glaucoma affects more than 60 million people worldwide, which has greatly increased the level of academic interest in its pathology and treatment[47,177,262]. It has been estimated that there is a 4% loss of retinal ganglion cells per year in patients diagnosed with glaucoma, and that at 25-35% loss of RGCs there is a significant visual impairment with approximately 10% of patients losing full vision[49,303–305]. However, existing treatments are only capable of lowering the increased intraocular pressure (IOP) associated with only a subpopulation of glaucoma patients and, consequentially, current treatment options are not effective for the entire patient population[48,51]. Therefore, development of alternative treatment methods is of great interest.

One promising approach is to replace the dying RGC population with healthy cells from an exogenous source. Significant work has been done to demonstrate our capability of transplanting retinal neurons in rodent models, particularly in the field of photoreceptor (PR) transplantation. Many studies have reported exogenous PR engraftment after injection into the subretinal space, with donor cells found in the outer nuclear layer (ONL) and remaining in the

host tissue for at least 90 days[77,79–81,306,307]. Although there is new evidence that the transfer of cellular material, such as fluorescent proteins, may be confounding these results, there is consistent evidence that 1. PR transplantation is a reliable technique that has been replicated by several and 2. PRs can survive and function after transplantation into the subretinal space[81,308–311]. While these achievements in transplantation push the field of retinal neuron cell replacement therapy forward, there remain several limitations of the current RGC transplantation methodology. Namely, most studies show that only 10% of transplantation attempts result in any RGCs surviving in the retina[193,194], with one exception demonstrating 50% success[192], and at most 3% of the transplanted cell population survive after the first 24hoursdfdf. Additionally, these studies saw only 10% of the successful transplantations (ie cells surviving in the eye) achieving donor cell engraftment into the host tissue[192–194]. While it is unclear why RGCs have such a high attrition rate post-transplantation, especially compared to PR transplantation, neuroprotective measures may serve as a potential solution.

Many neuroprotective factors that increase the survival of RGCs in vitro and in vivo have been identified within the last 20 years. Initial studies found that addition of neurotrophic factors that are produced by glia during development into adulthood could increase RGC survival in culture and various models of retinal injury. This includes nerve growth factor, brain-derived neurotrophic factor, and insulin-like growth factor 1[312]. Concurrently, an alternative approach was taken to understand how the RGC injury response signaling cascade could be manipulated to increase survival of RGCs[180,187,282,313]. In 2013, Watkins and colleagues demonstrated that knockout of dual leucine kinase (DLK-/-) improves RGC survival at a much higher rate[181]. As previously mentioned, DLK is a key mediator of axon injury response by activating the retrograde transport of stress signals[70,181–184,278]. However, DLK-/- prohibits axon regeneration, an unfortunate side effect of an otherwise attractive neuroprotective strategy[181]. Fortunately, we have shown that the inhibition of GCK-IV kinase family replicates the DLK-/- neuroprotective phenotype and synergizes with axon regenerative strategies[186]. Here, we use a MAP4K4 small molecule

inhibitor (PF-06260933, PF) to improve the survival of RGCs after intravitreal transplantation using two reporter RGC mouse lines, the Isl2-GFP mouse and the Brn3b-mCherry mouse.

Results

MAP4K4 inhibition may impact the survival of donor cells 48hours post-transplantation

To determine the effect of MAP4K4 inhibition on the survival of intravitreally transplanted RGCs, we compared reporter RGCs (50,000 cells/eye) intravitreally injected in a suspension of either 3uM PF to those suspended in only the vehicle (PBS) control. The donor RGCs were isolated from either postnatal day 0 (P0) – P3 Isl2-GFP or Brn3b-mCherry mice (donor fluorescence) and delivered into the eyes of adult mice with RGCs labelled with the other fluorescent protein (host fluorescence). The surface of the mouse retina was imaged with a custom scanning laser ophthalmoscopy (SLO) system after 48 hours to locate donor cells relative to the host animal retina. Previous studies found that less than 10% of transplants resulted in any cells surviving in the host eye[192–194]. Here we observed 5/18 and 10/18 injections with donor fluorescence visible in the SLO field of view (FOV) after resuspension in PBS or PF, respectively (fig. 1A). We observed a trend favoring the amount of fluorescence found in PF injections compared to the control (fig. 1B, n=18, p=0.0869). Additionally, there was no significant difference in the number of injections with detectable fluorescence between the two treatment groups (n=17, p=0.190).

Concurrently with SLO, we used optical coherent tomography (OCT) to examine a cross sectional view of the mouse retina[140]. We consistently observed hyperreflective vitreous opacities in all injected eyes directly above the retinal neural fiber layer (RNFL), that we hypothesize are a mix of injected RGCs and infiltrating inflammatory cells (fig. 1C)[314,315]. Quantification of these

opacities showed a significant increase within the vitreous of eyes injected with cells resuspended in PF compared to the vehicle controls (fig. 1D, n=14, p=0.0138). The contradiction of the OCT results with the SLO imaging may be due to the location of the injected cells within the eye. Our SLO system has a restricted FOV that does not allow us to image the entire retinal surface, including the retinal periphery where we observed large masses of these vitreous opacities via OCT (fig. 1C). Therefore, the injected cells were most likely delivered to an area outside of this specific view in most of the transplantation experiments. Together, these results suggest that MAP4K4 inhibition may affect the survival of donor cells immediately following transplantation, a time frame that seemingly accounts for most of the donor cell death[193,194].

MAP4K4 inhibition does not increase the long-term survival of transplanted RGCs post-injection

RGCs have been shown to survive for at least a year after intravitreal transplantation, albeit with an attrition rate of ~30% within the first week[193]. If RGC replacement therapy is to be a viable solution for RGC degenerative diseases, it is important to have enough cells that survive long enough to integrate into the host tissue and impact vision. Therefore, to determine how inhibition of MAP4K4 affects the survival of donor RGCs over time, we imaged mice with transplanted cells suspended with or without PF for up to 30 days. Using SLO, we imaged the same retinal area at 48 hours and 7 days post-transplantation and quantified the donor fluorescence (fig. 2A and C). We did not see any significant differences in the change of fluorescence from 48 hours and 7 days post-transplantation between the two groups (n=4 PF and 5 vehicle, p=0.505). This suggests that rate of donor cell death is not affected by MAP4K4 inhibition. Similarly, using OCT imaging, we did not see any significant differences in the percentage of vitreous particles lost over time (fig. 2B and D, n=9 PF and 6 vehicle, p=0.885).

However, we did observe hyperreflective particles remaining up to 30 days within the areas that maintained donor fluorescence (fig. 2C).

To further compare the transplant outcomes across the two treatments, we performed histological analysis on either whole mounted retina or cryosections generated from whole eyes. At 2 weeks post transplantation, we found cells expressing the donor cell fluorescence on the outer surface of both control and PF flat mounted retina. While the cells expressing donor fluorescence in both treatments colocalized with the pan-RGC marker RNA-binding protein with multiple splicing (RBPMS), they did not extend neurites and had a shrunken morphology compared to the endogenous RGCs (fig. 3A). Histological analysis of the cryosections revealed that there were large boluses of cells expressing donor cell fluorescence within the vitreous, which has been shown in previous studies. Similarly, these cells had a shrunken morphology, deteriorating nuclei, and did not extend neurites, suggesting that these cells may be undergoing apoptosis (fig. 3B). Thus, there does not seem to be an effect of MAP4K4 inhibition on the long-term donor cell survival as apoptotic cells were observed at the same frequency in both conditions.

Intravitreal injections of RGCs can cause retinal inflammation

Throughout these experiments we also observed morphological changes within the retina post injection. Beginning as early as 2 days post-injection, discrete sections of the retina had a 15% increase within the ONL when compared to the same area before injection (n= 4 PF, p=0.000265, occurring in 4/15 of the PF suspended transplantations and 0/15 of the vehicle suspended transplantations (fig. 3A). We also observed large clusters of vitreous opacities surrounding the areas of retinal thickening that remained at least five days post-transplantation (fig. 3A). Interestingly, the ONL returned to roughly the same size after 1-month post-transplantation, although the retinal lamination remained disrupted compared to the rest of the retina. The morphological changes within the retina we observed mimics phenotypes within mouse models of retinal inflammation, which is often accompanied by infiltrating immune cells[315–

[317]. Therefore, we performed a series of histological experiments with activated immune cell markers Iba1 and CD11b to determine if and where there was any immune cell activation post-transplantation. We observed an increase in Iba1+ cells within the areas of thickening compared to the rest of the retina (fig. 3B). We also observed colocalization of CD11b and donor cell fluorescence found directly outside of the retina. The CD11b+ cells possessed an ameboid morphology and aggregated at the site of donor fluorescence (fig. 3C). These findings suggest that the ocular immune system plays a larger role in the survival of transplanted cells than initially thought.

Discussion

RGC transplantation is a promising technique to help restore vision to glaucoma patients. This technique should be seen as a last resort due to its invasive nature and potential for ocular damage via trauma or infection. Additionally, there are still several roadblocks in place before bringing this technique to the clinic. The first being sourcing cells for transplantation, mentioned previously, which can be remedied using advancing stem cell technology. For example, several labs have shown that RGCs can be produced *in vitro* through stem cell differentiation and then used as an unlimited source of donor cells[163,192,195]. The second roadblock is the survival of cells within the eye post transplantation. All published transplantation studies have resulted in, at most, a 3% survival rate of intravitreally transplanted RGCs within the first 24 hours post-transplantation[192–195,263]. Therefore, efforts to increase cell survival are of utmost importance. To that point, we investigated how the inhibition of the GCK-IV kinase MAP4K4 with a small molecule affects the survival of RGCs after intravitreal transplantation.

MAP4K4 may only affect the initial survival and have no effect on long-term survival

RGC transplantation applies many stressors to the donor cells throughout the entire process. This includes the initial dissociation of tissue, purification of the cell population, and finally the injection itself. Therefore, it is assumed that some amount of the RGC population will not be viable at the protocol's conclusion. However, it has been shown that in the days following the delivery of the cells into the host eye, there is a continued attrition of the donor RGCs due to currently unknown mechanisms[193,194]. In this study, we show that injecting donor cells with a MAP4K4 inhibitor may alleviate some of this initial cell death due to an increase in donor cell fluorescence for cells suspended with the inhibitor (fig. 1). Similarly, we observed an increase in hyperreflective opacities within the vitreous of inhibitor treated eyes using OCT imaging. Interestingly, this effect does not seem to last more than a couple days post-injection; post-mortem histological analysis showed that by 2 weeks post injection, most of the donor RGCs were either dead or dying (fig. 2E-F). The short window of increased survival may be due to the constant flow of intraocular fluid throughout the posterior and anterior chambers of the eye, leading to a diffusion and eventual removal of the inhibitor post-injection[318].

RGC transplantation activates the ocular immune system

In several of our transplantation attempts we observed a thickening of the retina that was attributed to the enlargement of the ONL and the inner and outer segments of the PRs (fig. 3A). The specificity of the ONL thickening distinguishes itself from other sources of gross morphological changes to the retina, like retinal detachments (RD). RDs occur when the neural retinal delaminates from the retinal pigmented epithelium typically caused by an ingress of fluid into the subretinal space due to physical trauma or retinal degenerative diseases[319]. In this case, RDs can occur accidentally during the intravitreal injection process if the instrument slips between the neural retina and the RPE. The resulting cavity can be mistaken for an increase in retinal

thickness in OCT B-scans if not properly imaged[320,321]. However, we observed retinal thickening more characteristic of retinal inflammation, specifically mirroring the phenotypes of mouse uveitis models (fig. 3A)[314–317,322,323]. An umbrella term for retinal inflammation, uveitis encompasses more than 30 inner eye inflammatory conditions, typically caused by viral infections or systemic diseases like sarcoidosis. Uveitides are the sixth leading cause of blindness worldwide and affect patients of all age groups[322]. Mouse models of spontaneous or induced uveitis are characterized by retinal folds, inflammatory cell infiltrations, vasculitis, and chorioretinal lesions, similar to what we observed in our post injection analysis[323]. Macrophage co-localization with donor cell fluorescence suggests that the donor cells are actively phagocytized upon entering the host eye (fig. 3C). Immunosuppressive measures are one way to counter the observed inflammation, but it is unclear if this method will be effective over the length of time needed for donor cells to engraft in the host tissue[197]. Thus, further studies into the specificities of how the ocular immune system is activated is necessary.

Materials and Methods

Animals

Adult mice (*Mus musculus*, CD-1 IGS) were obtained from Charles River Laboratories (Wilmington, MA). Isl2-GFP mice were cryogenically revived by the UC Davis Mutant Mouse Resource and Research Center (MMRC) on the CD-1 IGS background. The Brn3b-mCherry CRISPR knock-in mouse line was generated by Biocytogen (Worcester, MA, USA) in the C57BL/6N background. We have not performed whole-genome sequencing to screen for off-target effects, but we have not detected any abnormalities, viability, fertility or any developmental problems (9 different generations have been analyzed to date). All the animals had *ad libitum* access to food and water and were kept at a constant temperature of 21°C on a 12h light/ 12h dark cycle. All mouse husbandry and handling were performed in accordance with protocols

approved by the University of California Davis Animal Care and Use Committee (IACUC protocol #22905), which strictly adheres to all NIH guidelines and satisfies the Association for Research in Vision and Ophthalmology guidelines for animal use.

Immunopurification of RGCs

Retinal ganglion cells (RGCs) were purified from whole mouse retina as previously described by Winzeler and Wang[300]. Briefly, retinas were dissected from postnatal day 0 (P0)-P3 mice with lens and vitreous removed. Retinas were then dissociated with a 0.6mg/mL of papain dissolved in Dulbecco's phosphate buffered saline (DPBS) (LS003126, Worthington Biochemical; 14287080, Life Technologies) for 14 minutes at 37 °C. Digestion was stopped by addition of a 15mg/mL bovine serum albumin (BSA)/trypsin inhibitor solution (LS003587, Worthington Biochemicals) at pH 7.4 and retina were triturated by dropwise release of the retina suspension. Macrophages were depleted by incubating cell suspension for 15 minutes at room temperature (RT) with mouse anti-rat CD11b/c; [OX-42] (ab1211, Abcam) bound magnetic beads (11531D, Thermo Fisher). The cell suspension was then plated onto a mouse anti-Thy1.2 (MCA02R, Bio-Rad) coated 10cm plate and incubated for 45 minutes at RT. The panning plate was washed with PBS to remove non-RGCs. RGCs were detached from the plate by incubation with 0.05% trypsin/Earl's balanced salt solution and resuspended in injection media at a concentration of 50,000 cells/µL.

Intravitreal injection

Intravitreal injections into adult mice were performed under general anesthesia (1.5% isoflurane) with mice on a heating pad (37 °C). Prior to injection, proparacaine and tropicamide drops were applied to the eye for local anesthesia and pupil dilation, respectively. The corneal surface was wetted Gel Tears hypromellose gel (GenTeal Tears Severe, Alcon) to prevent cold cataract. A small incision was made in the conjunctiva slightly posterior to the ora serrata using

ophthalmic scissors. An insertion hole into the vitreous was made at this incision using a 31-gauge insulin syringe (BD Insulin syringe with ultra-fine needle). Next, 1µL of vitreous was removed using a 33-gauge syringe (Hamilton Company, Reno, NV) followed by an injection 1µL of RGC suspension (50,000 cells/µL) over the course of 30 seconds, pausing for 10 seconds before removal. Finally, a triple antibiotic was added to the eye.

In vivo imaging

A custom-built scanning laser ophthalmoscopy (SLO) system was used to image GFP+ and mCherry+ cells within the retina, simultaneously collecting the reflectance and fluorescence images[324]. For imaging, mice were anesthetized with 2–2.5% isoflurane and positioned on a heating pad (37 °C) with a custom built bite-bar (Bioptigen, Morrisville, NC) that allowed rotational and translational adjustment for positioning the mouse with respect to the contact lens. The pupils were dilated and anesthetized with tropicamide and phenylephrine, and the corneal surface wetted with Gel Tears hypromellose gel (GenTeal Tears Severe, Alcon). Gel Tears helped maintain a homogeneous refractive surface between the cornea and the custom 0 diopter contact lens (Unicon Corporation, Osaka, Japan). GFP and mCh excitation was achieved with OBIS LX 488 nm and 561 nm lasers, respectively (Coherent Inc., US). Images were collected over 51° of visual angle at 43 µm per degree. In Fiji, images were registered[325], averaged, and pseudo-colored.

Optical coherence tomography (OCT) imaging was performed with a superluminescent diode centered at 860nm with a 132nm bandwidth (Broadlighter T-860-HP, Superlum), approximately 600µW at the pupil. A custom Python script was used to flatten the B-scans and then register those flattened B-scans using a strip-registration algorithm to generate complete flattened OCT volumes.

Tissue processing

Whole eyes were fixed in 4% PFA for 30 minutes then washed with PBS (pH 7.0). Eyes intended for cryosectioning were then embedded in successive sucrose solutions of 10%, 20%, and 30% with a final embedding step in 30% sucrose:OCT. Eyes were sectioned with a cryostat as 12-14um thick sections. Retinas were dissected from eyes intended for whole mount and were flattened by making four radial cuts around the retina (flat mount). Flat mounts were fixed for another 30 minutes in 4% PFA then washed in PBS.

Immunohistochemistry

Flat mounted retinas were permeabilized in 1% Triton X-100 in PBS; retina cryosections were permabilized in 0.3% Triton X-100 in PBS. After blocking non-specific antigens with blocking buffer (10% Normal Donkey Serum and 0.1% Triton X-100 in PBS), the tissue was incubated with primary antibodies at a dilution indicated in Table 1 at 4ºC overnight. The next day, the tissue was extensively washed with PBS at RT and incubated with Alexa Fluor secondary antibodies for either 3 hours (whole) or 1 hour (sections) at RT, as indicated in Table 1. Subsequently, the tissue was washed with PBS, the cell nuclei were labeled with 4',6-diamidino-2-phenyindole (DAPI) at a dilution of 1:10,000, and the sections or whole retinas were then mounted with Fluoromount-G (Southern Biotech, Birmingham, AL). Tissue was imaged using an Olympus FV1000 confocal microscope.

Statistical analysis

In all figures, data are represented as mean ± standard error and significance levels are indicated as follows: *p < 0.05, **p < 0.01, ***p < 0.001. All statistical analyses were performed using R. Two group comparisons were performed using Student's T-tests.

Figures

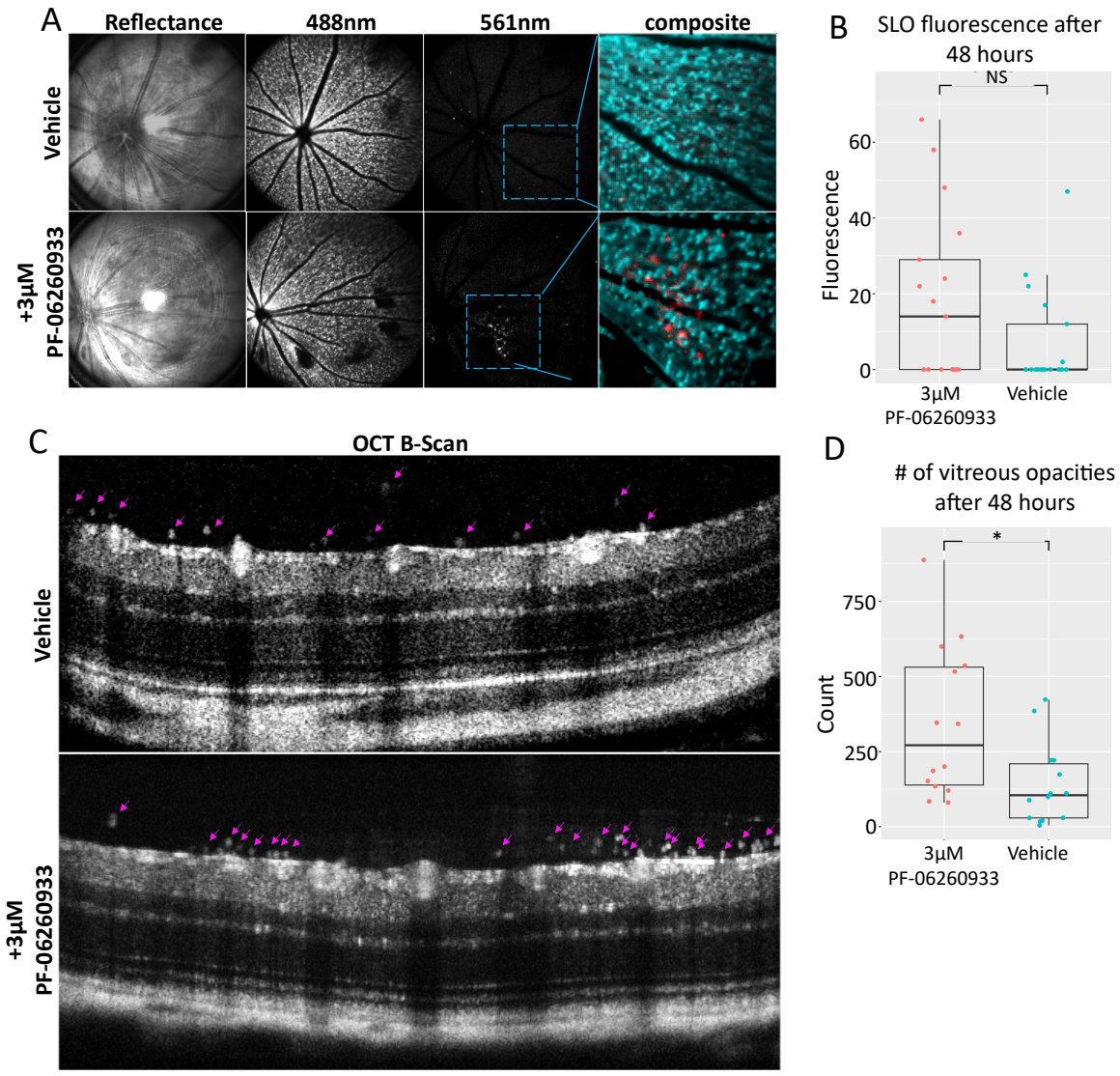

Figure 3.1: In vivo imaging after 48 hours post. Adult Isl2-GFP or Brn3b-mCherry mice were intravitreally injected with 50,000 RGCs immunopurified from P2 Brn3b-mCh or Isl2-GFP mouse retina in either vehicle (PBS) or PF-06260933 (3µM). A) SLO imaging shows clusters of donor cell fluorescence distinct from host fluorescence B) Quantification of SLO fluorescence for each treatment (n=18, p=0.0869). C) Registered OCT B-scans of eyes transplanted with RGCs. Magenta arrows indicate hyperreflective opacities in the vitreous D) Quantifications of vitreous opacities for each treatment (n=14, p=0.0138). Students t-test for all comparisons.

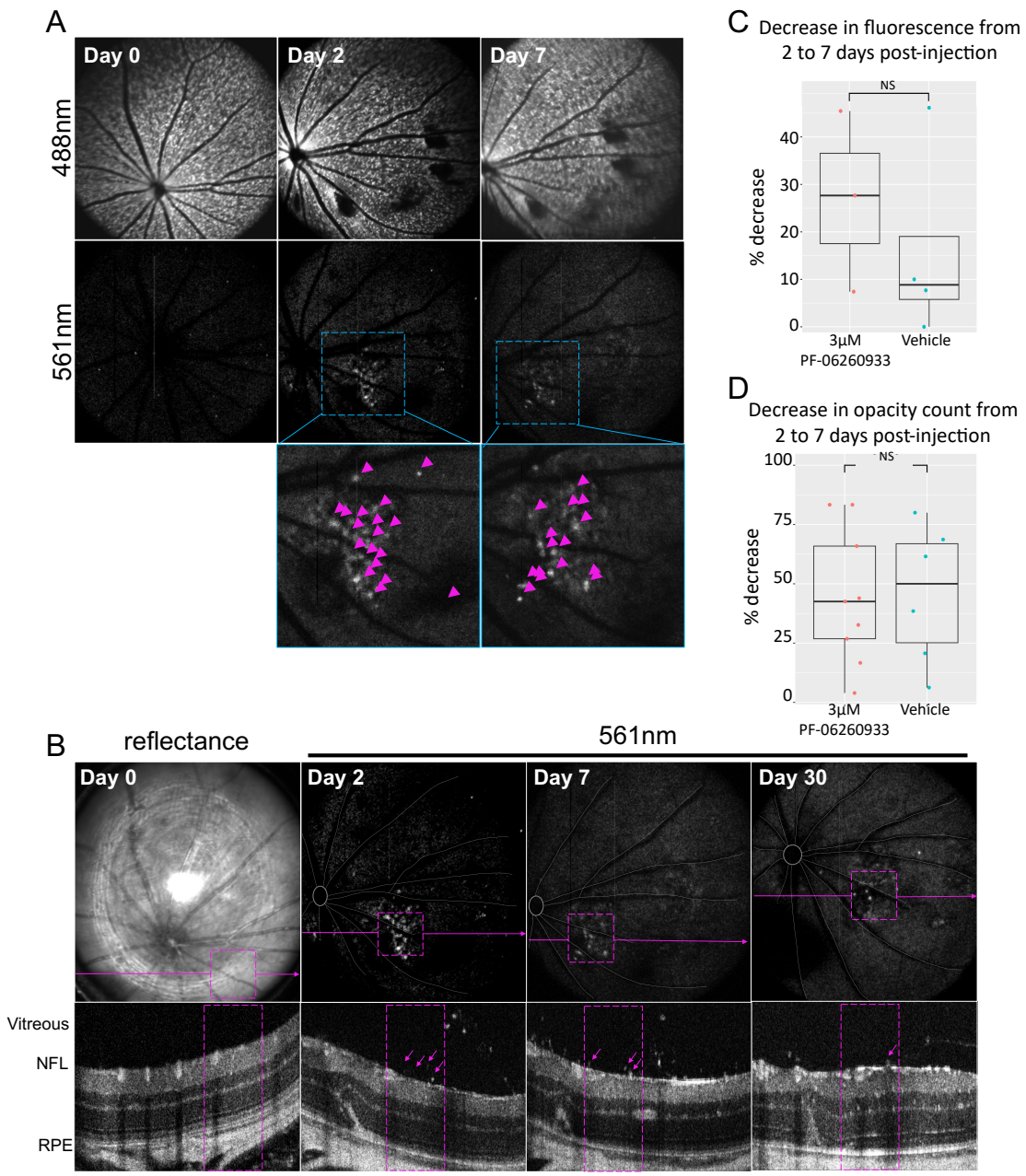

Figure 3.2: MAP4K4 inhibition does not increase long term cell survival. Adult Isl2-GFP mice were intravitreally injected with 50,000 RGCs immunopurified from P2 Brn3b-mCh mouse retina in either vehicle (PBS) or PF-06260933 (3µM). Mice were imaged 48hrs and up to 5 days post-injection with SLO. A) SLO images of a single eye over time. Magenta arrows indicate donor cell fluorescence. B) SLO and OCT imaging of the same retinal area over time. Purple arrows on the A-scan (fundus) indicate the position that the OCT B-scan was imaged. Purple boxes mark the

same area on both fundus and cross-sectional views. C-D) Comparison of the change in fluorescence and vitreous particles over time between cells transplanted in PF or vehicle (n=3 PF, 4 vehicle, p=0.505; n=6-9, p=0.918, Student's T-test). NFL: nerve fiber layer, RPE: retinal pigment epithelium.

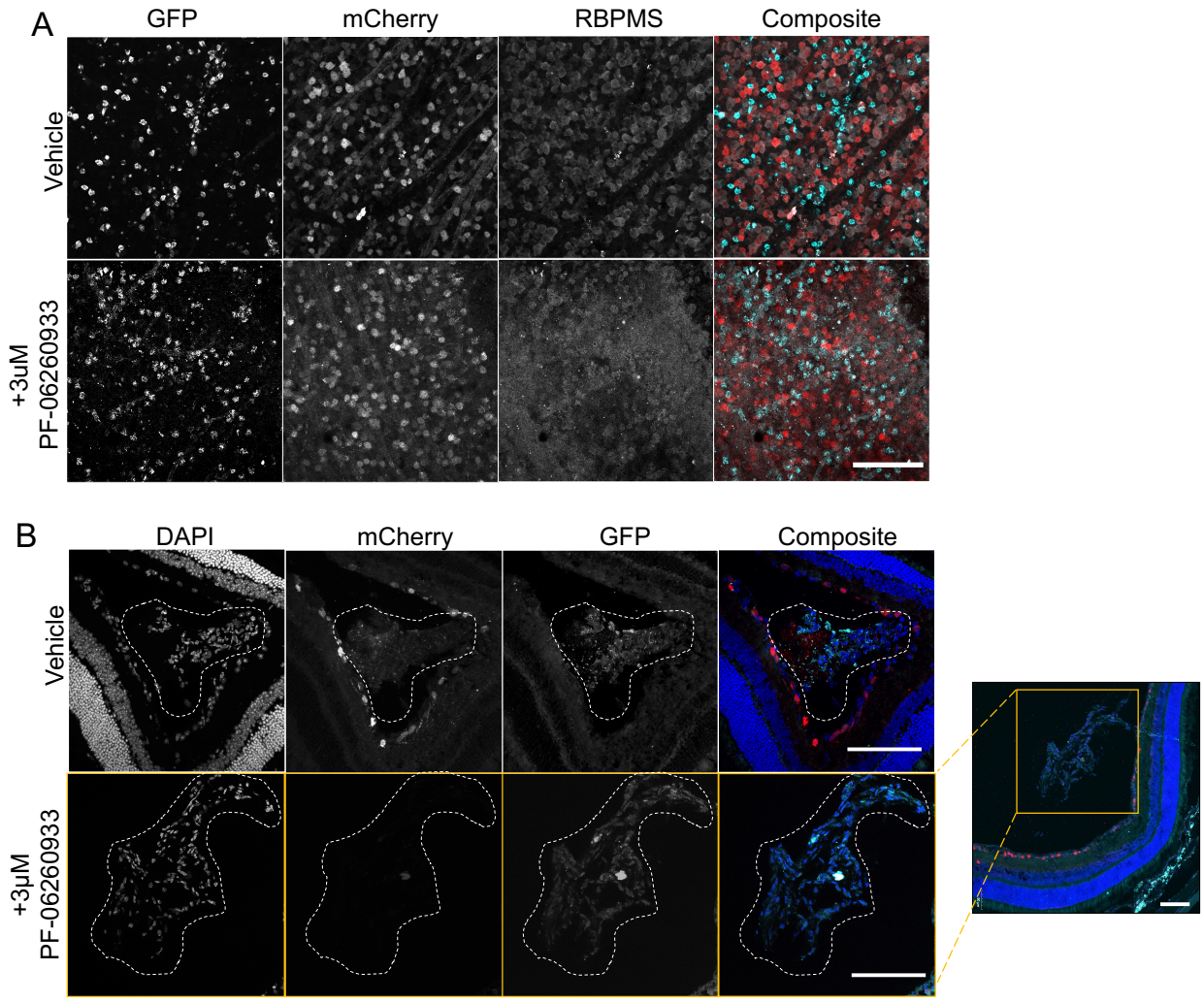

Figure 3.3: MAP4K4 inhibition does not affect transplanted cell morphology or location. Immunolabelled flat mount A) or cryosections B) of adult Isl2-GFP mice intravitreally injected with 50,000 RGCs immunopurified from P2 Brn3b-mCh mouse retina in either vehicle (PBS) or PF-06260933 (3µM). A) GFP+ cells have shrunk morphology compared to endogenous RGCs. B) Transplanted cells are consistently found in the vitreous. Scale bars = 100µm.

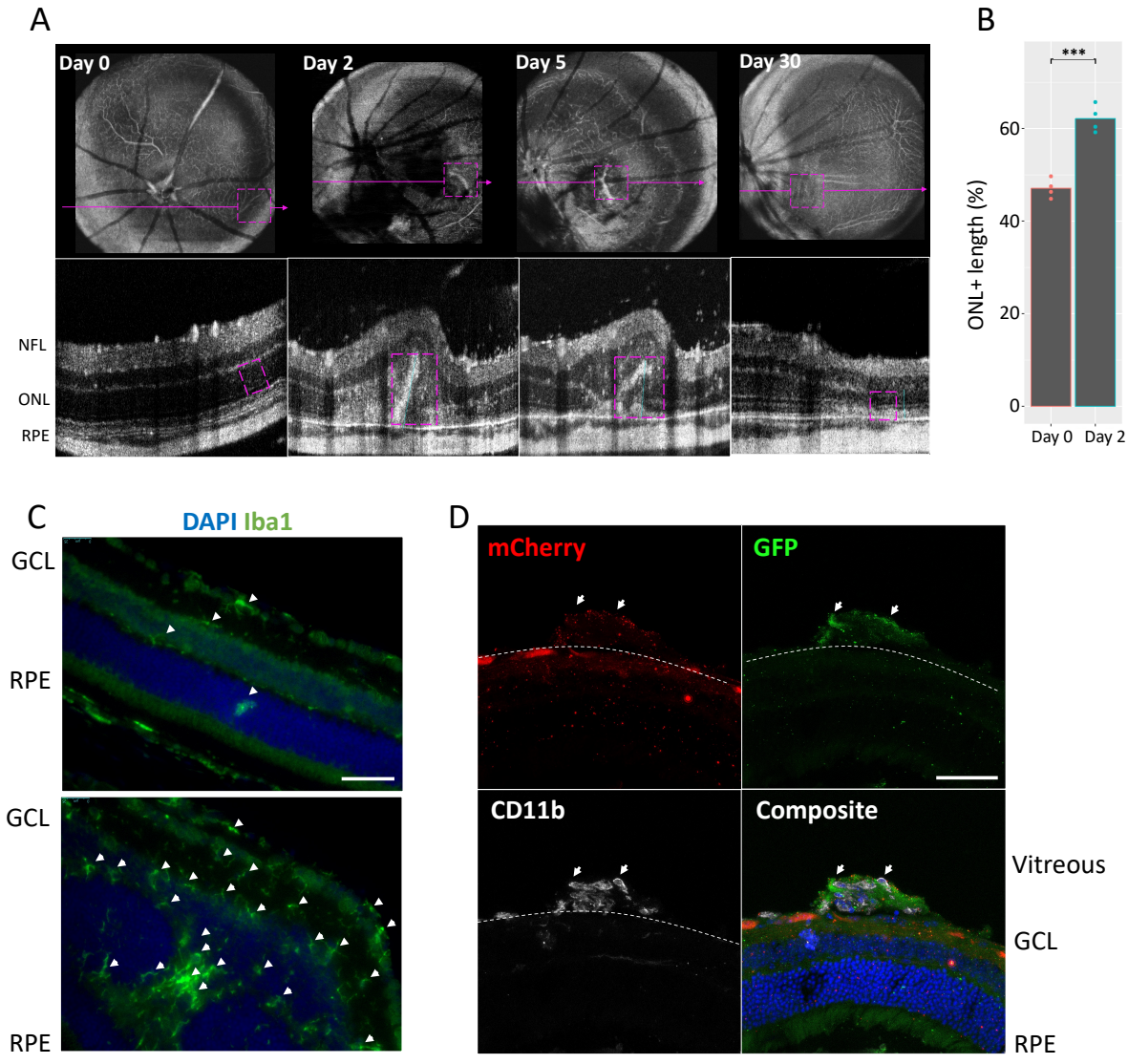

Figure 3.4: In vivo imaging and histological evidence of retinal inflammation following RGC transplantation. A) A and B OCT scans of the same mouse of the course of one-month post-transplantation. Purple arrows on the A-scan (fundus) indicate the position that the OCT B-scan was imaged. Purple boxes mark the same area on both fundus and cross-sectional views. B) ONL/IS/OS (ONL+) thickness was evaluated at these timepoints and normalized to the total retinal thickness (n=4, p=0.000265, Student's T-test). C) Retinal cross sections of areas with and without retinal thickening labeled with anti-Iba1 antibody. White arrows indicate Iba1+ cells. D) Cross

section of an adult Brn3b-mCherry mouse transplanted with Isl2-GFP RGCs labeled with mCherry, GFP, and CD11b. CD11b co-localizes with the GFP bolus within the vitreous (white arrow). Dotted white line indicates the inner limiting membrane. NFL: nerve fiber layer, ONL: outer nuclear layer, RPE: retinal pigment epithelium, GCL: ganglion cell layer. Scale bars = 50μm.

Chapter 4

The ocular immune response to intravitreal injection of RGCs

Introduction

The central nervous system (CNS) has no regenerative capacity; therefore, replacement of the dead/dying cell population is one of few methods to cure neurodegenerative diseases[1]. Many advancements have been made in the generation and delivery of exogenous cells to the retina. One of the major achievements is the differentiation of stem cells into retinal neurons that are nearly identical to those produced in vivo, and development of transplantation protocols that result in the survival of these cells within a living host animal[79,163,192–195,245,264,265,326–328]. However, several labs have shown that there is a significant loss (~5% survival) of RGCs within the first few days of transplantation[192–195,265]. While it is still unclear exactly what causes such acute loss, work has been done to determine some of the affecting factors. One factor may be how the cell purification process affects RGC viability. There are generally two methods to isolate RGCs from whole retina: fluorescence activated cell sorting (FACS), which requires fluorescently labeled target cells, and immunopurification, which can be done on wild type animals. These two processes are both lengthy protocols that subject the retinal tissue to digestive enzymes and unsustainable culture environments. Therefore, it is assumed that many cells will die through this

process and possibly injure the surviving cells. Indeed, several studies have shown that very few (find amount) RGCs survive after 72 hours post-immunopurification, but this widespread death can be remedied by introduction of neuroprotective factors[184,186,279]. The age of the donor RGCs is also an important factor for transplantation success. Hertz and colleagues showed that RGCs from E18-P9 survived better than adult cells 24 hours after culturing on retinal explants (~70% survival compared to ~15%), although the exact mechanisms that allow younger cells to survive more have not been described[193]. However, there are still many unexplored factors that affect the success of transplantation. One such factor is the ocular immune system, an environment distinguished by local mechanisms that suppress responses to antigens, also known as immune privilege[197,208].

Integral to maintaining ocular homeostasis and its immune privileged status are microglia, the resident macrophages of the retina that originate from a cell population independent from bone marrow-derived monocytes[210,223,329]. These cells monitor the retinal microenvironment and support the surrounding cells by secreting neurotrophic factors, phagocytizing cellular debris, and pruning synapses to contribute to overall retinal health[34,218,330,331]. Microglia in a healthy retina reside in the inner and outer plexiform layers, adopting a ramified morphology that consists of several branching processes from a small soma[212]. Non-reactive microglia are largely maintained through the interaction of retinal neurons and microglia. For example, CD200 (formerly known as orexin2/OX2), expressed on the cell surface of retinal ganglion cells, photoreceptors, vascular endothelium, and retinal pigmented epithelium (RPE), has been shown to regulate inflammatory responses in animal models of uveitis through CD200 receptor (CD200R), expressed by retinal microglia[212,332]. Similarly, fractalkine (CXCL1), expressed by retinal neurons, binds to its receptor only found on microglia, CX3CR1, to keep retinal microglia in a quiescent state[214,215]. In a pathological retina, microglia are the first responders that converge on the injury site after detecting changes in the microenvironment, such as increases in cytokines and chemokines, presence of complement components, and release of apoptotic signals by the surrounding cells.

After arriving at the insult, microglia transform into ameboid phagocytes to clear apoptotic cells[210,218]. Additionally, they begin the signaling cascade to mount an inflammatory response through upregulation of inducible nitric oxide synthase (iNOS) and production of proinflammatory cytokines, such as tumor necrosis factor (TNF), interleukins, and interferons[212,218,219]. Several studies have also shown that monocytes can also infiltrate into the retina, most commonly after damage to the outer blood retina barrier formed by the RPE. Here these cells differentiate into macrophages, but the full capacity of their role in retinal inflammation has yet to be defined[224–227].

Currently, only bone marrow mesenchymal stromal cells (BM-MSCs) have been used to specifically study the inflammatory response to intravitreal cell transplantation[198,237]. A study by Norte-Muñoz and colleagues showed that, although the eye holds an immune privilege status, allogeneic and xenogeneic (human) transplantation of BM-MSCs into mouse host causes activation of microglia and recruitment of cluster of differentiation 45 (CD45)+ cells, a surface protein expressed by leukocytes. In contrast, syngeneic transplantation resulted in no significant microglia activation or recruitment of CD45+ cells. Additionally, immunosuppression with cyclosporine did not dampen the microglia activation after allogeneic transplantation of BM-MSCs, which the authors hypothesize may be due to cyclosporine only affecting the adaptive immune response[238]. Therefore, intravitreal injection of genetically dissimilar cells, even with immunosuppression, activates the ocular immune system and causes the loss of the transplanted cell population, something that must be considered when attempting to transplant cells from an exogenous source.

To characterize the ocular immune response to intravitreal RGC transplantation, we transplanted isolated RGCs from the Brn3b-mCherry reporter mouse into microglia reporter Cx3xr1-GFP mice. We then used *in vivo* imaging to observe the changes within 5 days post-transplantation. Our results suggest that intravitreal RGC injection activates the ocular immune system and most likely contributes to the acute decrease of surviving RGCs within the host eye.

Results

The immediate immune response to intravitreal injection

To characterize the immune response to intravitreal injection, adult Cx3CR1-GFP mice were transplanted with immunopurified Brn3b-mCherry RGCs from postnatal day 0 (P0) – P3 mice into one eye and the other with PBS for the vehicle control. Previous studies have established the baseline morphology and densities of microglia labeled within Cx3CR1-GFP mice *in vivo*[333]. Our *in vivo* imaging using scanning laser ophthalmoscopy (SLO) reproduced the retinal maps observed previously in that GFP expression was evenly distributed throughout the retinal surface. Thus, the preinjected eyes were used as the day 0 timepoint throughout these experiments (fig. 1A). 48 hours after transplantation, we observed areas of dense GFP expression using SLO, suggesting that microglia migration had occurred. OCT imaging revealed various hyperreflective opacities and hyperreflective vessels located within the vitreous at these areas of dense GFP expression (fig. 1A). Interestingly, we observed these vitreous opacities within both the cell and vehicle groups, although there were more opacities in eyes that were injected with cells (fig. 1C; n=8, p=0.0863).

To further analyze the activation state of the retinal microglia, we flat mounted and stained retina for GFP 5 days post injection. Morphologically, the GFP+ cells within the cell group had larger somas (n=7 mice, $p<0.0001$) and were more densely grouped than the vehicle controls, which had smaller somas and were more evenly distributed throughout the retinal tissue (fig. 1B and E). Next, we used Sholl analysis with a 6μm starting radius and a 2μm radius step size to quantify the differences in branching between the two conditions[334]. We found that most microglia within the RGC transplanted eyes had processes that did not extend as far and were less complex than processes of microglia in control conditions. The microglia from cell transplants also had a

lower ramification index compared to those in eyes injected with only vehicle (fig. 1F-G; n=7, $p<0.0001$). The less ramified more ameboid morphologies suggest that these cells were indeed transformed into their phagocytic state. Additionally, the complexity and number of processes extended by the vehicle control microglia were not significantly different from microglia within eyes that were not operated on, indicating that the differences in morphology are most likely due to the presence of exogenous cells and not merely the injection procedure (fig. 1F-G). However, there were some microglia within the vehicle controls that had a more ameboid morphology, although this was a minority and most likely due to the invasive (<5%).

Phagocytosis of exogenous cells by microglia

Next, we examined the interactions between the donor and endogenous immune cells using SLO. 561nm signal was found throughout the eyes transplanted with Brn3b-mCherry cells that persisted for at least 5 days. Overlay of the 561nm and 488nm channels revealed co-localization of the two signals within a single retina, suggesting that the microglia are migrating towards the mCherry cells (fig. 2A). After 7 days, the mice were sacrificed and collected for histological analysis. Co-localization experiments revealed that mCherry was present within GFP+ ameboid microglia (fig. 2B). Within these microglia, the mCherry signal appeared as puncta-like structures within the Cx3cr1-GFP cells. Immunolabeling of cryosections showed that microglia migrate into the vitreous and to converge on donor cells (fig. 2C). Furthermore, co-localization with the pan-RGC marker RBPMS resulted in a decreased, speckled RBPMS expression pattern within transplanted cells, suggesting that these are actively dying cells (fig. 2C). Thus, our data suggests that the phagocytic activity of the host immune system strongly impacts the survival of donor cells after intravitreal injection.

Discussion

Previous work in the field of photoreceptor transplantations can help guide our approach to RGC transplantation. Several studies have described the acute loss of transplanted cells (~10%) after one month[77,79,80,195]. This was defined by one study as convergence of macrophages at the transplanted cell mass and the inflammatory response was alleviated by chemical immunosuppression of the host animal with a small molecule such as cyclosporine[307]. However, these findings were mainly observed in the transplantation of photoreceptors or RPE into the subretinal space, an artificial cavity formed by separating the photoreceptors from the RPE. This caveat has potentially significant impacts on how the immune system reacts to intravitreal injections because this protocol requires a needle to pass through all layers of the retina as opposed to only the most peripheral layers. Therefore, our data helps to illustrate the extent of the immune system's role within intravitreal injections.

Here we show that RGCs are readily targeted for phagocytosis. Given the previously investigated cell survival rates, this is not the most surprising observation. When cells die there is a cascade of apoptotic signaling to activate phagocytic cells to "clean up their mess". This allows the organ system to maintain a healthy environment for the rest of the cells. Therefore, it's very possible that the donor RGCs are giving off these signals to the host eye and recruiting macrophages that way. Similarly, tissue rejection is an important consideration for transplantation procedures with acute transplantation rejection occurring in as early as one week post transplantation[335]. However, immune privilege was first defined by an organ that does not reject foreign antigens, like those found in transplanted tissue. Within the eye, this phenomenon has been mainly demonstrated through introduction of exogenous antigens to the anterior chamber, that results in the inhibition of the initial T cell activation, beginning a cascade of deviant immune regulation[336]. Therefore, it is surprising how aggressively immune cells target the transplanted RGCs if the eye has so many mechanisms in place to reduce inflammation.

Experiments specific to internal transplants within the eye helped to further define the extent of the eye's privileged status. The first of these experiments was performed in 1993 when Jiang and colleagues transplanted whole retinal allografts into mouse eyes. In this study, the authors reported little inflammation 12 days after transplantation into the vitreous[236]. Why, in this case of transplanting single cell RGCs, we observe an immune response is still unknown. Future experiments in host immunosuppression can shed light on the exact mechanisms acting with the specific immune response to intravitreally injected RGCs.

Materials and Methods

Animals

Adult mice (*Mus musculus*, CD-1 IGS) were obtained from Charles River Laboratories (Wilmington, MA). Homozygous Cx3cr1$^{GFP/GFP}$ (strain 005582) mice were obtained from The Jackson Laboratory. The Brn3b-mCherry CRISPR knock-in mouse line was generated by Biocytogen (Worcester, MA, USA) in the C57BL/6N background. We have not performed whole-genome sequencing to screen for off-target effects, but we have not detected any abnormalities, viability, fertility or any developmental problems (9 different generations have been analyzed to date). All the animals had *ad libitum* access to food and water and were kept at a constant temperature of 21°C on a 12h light/ 12h dark cycle. All mouse husbandry and handling were performed in accordance with protocols approved by the University of California Davis Animal Care and Use Committee (IACUC protocol #22905), which strictly adheres to all NIH guidelines and satisfies the Association for Research in Vision and Ophthalmology guidelines for animal use.

Immunopurification of RGCs

Retinal ganglion cells (RGCs) were purified from whole mouse retina as previously described by Winzeler and Wang[300]. Briefly, retinas were dissected from postnatal day 0 (P0)-P3

mice, then dissociated with a 0.6mg/mL of papain dissolved in Dulbecco's phosphate buffered saline (DPBS) (LS003126, Worthington Biochemical; 14287080, Life Technologies) for 14 minutes at 37 °C. Papain digestion was stopped by addition of a 15mg/mL bovine serum albumin (BSA)/trypsin inhibitor solution (LS003587, Worthington Biochemicals) at pH 7.4. Retina were mechanically dissociated by dropwise release of the tissue suspension into 15mL conical tubes. Mouse anti-rat CD11b/c; [OX-42] (ab1211, Abcam) bound magnetic beads (11531D, Thermo Fisher) were used for macrophage depletion by incubation with the cell suspension for 15 minutes at room temperature (RT). The cell suspension was then plated onto a mouse anti-Thy1.2 (MCA02R, Bio-Rad) coated 10cm plate and incubated for 45 minutes at RT with gentle swirling. The cell bound plate was then washed with PBS to discard non-RGCs. RGCs were detached from the plate by incubation with 0.05% trypsin/Earl's balanced salt solution and resuspended in injection media at a concentration of 50,000 cells/µL.

Intravitreal injection

Adult mouse intravitreal injections were performed under general anesthesia (1.5% isoflurane) with mice on a heating pad (37 °C). Proparacaine and tropicamide drops were applied to the eye for local anesthesia and pupil dilation before injection, respectively. The corneal surface was wetted with Gel Tears hypromellose gel (GenTeal Tears Severe, Alcon) to prevent cold cataract. To begin the surgical procedure, a small incision was made in the conjunctiva slightly posterior to the ora serrata using ophthalmic scissors. A 31-gauge insulin syringe (BD Insulin syringe with ultra-fine needle) was used to make an insertion hole at the incision point. Next, 1µL of vitreous was removed using a 33-gauge syringe (Hamilton Company, Reno, NV) followed by an injection 1µL of RGC suspension (50,000 cells/µL) over the course of 30 seconds, pausing for 10 seconds before removal. Finally, a triple antibiotic was added to the eye and the mouse was allowed to recover on the heating pad.

In vivo imaging

A custom in vivo imaging system was used to image GFP+ and mCherry+ (mCh) cells within the eye of post operation mice, collecting back reflectance and fluorescence images[324]. Mice were anesthetized with 2–2.5% isoflurane and positioned on a heating pad (37 °C) with a custom-built bite-bar (Bioptigen, Morrisville, NC) that allowed rotational and translational adjustment for positioning the mouse with respect to the contact lens. The mouse pupils were dilated, and eyes anesthetized with tropicamide and phenylephrine, and the corneal surface wetted with Gel Tears hypromellose gel (GenTeal Tears Severe, Alcon). Gel Tears maintain a homogeneous refractive surface between the cornea and the custom contact lens (Unicon Corporation, Osaka, Japan). GFP and mCh excitation was achieved with 488 nm and 561 nm lasers, respectively (OBIS LX, Coherent Inc., US). Images were collected over 51° of visual angle at 43 μm per degree. In Fiji, fundus images were registered[325], averaged, and pseudo-colored.

Optical coherence tomography (OCT) imaging was performed with a superluminescent diode centered at 860nm with a 132nm bandwidth (Broadlighter T-860-HP, Superlum), approximately 600μW at the pupil. A custom Python script was used to flatten the B-scans and then register those flattened B-scans using a strip-registration algorithm to generate complete flattened OCT volumes.

Tissue processing

Whole eyes were fixed in 4% PFA for 30 minutes then washed with PBS (pH 7.0). Eyes for cryosectioning were embedded in successive sucrose/PBS solutions of 10%, 20%, and 30% with a final embedding step in 30% sucrose:OCT. Eyes were sectioned with a cryostat as 12-14um thick sections. Retinas were dissected from eyes intended for whole mount and were flattened by making four radial cuts around the retina (flat mount). Flat mounts were fixed for another 30 minutes in 4% PFA then washed in PBS for 5 minutes at RT.

Immunohistochemistry

Flat mounted retinas were permeabilized in 1% Triton X-100 in PBS; retina cryosections were permabilized in 0.3% Triton X-100 in PBS at RT. Non-specific antigens were blocked by blocking buffer (10% Normal Donkey Serum and 0.1% Triton X-100 in PBS) and the tissue was incubated with primary antibodies at a dilution indicated in Table 6.1 at 4ºC overnight. The next day, the tissue was washed with PBS at RT and incubated with Alexa Fluor secondary antibodies for either 3 hours (whole) or 1 hour (sections) at RT, as indicated in Table 6.1. The tissue was then washed with PBS, the cell nuclei were labeled with 4',6-diamidino-2-phenyindole (DAPI) at a dilution of 1:10,000, and the sections or whole retinas were then mounted with Fluoromount-G (Southern Biotech, Birmingham, AL). Tissue was imaged using an Olympus FV1000 confocal microscope.

Statistical analysis

In all figures, data are represented as mean ± standard error and significance levels are indicated as follows: *$p < 0.05$, **$p < 0.01$, ***$p < 0.001$. All statistical analyses were performed using R. Two group comparisons were performed using Student's T-tests. Multiple group comparisons of immunohistochemistry and flow cytometry data were performed using a one-way ANOVA followed by a Tukey's honest significant differences (HSD) test. Multiple group comparisons over time were performed using a two-way ANOVA followed by a Tukey's HSD test.

Figures

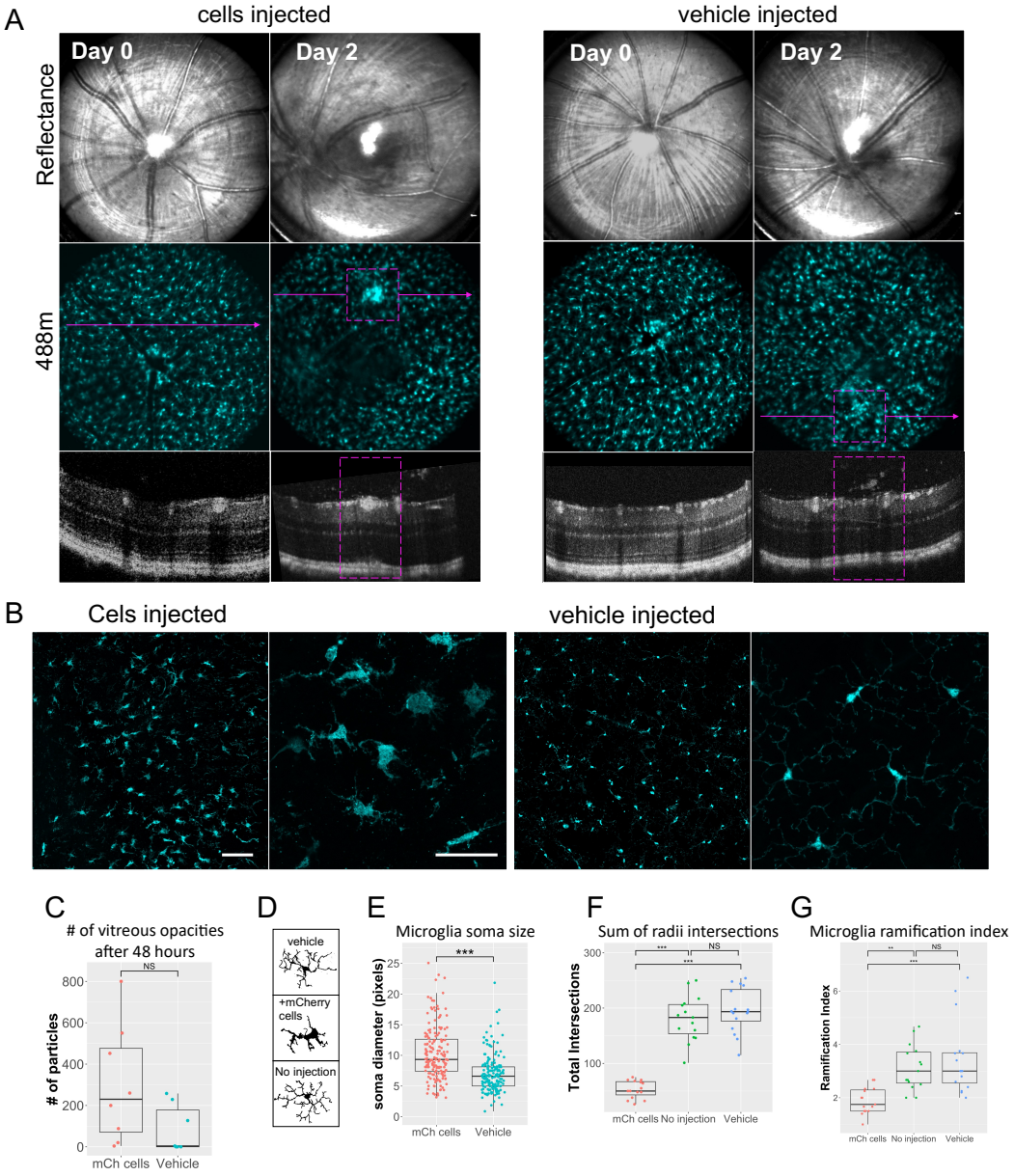

Figure 4.1: Microglia response to injected cells. Cx3cr1-GFP mice were injected with 50,000 RGCs immunopurified from P2 Brn3b-mCh mouse retina and live imaged with SLO 2- and 5-days post injection. Eyes were collected 7 days post injection and immunolabeled for GFP to identify microglia and macrophages. A) Live imaging of the same retina two days post transplantation. Purple arrows on the SLO image indicate the position that the OCT B-scan was imaged. Purple

boxes mark the same area on both fundus and cross-sectional views. B) immunolabeling against GFP. White arrows represent microglia with activated morphologies. C) Quantification of macrophage/microglia somas using FIJI (n=7, $p=9.57x10^{-15}$, Student's t-test). D) Binary images examples of microglia used in Sholl analysis. E) Total intersections (n=5, 15 per group, mCh cells-no injection $p=2.70x10^{-12}$, mCh cells-vehicle $p=1.14x10^{-12}$, vehicle-no injection p=0.442) F) Ramification index (n=5, 15 per group, mCh cells-no injection p=0.003, mCh cells-vehicle p=0.00013, vehicle-no injection p=0.585). ANOVA with Tukey's HSD. Scale bars = 50μm.

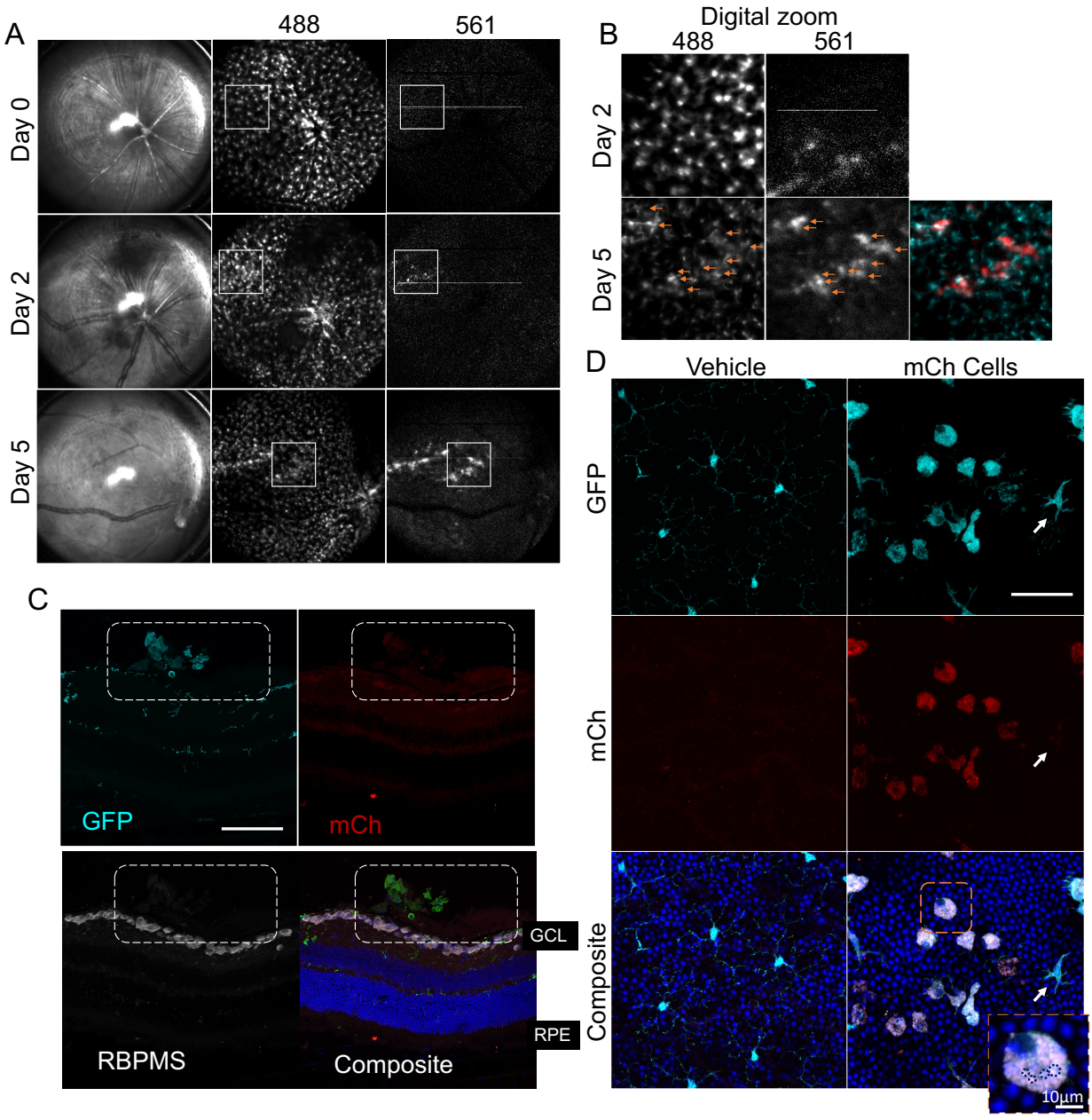

Figure 4. 2: Phagocytosis of mCh cells injected intravitreally. Adult Cx3cr1-GFP mice were intravitreally injected with either 50,000 RGCs immunopurified from P2 Brn3b-mCh mouse retina or 1µL of vehicle (PBS). Retinae were dissected 7 days post injection, flat mounted and immunolabeled for mCh to identify injected cells and GFP to identify Cx3cr1-GFP cells. A) Live imaging of retina with SLO over time. White boxes denote the same area within each time point. B) digital zoom of regions of interest from (A). Arrows represent colocalization between 488nm

and 561nm signal. C) Cryosections with donor cells immunolabeled for GFP and RBPMS. White dashed box is drawn around the cell bolus. D) Flat mounted retina stained with anti-mCherry and anti-GFP antibodies. Orange box indicates the digitally zoomed image of a single immune cell with black circles surrounding puncta. White arrow indicates GFP+ cell with no mCherry expression. GCL: ganglion cell layer, RPE: retinal pigment epithelium. Scale bars = 50μm, unless noted otherwise.

Chapter 5

Disruption of the inner limiting membrane activates the ocular immune system

Introduction

The retina is the highly organized neural tissue located at the back of the eye. It is split into several layers of interconnected neurons that transform light stimuli into signals sent to the visual processing centers of the brain. These layers are generally split into where the retinal neuron somas reside, or the outer and inner nuclear layer (O/INL), and the regions where neurons synapse, called the outer and inner plexiform layers (O/IPL)[20,32]. This system is also very fragile, loss of any layer will result in loss of vision because there is no redundancy in the circuitry between the light sensitive photoreceptors and the output ganglion cells[27,32]. Unfortunately, like most of the central nervous system, the retina cannot regenerate its neurons and once neurons are lost, most often due to a retinal degenerative disease, there are no endogenous mechanisms to regrow these cells[312,337,338]. Retinal cell replacement therapy is a promising, but not yet perfect, method to treat retinal diseases. There are several factors that must be considered while developing this technique: first is having a reliable source of cells, second is keeping those cells alive through

and after the transplantation process, and third is engraftment of the donor cells into the correct area of the recipient's tissue. Of these barriers, engraftment has been the least successful aspect of the method to date[163,164,192–195,273,275]. This holds especially true for retinal ganglion cell (RGC) replacement therapy compared to photoreceptor (PR) transplantation. PR transplantation typically involves injection into the subretinal space, an artificial region between the retinal pigmented epithelium and the photoreceptors created during the procedure. Placement of exogenous PR in this area has an advantage compared to GCL because there are no physical barriers between the injected cells and the endogenous PRs[77,79–81,307]. To date, very few studies have successfully shown cells migrating to the GCL, even though they can survive in the vitreous for at least a year[78,192–195,263]. One of the main hypotheses as to why the cells do not cross into the host tissue is that the inner limiting membrane (ILM) acts as a physical barrier to engraftment.

The ILM is the basement membrane that separates the retinal tissue from the vitreous and consists of mainly extracellular matrix proteins, mainly laminin and collagen, that originate from the lens and ciliary body. Data suggests that the ILM is necessary for proper retinal development by helping to establish the apical/basal polarity by promoting directional microtubule assembly within RGC axons through laminin activated integrin signaling[240]. In mice, the ILM is a consistent thickness (~70nm), whereas the human ILM differs in thickness depending on the retinal region. For example, the ILM in the human fovea is thickest at ~400nm, whereas the periphery is closer to 70nm[240–242]. The retinal side of the ILM interfaces with the end processes (endfeet) of Müller Glia (MG), the radial glia that spans the entire retina. Here, laminin binds to the high concentrations of dystroglycans found within the MG endfeet, which is suggested to be a necessary interaction for proper retinal development[239]. Previous studies have shown that removal of the ILM helps the engraftment of donor cells. This was first shown by Johnson and colleagues in 2010, where they showed that removal of the ILM ex vivo increases the infiltration of donor mesenchymal stem cells (MSC) into the cultured tissue[196]. In a follow-up study, Zhang and colleagues showed that enzymatic disruption of the ILM with low concentrations (0.6U/mL)

Pronase E increases neurite engraftment of stem cell derived RGCs when co-cultured with ex vivo mouse retina[245]. However, due to the nature of these studies, the ocular immune system is not accounted for because the rest of the mouse body is not present. Therefore, it is still unclear how impactful ILM disruption is for clinical applications of RGC transplantation.

As mentioned previously, the retina is an immune privileged tissue that has endogenous mechanisms to suppress inflammatory responses[204,208]. This resting state is maintained by the interactions between glia and retinal neurons to prevent chronic inflammation and the subsequent damage to the retina it may cause. However, in a pathological retina, which often occurs due to the targeted degeneration of a specific retinal neuron population, these mechanisms can be overrode by an influx of pro-inflammatory signals from the dying cells[210–212,218,219,339]. This begins the signaling cascade to mount an inflammatory response through upregulation of inducible nitric oxide synthase (iNOS) and production of proinflammatory cytokines, such as tumor necrosis factor (TNF), interleukins, and interferons[210,330,340]. Additionally, circulating bone marrow (BM) derived monocytes can infiltrate into the retina through the blood retina barrier (BRB) formed by either epithelial cells within the inner retinal vasculature or the interface between the choroidal vasculature and retinal pigmented epithelium (RPE)[222–224,226]. Although it is still unclear exactly how monocytes are mobilized to CNS tissues, the C-C motif chemokine receptor 2– C-C motif chemokine ligand 2 (CCR2-CCL2) axis is crucial for migration of BM monocytes during retinal degeneration[226,341]. Within the inflamed retina, BM monocytes differentiate into macrophages to assist resident microglia activity, but the full capacity of their role in retinal inflammation has yet to be defined[223–226,341,342].

In this study we explored the immune response to in vivo mechanical disruption of the ILM. After 24 hours post-peel, we observed ameboid CD11b positive cells surrounding areas of disrupted laminin on the retinal surface. After 5 days, the total number of ameboid cells (decreases?) and the fluorescence intensity of CD11b decreases from the 24hour time point.

Together, this data suggests that mechanical disruption of the ILM illicits microglia activation and monocyte infiltration.

Results

The immune response after 24 hours post ILM disruption is localized

To determine the immediate immune response to *in vivo* mechanical disruption of the ILM, we used a 31g needle to gently scrape the vitreal surface of the retina of adult mice and collected them after 24 hours to compare them to their untouched controls (fig. 1A). Then to determine the distribution and morphology of the retinal immune cells, we performed histological analysis on the resulting flat mounts by immunolabeling the tissue with antibodies targeting CD11b, a marker for activated microglia, and laminin, one of the main components of the ILM. Previous studies of retinal injury have demonstrated that microglia are actively recruited to an injury site after morphing from a ramified state into an ameboid state, and here we observed similar microglia behavior[218,225,333]. Scraped retina contained areas of dense CD11b expression that co-localized with areas of disrupted laminin expression, while the unscraped controls had an even distribution of CD11b+ cells and a uniform layer of laminin. At the scrape areas, the RGC layer was often clearly visible when imaged at the vitreal surface of the retina, signaling that the scrape itself did not fatally damage the retinal neurons (fig. 1B).

Additionally, we further classified the scraped retina as regions of either “disruption” or “no disruption” to investigate the differences between microglia recruited to the injury compared to the rest of the retina. Microglia that surrounded the scrape site did not extend processes and were found within the same plane as the ILM (fig. 1B). Additionally, microglia within ILM disrupted eyes had larger somas than those within unscraped controls, regardless of their proximity to a scrape site (fig. 1C; n=5, *$p<0.05$, ***$p<0.0001$). We next used Sholl analysis to examine the differences in morphologies between the microglia within the regions without disruption and the unscraped

controls. Using a 6μm starting radius and a 2μm step size, Sholl analysis revealed no significant differences in total intersections, furthest radii reached, or ramification index between the microglia within regions without disruption and unscraped controls (fig. 1D-E). Thus, we observed a localized response to the disruption site by microglia that did not spread to areas outside where the ILM was broken.

Effect of ILM disruptions on the ocular immune response over time

As we have previously shown, donor RGCs are targeted by microglia after intravitreal injection. If ILM disruption is to be a viable technique to help improve RGC engraftment as a pre-treatment before transplantation, then it would be valuable to know when microglia return to their quiescent state. To look closely at the morphologies of the microglia over time, we disrupted the ILM of CD-1 mice and collected their eyes on day 1, day 3, and day 5 for histological analysis. First, we compared the morphologies between the time points using Sholl analysis. As in the previous section, we used a starting radius of 6μm and a step size of 2μm. Over time, CD11b+ cells surrounding the ILM disruptions became more morphologically complex, extending increasingly branched processes further from their soma ($n=3$, $p<0.001$). The microglia within areas of no disruption maintained their ramified morphology overtime, showing no significant differences in process length or branching ($n=3$, $p>0.05$). However, when the microglia at 5 days were significantly different than the unscraped controls, suggesting that although there are less activated microglia, they have not returned to homeostasis (2A and C-D). We then calculated the ratio of ameboid to ramified microglia within the disrupted areas to help determine how long microglia remain activated at the scrape site. The percentage of CD11b+ cells converging directly on the disruption decreased over time (fig. 2A and E), additionally supporting conclusion that the inflammation is reduced at the scrape.

Macrophages infiltrate the retina through the vasculature in some cases of retinal injury, with the largest vessels located at the optic nerve head (ONH)[222,223]. Therefore, to determine if

monocytes infiltrate into the retina, and if that rate is consistent over time, we quantified the fluorescence of CD11b of the ONH in the flat mounts. Within the initial 24 hours, we observed an increase in CD11b signal at the ONH compared to an unscraped eye. However, by day 3 there was a decrease of fluorescence from day 1, suggesting that less monocytes are infiltrating into the retina (fig. 2B and F, n=4, $p<0.001$). Additionally, the average fluorescence from day 3 onwards is not significantly different than that from an unscraped control (day 0) (fig. 2F-G, n-4, $p>0.05$). Thus, we conclude that mechanical disruptions to the ILM will initiate an acute immune response that slows over time but does not see microglia return to a quiescent state within five days.

Discussion

Although promising in its current state, methods for robust cell replacement therapy to treat retinal degenerative diseases remain elusive. One of the clearest barriers is the physical barriers within the eye. Specifically, the ILM has been shown to prevent RGCs from entering the host tissue. When disrupted either mechanically or enzymatically, there is a significant increase in exogenous cell integration[196,245]. Therefore, methods to remove this membrane have been of great interest. However, all the studies to date have only performed ILM disruption *ex vivo*, limiting the experiments to a system that excludes the rest of the body[196,245]. Importantly, the immune system does not function properly in these conditions. Previously we have shown that the immune system plays a large role in the survival of donor RGCs, with most of the donor cells being engulfed by CD11b+ cells within the vitreous (see Chapter 3). Thus, if we are to consider ILM disruption as a pre-treatment to RGC replacement therapy, we must understand the response from the ocular immune system to such an insult.

Here we show that disruption of the ILM recruits microglia to the injury site and that monocyte infiltration slows over time, although the microglia do not fully return to their surveillance state within five days. One way to address the remaining activated cells is to simply extend the

recovery time. However, it has been shown that within models of retinal degeneration some retinal immune cells never return to their quiescent state and continue to express activation/inflammation genes[225,228,343]. Since ILM disruption is acute and less detrimental compared to injury to specifically cause retinal degeneration, this procedure may be less likely to cause chronic inflammation than say laser induced photoreceptor damage[225,333]. Another method to circumvent the longitudinal immune activation may be to use immunosuppressives. This may be especially useful if the next operation is RGC transplantation because the cells will be delivered to the disrupted area and reduction of activated cells will most likely help donor cell survival.

Previous studies have shown that MG gliosis may play a large role in the success of donor RGC engraftment[196,245]. MG, the largest and most abundant glia within the retina, span through all layers of the retina and provide structure and biochemical support to the surrounding cells and serve as the binding site for extracellular matrix proteins within the ILM[32,240]. In response to retinal injury or infection, MG undergo reactive gliosis that is characterized by hypertrophy, proliferation, and upregulation of intermediate filaments: glial fibrillary acid protein (GFAP), vimentin and nestin[344]. Additionally, MG play a large role in retinal immunity by releasing pro-inflammatory factors, regulating T-cell proliferation, and have even been shown to phagocytize foreign molecules injected into the vitreous[344]. In the context of RGC transplantation, reactive gliosis may be one of the “gatekeepers” to successful engraftment. Johnson and colleagues described a reduction of reactive gliosis at mechanically disrupted regions of the ILM that correlated with an increase in donor cell engraftment at these regions lacking gliotic MG[196]. Further examination into the role of MG in donor cell engraftment found that direct inhibition of gliosis increases cell engraftment[196,245]. However, these experiments were performed *in vitro*, so it is unclear how the innate and adaptive immune systems interact specifically with MG after ILM disruption. Thus, future experiments to understand the interactions between MG and microglia after *in vivo* ILM disruption may help inform the development of new methods to increase donor cell integration into the retina.

Methods

Animals

Adult mice (*Mus musculus*, CD-1 IGS) were obtained from Charles River Laboratories (Wilmington, MA). Homozygous Cx3cr1$^{GFP/GFP}$ (strain 005582) mice were obtained from The Jackson Laboratory. The Brn3b-mCherry CRISPR knock-in mouse line was generated by Biocytogen (Worcester, MA, USA) in the C57BL/6N background. We have not performed whole-genome sequencing to screen for off-target effects, but we have not detected any abnormalities, viability, fertility or any developmental problems (9 different generations have been analyzed to date). All the animals had *ad libitum* access to food and water and were kept at a constant temperature of 21°C on a 12h light/ 12h dark cycle. All mouse husbandry and handling were performed in accordance with protocols approved by the University of California Davis Animal Care and Use Committee (IACUC protocol #22905), which strictly adheres to all NIH guidelines and satisfies the Association for Research in Vision and Ophthalmology guidelines for animal use.

ILM disruption

Adult mouse procedures were performed under general anesthesia (1.5% isoflurane) with mice on a heating pad (37 °C). Proparacaine and tropicamide drops were applied to the eye for local anesthesia and pupil dilation, respectively and the corneal surface wetted with Gel Tears hypromellose gel (GenTeal Tears Severe, Alcon) to prevent cold cataract. To begin the surgical procedure, a small incision was made in the conjunctiva slightly posterior to the ora serrata using ophthalmic scissors. A 31-gauge insulin syringe (BD Insulin syringe with ultra-fine needle) was used to make an insertion hole at the incision point. Next, another 31-guage insulin syringe with the tip blunted was inserted and used to gently scrape along the retina opposite from the insertion

hole. Finally, a triple antibiotic was added to the eye and the mouse was allowed to recover on the heating pad.

In vivo imaging

A custom in vivo imaging system was used to image GFP+ and mCherry+ (mCh) cells within the eye of post operation mice, collecting back reflectance and fluorescence images[324]. Mice were anesthetized with 2–2.5% isoflurane and positioned on a heating pad (37 °C) with a custom-built bite-bar (Bioptigen, Morrisville, NC) that allowed rotational and translational adjustment for positioning the mouse with respect to the contact lens. The mouse pupils were dilated, and eyes anesthetized with tropicamide and phenylephrine, and the corneal surface wetted with Gel Tears hypromellose gel (GenTeal Tears Severe, Alcon). Gel Tears maintain a homogeneous refractive surface between the cornea and the custom contact lens (Unicon Corporation, Osaka, Japan). GFP and mCh excitation was achieved with 488 nm and 561 nm lasers, respectively (OBIS LX, Coherent Inc., US). Images were collected over 51° of visual angle at 43 μm per degree. In Fiji, fundus images were registered[325], averaged, and pseudo-colored.

Optical coherence tomography (OCT) imaging was performed with a superluminescent diode centered at 860nm with a 132nm bandwidth (Broadlighter T-860-HP, Superlum), approximately 600μW at the pupil. A custom Python script was used to flatten the B-scans and then register those flattened B-scans using a strip-registration algorithm to generate complete flattened OCT volumes.

Tissue processing

Whole eyes were fixed in 4% PFA for 30 minutes then washed with PBS (pH 7.0). Eyes for cryosectioning were embedded in successive sucrose/PBS solutions of 10%, 20%, and 30% with a final embedding step in 30% sucrose:OCT. Eyes were sectioned with a cryostat as 12-14um thick sections. Retinas were dissected from eyes intended for whole mount and were

flattened by making four radial cuts around the retina (flat mount). Flat mounts were fixed for another 30 minutes in 4% PFA then washed in PBS for 5 minutes at RT.

Immunohistochemistry

Flat mounted retinas were permeabilized in 1% Triton X-100 in PBS; retina cryosections were permabilized in 0.3% Triton X-100 in PBS at RT. Non-specific antigens were blocked by blocking buffer (10% Normal Donkey Serum and 0.1% Triton X-100 in PBS) and the tissue was incubated with primary antibodies at a dilution indicated in Table 6.1 at 4ºC overnight. The next day, the tissue was washed with PBS at RT and incubated with Alexa Fluor secondary antibodies for either 3 hours (whole) or 1 hour (sections) at RT, as indicated in Table 6.1. The tissue was then washed with PBS, the cell nuclei were labeled with 4',6-diamidino-2-phenyindole (DAPI) at a dilution of 1:10,000, and the sections or whole retinas were then mounted with Fluoromount-G (Southern Biotech, Birmingham, AL). Tissue was imaged using an Olympus FV10000 confocal microscope or a Leica DM inverted scope.

Statistical analysis

In all figures, data are represented as mean ± standard error and significance levels are indicated as follows: *$p < 0.05$, **$p < 0.01$, ***$p < 0.001$. All statistical analyses were performed using R version. Two group comparisons were performed using Student's T-tests. Multiple group comparisons of immunohistochemistry were performed using a one-way ANOVA followed by a Tukey's honest significant differences (HSD) test. Multiple group comparisons for Sholl analysis data were performed using a two-way ANOVA followed by a Tukey's HSD test. Diameter experiment populations was tested for normalcy using a Shapiro-Wilk test (failed). Comparison of region diameters was then performed using a Kruskal-Wallis one-way analysis of variance test followed by a pairwise Wilcox rank sum test.

Figures

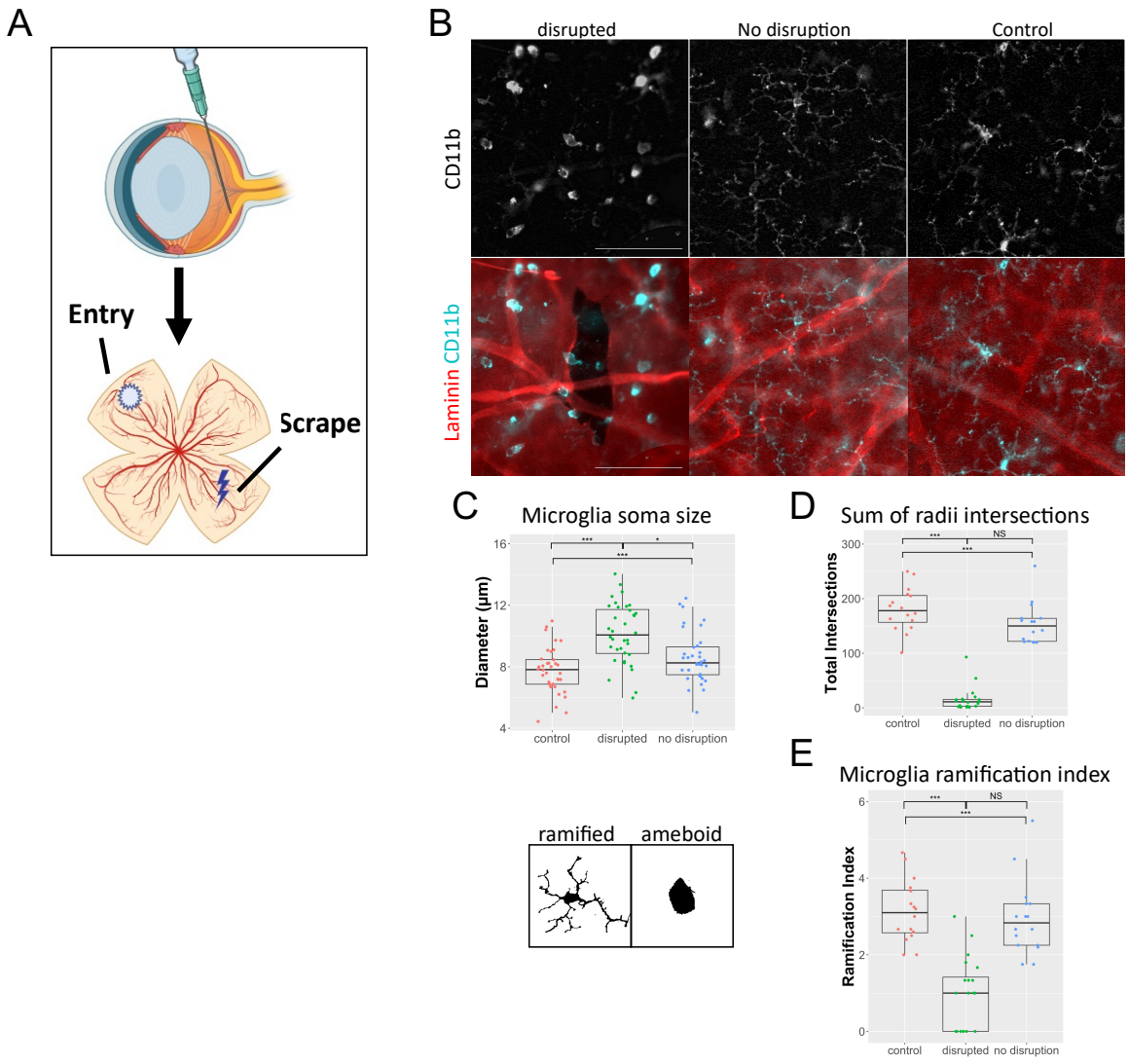

Figure 5.1: Immune response 24hours after ILM disruption. A) Schematic of ILM disruption technique. B) Flat mount retina immunostained with CD11b and laminin 24hours after disruption. Representative images of areas with mechanical disruption, areas that have not been disrupted, and areas from retina that were not disrupted at all. C) Comparison of microglia soma size within each region (n=3, 15/group, control-disrupted $p=2.60x10^{-6}$, disrupted-no disruption $p=7.70x10^{-4}$, control-no disruption p=0.034). ANOVA with Tukey's HSD.

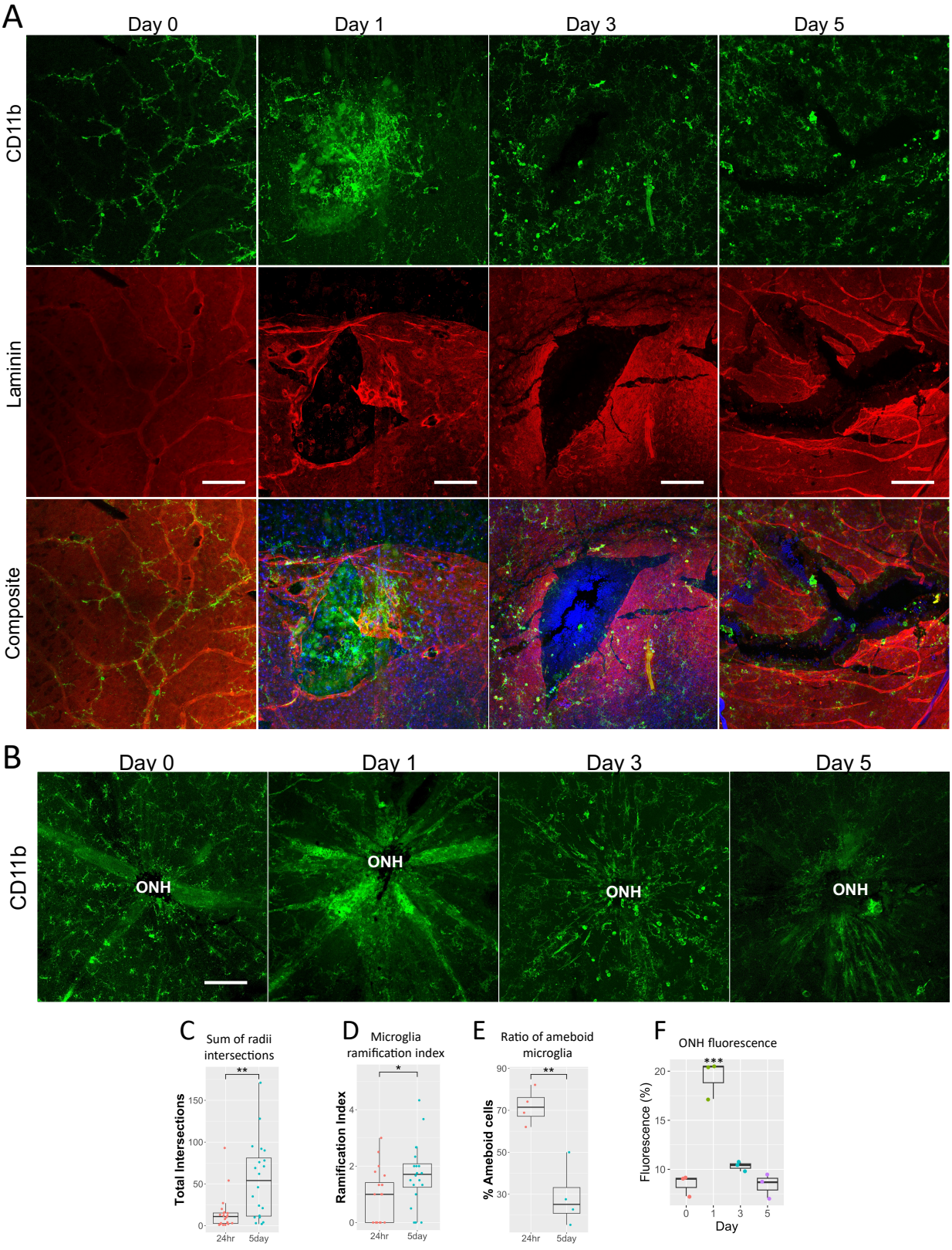
A
Day 0
Day 1
Day 3
Day 5
CD11b
Laminin
Composite
B
Day 0
Day 1
Day 3
Day 5
CD11b
ONH
ONH
ONH
ONH
C
Sum of radii intersections
Total Intersections
24hr
5day
D
Microglia ramification index
Ramification Index
24hr
5day
E
Ratio of ameboid microglia
% Ameboid cells
24hr
5day
F
ONH fluorescence
Fluorescence (%)
Day

Figure 5.2: Immune response to ILM disruption over time. Comparisons between 24hr and 5days post ILM disruption shown by A) flat mounted retina immunolabeled for CD11b and laminin over time. B) CD11b expression at ONH of flat mounted retina shows acute increase then slowly decreases over time. C) Total intersections for individual microglia by Sholl analysis (n=5, 20/group, $p=0.002$). D) Ramification index by Sholl analysis (n=5, 20/group, $p=0.028$). E) Ratio of ameboid to total microglia in 200x200μm area (n=4, $p=0.005$). F) Quantification of CD11b fluorescence at ONH over time (n=3, $p<0.0001$ for comparisons with day 1, $p>0.05$ for all other comparisons). Students T-test for C-E, ANOVA with Tukey's HSD for F. Scale bars = 100μm.

Chapter 6

Optimization of RGC transplantations

Immunopurification of RGCs

Retinal ganglion cells (RGCs) were purified from whole mouse retina based on the protocol previously described by Winzeler and Wang[300]. To start, postnatal day 0 (P0)-P3 mice were sacrificed and their eyes enucleated. Retinae were dissected in room temperature (RT) phosphate buffered saline (PBS) with lens and vitreous removed. When using more than 3 litters, pups were screened for fluorescence to enrich the purified cell population, else all pups were used to collect enough RGCs. Retinas were then dissociated with a solution of 0.6mg/mL of papain, 1mg/uL cysteine, and DNAse in Dulbecco's phosphate buffered saline (DPBS) (LS003126, Worthington Biochemical; 14287080, Life Technologies) for 14 minutes at 37 °C, with gentle swirling after the first 7 minutes. Digestion was stopped by addition of a 15mg/mL bovine serum albumin (BSA)/trypsin inhibitor solution (LS003587, Worthington Biochemicals) at pH 7.4. Whole retinae were triturated by gentle dropwise release of the retina suspension into a clean 15mL conical tube. Macrophages were depleted by incubating the cell suspension for 15 minutes at room RT with mouse anti-rat CD11b/c; [OX-42] (ab1211, Abcam) bound magnetic beads (11531D, Thermo Fisher) then separating the cell populations by increasing the total suspension volume with panning buffer (0.05mg/mL insulin in 0.5% PBS/BSA) using a strong magnet. To avoid any contaminating beads, extra panning buffer was added to wash and magnetically separate the beads if needed. The macrophage depleted cell suspension was then plated onto a

mouse anti-Thy1.2 (MCA02R, Bio-Rad) coated 10cm bacterial plate and incubated for 45 minutes at RT, swirling every 15 minutes. The panning plate was gently washed with DPBS (with Ca^{2+} and Mg^{2+}) several times to remove non-RGCs (fig. 1A). Extra care was taken to prevent RGCs from prematurely detaching by adding new PBS wash to the same area of the plate, so only one section would experience the force of wash solution's initial impact. Next the plate was washed with Earl's Balanced Salt Solution (without Ca^{2+} and Mg^{2+}) to remove calcium and magnesium ions that would otherwise inhibit trypsinization. RGCs were detached from the plate by incubation with 0.05% trypsin/Earl's balanced salt solution at 37 °C for 7 minutes, followed by inhibition with 30% FBS/PBS trypsin inhibition. The RGCs were further detached by gently pipetting the solution within the dish over the surface of the plate and resuspended in injection media at a concentration of 50,000 cells/µL.

Intravitreal injection

Intravitreal injections into adult mice were performed under general anesthesia (1.5% isoflurane) with mice on a heating pad (37 °C). Prior to injection, proparacaine and tropicamide drops were applied to the eye for at least 30 seconds for local anesthesia and pupil dilation, respectively. The corneal surface was wetted with Gel Tears hypromellose gel (GenTeal Tears Severe, Alcon) to prevent cold cataract and provide optimal visibility into the mouse eye. A small incision was made in the conjunctiva slightly posterior to the ora serrata using ophthalmic scissors. Next, a round glass coverslip was placed over the eye to clearly view the back of the eye. An insertion hole into the vitreous was made at this incision using a 31-gauge insulin syringe, with care taken to avoid hitting the lens and retina (BD Insulin syringe with ultra-fine needle). Next, 1µL of vitreous was removed using a 33-gauge syringe (Hamilton Company, Reno, NV) followed by an injection 1µL of RGC suspension (50,000 cells/µL) as close to the retina as possible over

the course of 30 seconds, pausing for 10 seconds before removal. Finally, a triple antibiotic was added to the eye and mice were allowed to recover on the heating pad.

In vivo imaging

A custom-built scanning laser ophthalmoscopy (SLO) system was used to image GFP+ and mCherry+ cells within the retina, simultaneously collecting the reflectance and fluorescence images[324]. For imaging, mice were anesthetized with 2–2.5% isoflurane and positioned on a heating pad (37 °C) with a custom-built bite-bar (Bioptigen, Morrisville, NC) that allowed rotational and translational adjustment for positioning the mouse with respect to the contact lens. The pupils were dilated and anesthetized with tropicamide and phenylephrine, and the corneal surface wetted with Gel Tears hypromellose gel (GenTeal Tears Severe, Alcon). Gel Tears helped maintain a homogeneous refractive surface between the cornea and the custom 0 diopter contact lens (Unicon Corporation, Osaka, Japan). GFP excitation was achieved with OBIS LX 488 nm laser (Coherent Inc., US) filtered through single bandpass filter (name), delivering 99μW of power at the mouse pupil. mCherry excitation was achieved OBIS LX 561 nm laser (Coherent Inc., US) filtered through single bandpass filter (name), delivering 250μW of power at the mouse pupil. 100 serial images, including both reflectance and fluorescence, were collected over 51° of visual angle at 43 μm per degree. In Fiji, images were registered using the TurboReg plugin with “Rigidbody” transformation[325], averaged, and pseudo-colored for display.

Optical coherence tomography (OCT) imaging was performed with a superluminescent diode centered at 860nm with a 132nm bandwidth (Broadlighter T-860-HP, Superlum), approximately 600μW at the pupil. Several B-scan volumes were collected from the same position. Custom MATLAB and ImageJ macro code was used to compensate chromatic dispersion within B-scans then average and register the serial volumes using the MultiStackReg plugin with “Rigidbody” transformation.

Optimization of injection technique

Several factors contributed to the success of an intravitreal injection. Here we define success as transplanted cells found within the eye after at least 48 hours. First, there must be enough viable RGCs for injection. When using less than two litters of mice (ie less than 20 mice total), the number of RGCs bound to the panning plate decreased significantly. Additionally, when using 20< mice, the RGCs often extended short neurites when bound to the plate, suggesting that they were healthy and viable at this stage (fig. 1B). In both these conditions, there was a higher percentage of living cells after trypsinization, and more cells survived after 48hours of culture (fig. 1C).

The viscosity of the donor cell suspension also seems to contribute to the outcome of the transplantation. In general, the cell suspension was delivered as dissociated single cells or as a large mass/bolus. Although difficult to know if the cells remained dispersed or as a bolus due to fluid dynamics of the inner eye and movement of the mouse head, we found that transplantation of cells in a less viscous suspension immunofluorescence resulted in more host eyes donor cell fluorescence detectable by SLO (Table 2). Out of 36 total transplantation attempts, 15 contained fluorescent donor cells detectable by SLO and of these only 3 had donor cells as a bolus (Table 2). However, after sectioning and staining, most of the eyes injected with boluses contained aggregates of fluorescent cells within the vitreous (see figure 3.3). Previous studies have described a technique to ensure retinal contact with the cell bolus by using air bubbles within the eye[195]. This technique, which injects an air bubble into the vitreous, is used within ophthalmology clinics as a method to repair retinal detachments[345]. In our experiments, bubbles were placed within the eye using the Hamilton needle, followed by injection of a cell bolus. The results of this technique are inconclusive because when removing the needle, the cell bolus did not necessarily stay suspended within the bubble. We also observed vitreous backflow on some occasions, which

may have moved the cell bolus from its original spot. Additionally, cell boluses placed close to the lens were quick to adhere to the lens and difficult to remove. After sectioning and staining these eyes, we observed large masses attached to the lens that contained DAPI positive cells (fig. 2A). Thus, the boluses may be more difficult to image with SLO than single cell suspensions, especially if the cell aggregates can easily attach to the lens, bringing it out of focus. Therefore, optimization of the SLO imaging system to image objects outside of the retinal plane is key to utilizing its full capacity for RGC transplantation.

In vivo imaging also revealed several unknown factors that may affect the outcomes of RGC transplantation attempts. In some experiments, subsequent OCT imaging showed that the injection needle may have contacted the vitreal surface of the retina (fig. 2B). While this insult did not cause any hemorrhaging during the procedure, the damage is noticeable within the OCT by the indent from the nerve fiber layer (NFL) to the inner plexiform layer (IPL). Interestingly, we observed increased OCT scattering within the outer nuclear and outer plexiform layers (ONL/OPL) similar to that seen following near-infrared laser induced photoreceptor damage[333]. Additionally, there were few vitreous opacities found directly above the GCL, suggesting that this was not the location that the exogenous RGCs were delivered. It is unclear what effect the NFL injuries have on the outcome of RGC transplantation, specifically if the recruited macrophages also target the transplanted cells. However, due to the small space within the mouse vitreous injuries like this can happen easily without the experimenter noticing. Therefore, care must be taken to avoid these risks, such as anchoring the hand to a non-moving surface and proper magnification of mouse eye.

Together, our data suggests that the intravitreal transplantation protocol relies on several complex techniques to work in series, a feat not easily achieved. Thus, further experiments in developing the RGC delivery method should be pursued to create a robust and reproducible method for RGC transplantation.

Material Transfer

Material transfer (MT) between donor and host retinal neurons was first discovered in photoreceptor (PR) transplant studies. Prior to this discovery, published data showed that after fluorescently labeled exogenous PRs were delivered to the subretinal space of a wildtype animal, fluorescently labeled cells were found in the ONL. These cells were morphologically indistinguishable from and synapsed with other host neurons as if they were endogenous PRs, a groundbreaking discovery for the field[80,346]. However, upon further investigation, these cells that mimicked endogenous cells were, in fact, endogenous cells that had fluorescent protein molecules transferred to them by nanotube like processes with the donor cells[81,309,311]. It is currently unknown if MT occurs between other retinal neurons, like RGCs, or if it is a PR specific phenomenon. Therefore, it is critical to determine if RGCs can transfer material between endogenous and exogenous cells not only properly develop RGC replacement therapies, but to uphold a standard of rigor and reproducibility within this scientific field.

Using our duo RGC reporter approach, we have evidence that material transfer does occur between RGCs. Throughout our experiments we used two fluorescent RGC reporter lines, the Brn3b-mCherry mouse and the Isl2-GFP mouse (see chapter 3) to distinguish host and donor cells within a single animal. However, this system also gives us a simple method to study material transfer: if an RGC expresses both GFP and mCherry, then it has most likely undergone MT. Here we performed co-localization experiments with anti-mCherry and anti-GFP antibodies to determine if MT occurs. We observed several instances of GFP expression within the RGCs of a Brn3b-mCherry mouse after transplantation with Isl2-GFP cells (fig. 3). The expression ranged from expressed throughout the soma, partial expression within the soma, and seemingly within RGC axons (fig. 3). Additionally, we observed this in at least 3 mice, suggesting that this is not an artifact of the immunolabeling protocol. Furthermore, we observed GFP+ RGCs that did not express mCherry, suggesting that either 1) the cells did successfully integrate or 2) that material

transferred occurred (fig. 3) However, these observations are preliminary and require further experiments to concretely conclude that MT has occurred.

Figures

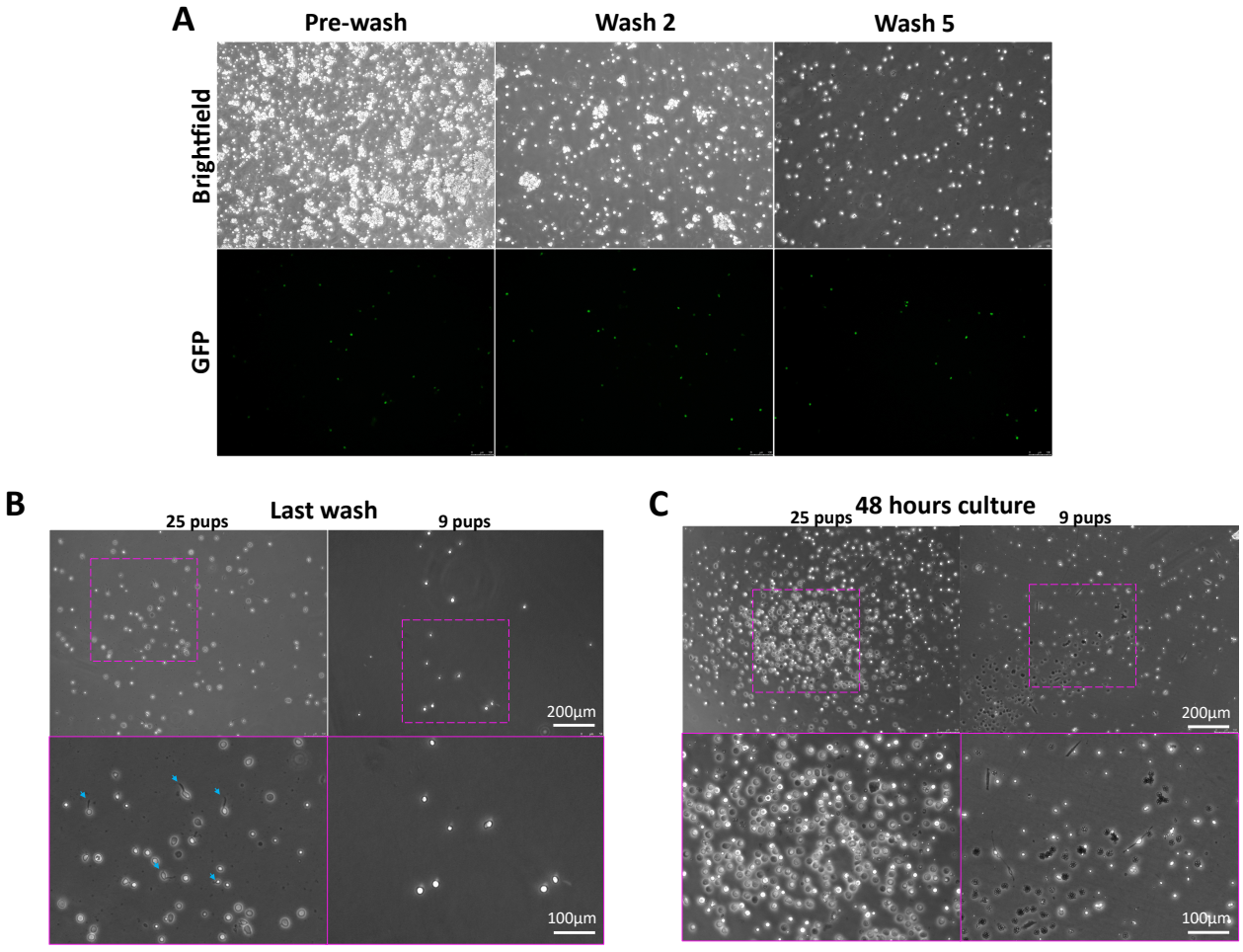

Figure 6.1: Optimization of immunopurification technique. A) Brightfield images of the panning plate wash step during immunopanning protocol. B) Comparison of the final panning plate pre-trypsinization using either 25 or 9 pups as starting material. Blue arrows represent cells projecting neurites C) Primary culture of RGCs isolated from experiments using 25 or 9 pups. Purple regions of interest are zoomed in on bottom row.

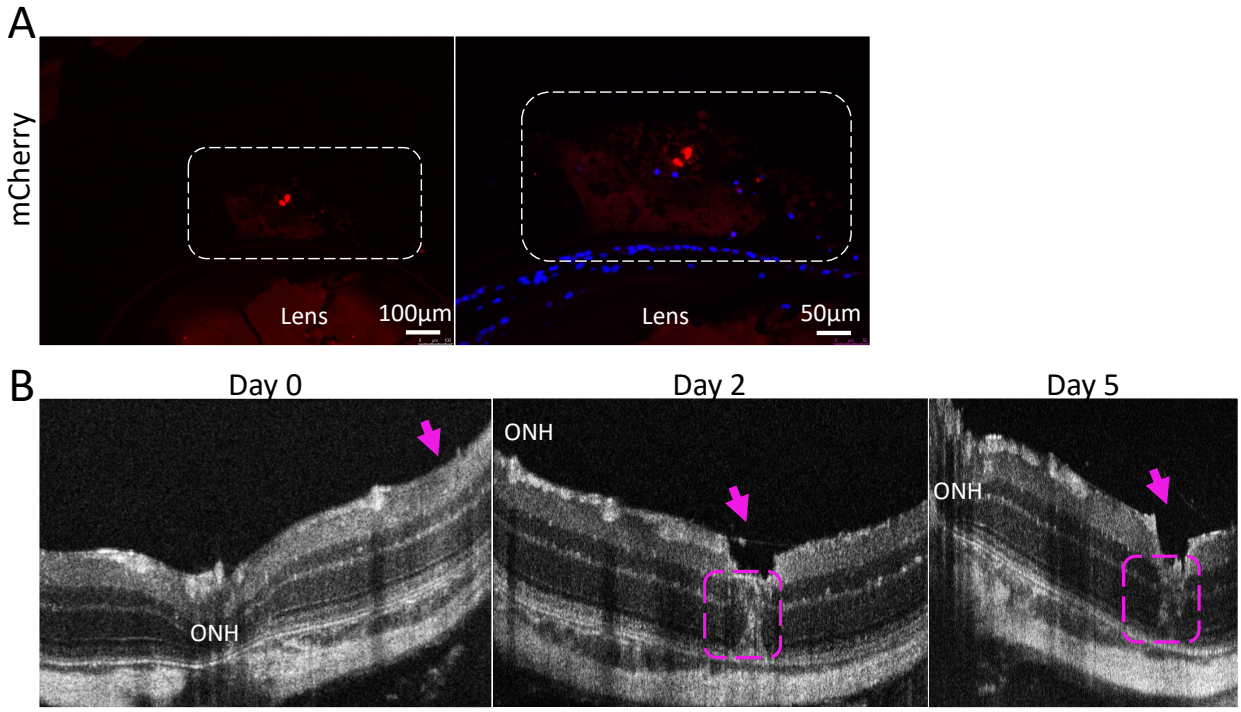

Figure 6.2: Artifacts of intravitreal injection. A) Cryosection of Isl2-GFP mouse with transplanted Brn3b-mCherry RGCs. White dotted box marks the bolus found attached to lens. B) OCT B-Scans of area of retinal damage after injection. Purple arrow marks damage on retinal surface, dotted purple box marks potential inflammation.

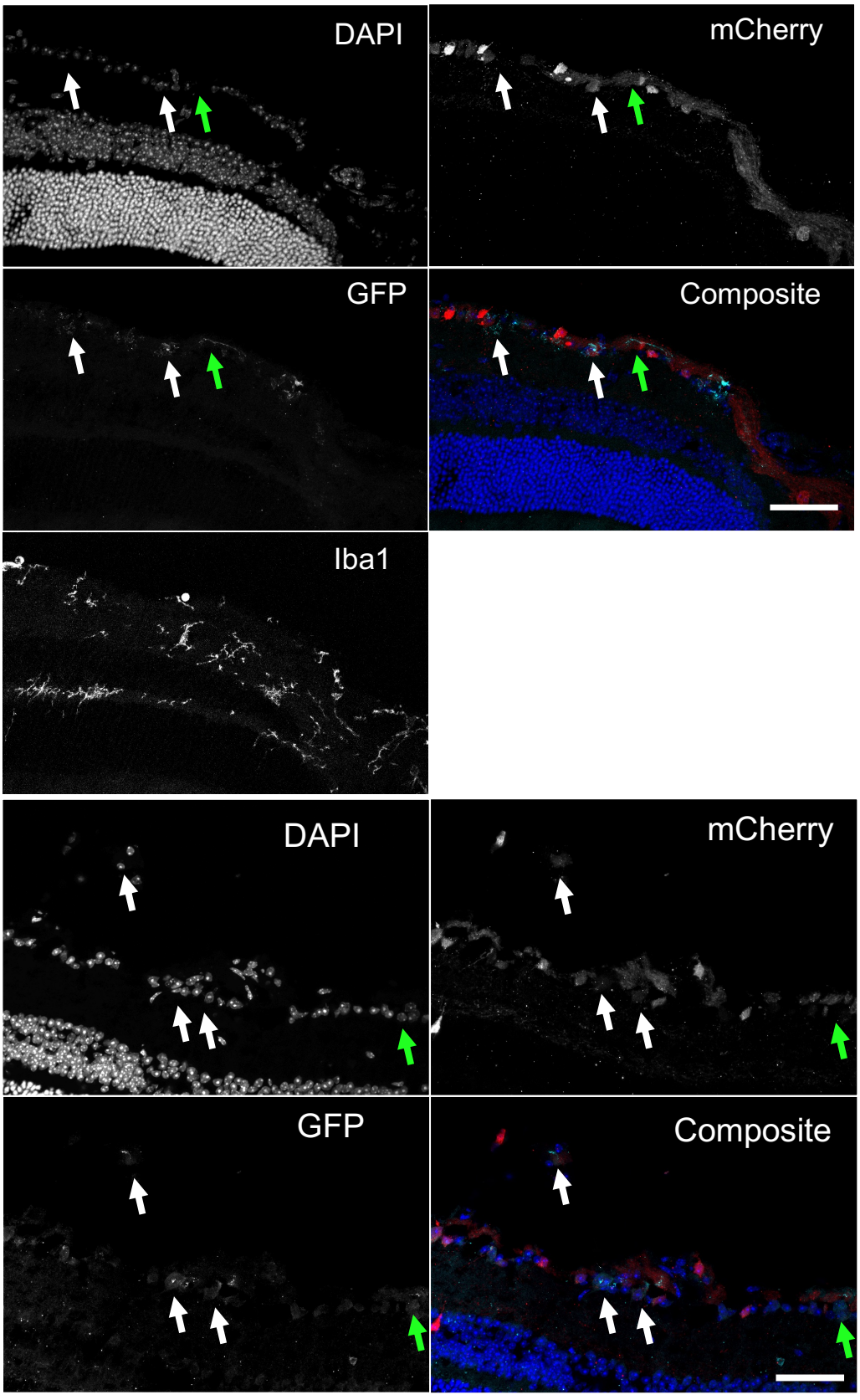
DAPI
mCherry
GFP
Composite
Iba1
DAPI
mCherry
GFP
Composite

Figure 6.3: Material transfer between donor and host RGCs. Cryosections of two different Brn3b-mCherry mouse retinae after transplantation with Isl2-GFP cells (1-week post-injection) immunolabeled for mCherry, GFP, and Iba1 (left retina only). White arrows mark colocalization of mCherry and GFP expression. Green arrows mark cells with only GFP expression. There is also no colocalization of Iba1 and cells marked with arrows.

Table 6.1: Antibodies used in chapters 3-5

Antibody	Specificity	Catalogue	Dilution	Source
mCherry		AB0040-200	1:500	Acris Antibodies
GFP		Ab13970	1:500	Abcam
RBPMS	RGCs	1832-RBPMS	1:500	Phosphosolutions
CD11b	Microglia/macrophages	101220	1:100	Biolegends
Iba1	Microglia/macrophages	019-19741	1:500	Wako
Laminin	Extracellular matrix/ILM	ab11575	1:500	abcam
Alexa 488 anti-chicken	Chicken IgG	A-11039	1:500	Thermo Fisher
Alexa 568 anti-goat	Goat IgG	A-11057	1:500	Thermo Fisher
Alexa 647 anti-rabbit	Rabbit IgG	A-21245	1:500	Thermo Fisher
Alexa 647 anti-Guinea Pig	Guinea Pig IgG	A-21450	1:500	Thermo Fisher

Table 6.2: RGC transplantation outcomes

Genotype	Eye	Bubbles	Suspension	Day	Cell location (OCT)	Fluorescence (SLO)
Brn3b-mCh	R		single cell	3	periphery	yes
Brn3b-mCh	R		single cell at ONH	7	spread throughout	no
	L		single cell at ONH	7	spread throughout	no
Brn3b-mCh	R		single cell	7	spread throughout	yes
Brn3b-mCh	L		single cell	11	periphery	no
Brn3b-mCh	R		single cell	11	periphery, shadow at ONH	yes
	L		single cell	11	none, shadow over retina	no
Brn3b-mCh	R		single cell	11	none	no
Brn3b-mCh	R		single cell	5	none	yes
	L		single cell	5	some at periphery	no
Brn3b-mCh	L		single cell	5	none	no
Brn3b-mCh	R		bolus	3	a lot between lens and retina	yes

	L		single cell	3	lens damage	NA
Brn3b-mCh	R		single cell	3	a lot between lens and retina	yes
	L		single cell	3	periphery	yes
Brn3b-mCh	R		bolus	6		no
	L		single cell	6		no
Brn3b-mCh	R		single cell	6		no
	L		bolus	6		no
Isl2-GFP	R		single cell	2	periphery	yes
	L		single cell	2	periphery	no
Isl2-GFP	R		single cell	2	periphery, ONH	no
	L		single cell	2	aggregation at periphery, ONH	no
Cx3cr1-GFP	R		single cell	2	throughout	yes
	R/L	yes	bolus			no
	R/L	yes	bolus			no
	R/L	yes	bolus			no
	R/L	yes	bolus			no
Isl2-GFP	R	no	single cell	2	periphery, ONH	yes
	L	no	single cell	2	periphery, ONH	no
Isl2-GFP	R	no	single cell	2	aggregation at periphery, ONH	yes
	L	no	single cell	2	periphery, ONH	no
Isl2-GFP	R	no	single cell	2	aggregation at periphery	yes
	L	no	single cell	2	some at periphery, ONH	no
Cx3cr1-GFP	R	no	single cell	2	throughout	yes
Cx3cr1-GFP	R	no	single cell	2	throughout	yes
Brn3b-mCh	R	no	single cell	2	aggregation close to ONH, periphery	no
	L	no	single cell	2	aggregation between lens and retina	no
Brn3b-mCh	R	yes	single cell	2	Large aggregation on lens, throughout	no

	L	yes	single cell	2	periphery	no
Cx3cr1-GFP	R	no	bolus	4		yes
Cx3cr1-GFP	R	no	single cell	4		no
Brn3b-mCh	R	yes	bolus	2	aggregation near ONH	no
	L	yes	bolus	2	mass on lens	no
Brn3b-mCh	R	yes	bolus	2	Large mass?	no
	L	no	single cell	2	aggregation in periphery near lens	no
Brn3b-mCh	R	yes	bolus	2		no
	L	yes	bolus	2		no
Cx3cr1-GFP	R	yes	bolus	2	throughout	yes
Cx3cr1-GFP	R	yes	bolus	2	periphery, near lens	no

Chapter 7

Concluding Remarks

In this dissertation I investigated the current barriers to retinal ganglion cell (RGC) replacement therapy. First, I addressed the barriers faced by the donor cells: sourcing and survival (Chapter 2 and 3) and then barriers within the host eye: the immune response and the inner limiting membrane (ILM) (Chapter 4 and 5). Throughout these studies I also optimized/troubleshooted a variety of tools and techniques for RGC transplantation, including intravitreal injection, scanning laser ophthalmoscopy and optical coherence tomography, and a method to mechanically disrupt the ILM *in vivo* (Chapter 6). Together, these studies have resulted in several findings that will help to inform the development of RGC replacement therapy.

One key finding within this dissertation is that donor cell treatments can impact transplantation success, with success defined as donor cells surviving within the eye regardless of location. It has been shown that RGCs isolated from early postnatal mouse retina have a higher chance of transplantation success than those from older mice[193]. This is not entirely surprising because RGC neurogenesis continues until shortly after birth and, therefore, RGCs isolated from early postnatal mice are primed to migrate and integrate into the GCL[347]. However, there is still an incredibly low percentage of cells that are found within the retina, even though these cells are theoretically in the best condition for transplantation[78,192–196,245]. Interestingly, no previous study has specifically examined methods to increase the donor cell survival rate, a gap this dissertation has helped address. Here I found that manipulation of axon injury response transcription factors, like the GCK-IV kinase family, can increase the number of successful transplantations, as well as

the number of surviving cells *in vivo*. However, the use of a small molecule inhibitor used here is limited by the volume injected into the eye; unless the host receives multiple doses of the inhibitor, whatever is initially injected is all that will be available to affect the donor cells within the eye. Therefore, the development of methods to increase the long-term survival of the donor cells, and perhaps the endogenous cells as well, will be necessary to advance RGC replacement therapy.

Another key finding is the consistent presence of immune cells after RGC transplantation and inner limiting membrane (ILM) disruption. While there are several studies examining the immune response to subretinal transplantation, only one study has investigated the immune response to intravitreal transplantation[197,237,307]. Here the authors showed that intravitreally transplantation of bone marrow mesenchymal stem cells is associated with reactive gliosis and recruitment of macrophages[237]. Similarly, I found that macrophages are recruited to transplanted RGCs regardless of donor cell location. I also found that macrophages are recruited to the disrupted areas within the ILM, although this recruitment seems to slow over the course of one week. However, the ocular immune system plays an additional role in neuron survival and regeneration. Several studies have shown that induction of sterile inflammation via lens damage is associated with an increase in RGC survival and axon regeneration[348]. This is most likely due to the neuroprotective “pre-treatment” by infiltrating monocytes expressing factors that have been shown to increase neuron survival and induce axon regeneration[348]. This may be promising in the context of using ILM disruption as a pre-treatment to both allow more access to the ganglion cell layer and induce the expression of neuroprotective factors. Additionally, monocyte derived macrophages, as opposed to differentiated retinal microglia, have been shown to be less response to a second retinal injury, although it is currently unclear which type of macrophage is responsible for donor cell phagocytosis[225]. Understanding the specific mechanisms that dictate the targeting of donor RGCs will help determine strategies to overcome, or enlist, the ocular immune system.

Finally, these studies have highlighted the variability within the transplantation experiments. Unsurprisingly, this highly technical multistep protocol has varying outcomes due to the isolated RGC viability, the location the donor cells are delivered, and the quality of the injection itself. Additionally, each lab performs these experiments differently, changing factors such as RGC isolation methods, needle gauge, cell suspension media, bringing into question which factors are actually responsible for successful transplantations[78,192–196,245]. However, an important factor that is often not controlled for is material transfer, the presence of which calls into question the robustness of the current transplantation studies[81,308,311]. Here I have found evidence for material transfer, which will undoubtedly be the focus of future studies.

Future studies continuing the work specifically from this dissertation include the effect of immunosuppression on RGC transplantation. From my studies, it is unclear what role the immune cells play in donor cell survival; are they targeting the donor cells in mechanisms similar to pathogen response or if they are clearing dying cells[218,349,350]? Immunosuppression will certainly help determine the role of activated immune cells on the overall survival rate of donor cells. Another follow up study is to determine if ILM disruption increases RGC engraftment. While several studies have shown that mechanically or enzymatically disrupting the ILM leads to an increase in donor cell engraftment, this has only been performed *ex vivo*[75,84,297].

RGC replacement therapy has made many strides towards its goal of clinical applications within the last 15 years. However, due to the complex nature of this technique there are many factors left unexamined. While the results of this dissertation help elucidate some of the mechanisms currently preventing successful donor cell engraftment, factors like the intraocular pressure and an increased resilience of some RGC subtypes may unknowingly impact experiment results[75,84,297]. Therefore, the continued interrogation of the barriers to RGC replacement therapy is necessary to help develop techniques that will ultimately treat vision loss due to retinal degenerative diseases.

References

1. Harper, R. *The Code of Hammurabi, King of Babylon, about 2250 B.C.* vol. 65 (F. Leypoldt, 1904).
2. Bryan, C. *The Papyrus Ebers: Translated from the German Version*. (D Appleton and Company, 1931).
3. Retief, F., Stulting, A. & Cilliers, L. The eye in antiquity. *South Afr. Med. J. Suid-Afr. Tydskr. Vir Geneeskd.* **98**, 697–700 (2008).
4. Hippocrates. *Hippocrates: Places in Man Translated by Elizabeth M. Craik*. (Clarendon Press, 1998).
5. Raju, V. K. Susruta of ancient India. *Indian J. Ophthalmol.* **51**, 119–122 (2003).
6. Sim, P. Y. History of Ophthalmology. *American Academy of Ophthalmology Eye Wiki* https://eyewiki.aao.org/History_of_Ophthalmology (2021).
7. Herophilus. *Herophilus: The Art of Medicine in Early Alexandria*. (Cabridge University Press, 1989).
8. Dobson, J. F. Herophilus of Alexandria. *Proc. R. Soc. Med.* **18**, 19–32 (1925).
9. Hippocrates & Galen. *The writings of Hippocrates and Galen with contributions by JR Cox*. (Lindsay and Blakiston, 1846).
10. Hirschberg, J. *The History of Ophthalmology: The renaissance of ophthalmology in the eighteenth century (pt.3). The first half of the nineteenth century (pt.1)*. (Wayenborgh, 1985).
11. Kepler, J. *Ad Vitellionem Paralipomena, Quibus Astronomiae Pars Optica Traditur*. (1604).
12. Fishman, R. S. Kepler's Discovery of the Retinal Image. *Arch. Ophthalmol.* **89**, 59–61 (1973).
13. Ramón y Cajal, S. *Die Retina der Wirbelthiere: Untersuchungen mit der Golgi-Cajalschen Chromsilbermethode und der Ehrlichschen Methylenblaufárbung*. (J.F. Bergmann, 1894).
14. Isawumi, M. A., Kolawole, O. U. & Hassan, M. B. Couching Techniques for Cataract Treatment in Osogbo, South West Nigeria. *Ghana Med. J.* **47**, 64–69 (2013).
15. Albert, D. M. & Blodi, F. C. Georg Joseph Beer: a review of his life and contributions. *Doc. Ophthalmol. Adv. Ophthalmol.* **68**, 79–103 (1988).
16. Keeler, C. R. The Ophthalmoscope in the Lifetime of Hermann von Helmholtz. *Arch. Ophthalmol.* **120**, 194–201 (2002).
17. Ehinger, B. & Grzybowski, A. Allvar Gullstrand (1862-1930)--the gentleman with the lamp. *Acta Ophthalmol. (Copenh.)* **89**, 701–708 (2011).
18. Kolb, H. Simple Anatomy of the Retina. in *Webvision: The Organization of the Retina and Visual System* (eds. Kolb, H., Fernandez, E. & Nelson, R.) (University of Utah Health Sciences Center, 1995).
19. Masland, R. H. The fundamental plan of the retina. *Nat. Neurosci.* **4**, 877–886 (2001).
20. Schmolesky, M. The Primary Visual Cortex. *Webvision* https://webvision.med.utah.edu/book/part-ix-brain-visual-areas/the-primary-visual-cortex/ (2007).
21. Baker, S. A. & Kerov, V. Chapter Seven - Photoreceptor Inner and Outer Segments. in *Current Topics in Membranes* (ed. Bennett, V.) vol. 72 231–265 (Academic Press, 2013).
22. Kolb, H. Photoreceptors. *Webvision* https://webvision.med.utah.edu/book/part-ii-anatomy-and-physiology-of-the-retina/photoreceptors/ (2013).
23. Terakita, A. The opsins. *Genome Biol.* **6**, 213 (2005).
24. Twig, G., Levy, H. & Perlman, I. Color opponency in horizontal cells of the vertebrate retina. *Prog. Retin. Eye Res.* **22**, 31–68 (2003).
25. Barnes, S., Grove, J. C. R., McHugh, C. F., Hirano, A. A. & Brecha, N. C. Horizontal Cell Feedback to Cone Photoreceptors in Mammalian Retina: Novel Insights From the GABA-pH Hybrid Model. *Front. Cell. Neurosci.* **14**, 595064 (2020).

26. Kolb, H. *et al.* Are there three types of horizontal cell in the human retina? *J. Comp. Neurol.* **343**, 370–386 (1994).
27. Yan, W. *et al.* Cell Atlas of The Human Fovea and Peripheral Retina. *Sci. Rep.* **10**, 9802 (2020).
28. Lu, Y. *et al.* Single-Cell Analysis of Human Retina Identifies Evolutionarily Conserved and Species-Specific Mechanisms Controlling Development. *Dev. Cell* **53**, 473-491.e9 (2020).
29. West, E. R. & Cepko, C. L. Development and diversification of bipolar interneurons in the mammalian retina. *Dev. Biol.* **481**, 30–42 (2022).
30. Yan, W. *et al.* Mouse Retinal Cell Atlas: Molecular Identification of over Sixty Amacrine Cell Types. *J. Neurosci. Off. J. Soc. Neurosci.* **40**, 5177–5195 (2020).
31. Diamond, J. S. Inhibitory Interneurons in the Retina: Types, Circuitry, and Function. *Annu. Rev. Vis. Sci.* **3**, 1–24 (2017).
32. Grünert, U. & Martin, P. R. Cell types and cell circuits in human and non-human primate retina. *Prog. Retin. Eye Res.* **78**, 100844 (2020).
33. Bringmann, A. *et al.* Cellular signaling and factors involved in Müller cell gliosis: Neuroprotective and detrimental effects. *Prog. Retin. Eye Res.* **28**, 423–451 (2009).
34. Vecino, E., Rodriguez, F. D., Ruzafa, N., Pereiro, X. & Sharma, S. C. Glia–neuron interactions in the mammalian retina. *Prog. Retin. Eye Res.* **51**, 1–40 (2016).
35. Kim, U. S., Mahroo, O. A., Mollon, J. D. & Yu-Wai-Man, P. Retinal Ganglion Cells—Diversity of Cell Types and Clinical Relevance. *Front. Neurol.* **12**, (2021).
36. Sanes, J. R. & Masland, R. H. The Types of Retinal Ganglion Cells: Current Status and Implications for Neuronal Classification. *Annu. Rev. Neurosci.* **38**, 221–246 (2015).
37. Hattar, S., Liao, H. W., Takao, M., Berson, D. M. & Yau, K. W. Melanopsin-containing retinal ganglion cells: architecture, projections, and intrinsic photosensitivity. *Science* **295**, 1065–1070 (2002).
38. Hastings, M. H., Maywood, E. S. & Brancaccio, M. Generation of circadian rhythms in the suprachiasmatic nucleus. *Nat. Rev. Neurosci.* **19**, 453–469 (2018).
39. Schmidt, T. M. *et al.* A Role for Melanopsin in Alpha Retinal Ganglion Cells and Contrast Detection. *Neuron* **82**, 781–788 (2014).
40. Zhang, Y., Kim, I.-J., Sanes, J. R. & Meister, M. The most numerous ganglion cell type of the mouse retina is a selective feature detector. *Proc. Natl. Acad. Sci. U. S. A.* **109**, E2391–E2398 (2012).
41. Fuhrmann, S. Eye Morphogenesis and Patterning of the Optic Vesicle. *Curr. Top. Dev. Biol.* **93**, 61–84 (2010).
42. Heavner, W. & Pevny, L. Eye Development and Retinogenesis. *Cold Spring Harb. Perspect. Biol.* **4**, a008391 (2012).
43. Kevany, B. M. & Palczewski, K. Phagocytosis of Retinal Rod and Cone Photoreceptors. *Physiol. Bethesda Md* **25**, 8–15 (2010).
44. Young, R. W. & Bok, D. PARTICIPATION OF THE RETINAL PIGMENT EPITHELIUM IN THE ROD OUTER SEGMENT RENEWAL PROCESS. *J. Cell Biol.* **42**, 392–403 (1969).
45. McBee, J. K., Van Hooser, J. P., Jang, G.-F. & Palczewski||, K. Isomerization of 11-cis-Retinoids to All-trans-retinoids in Vitro and in Vivo. *J. Biol. Chem.* **276**, 48483–48493 (2001).
46. Travis, G. H., Kaylor, J. & Yuan, Q. Analysis of the Retinoid Isomerase Activities in the Retinal Pigment Epithelium and Retina. in *Retinoids: Methods and Protocols* (eds. Sun, H. & Travis, G. H.) 329–339 (Humana Press, 2010). doi:10.1007/978-1-60327-325-1_19.
47. Tham, Y.-C. *et al.* Global prevalence of glaucoma and projections of glaucoma burden through 2040: a systematic review and meta-analysis. *Ophthalmology* **121**, 2081–2090 (2014).
48. K. Schuster, A., Erb, C., M. Hoffmann, E., Dietlein, T. & Pfeiffer, N. The Diagnosis and Treatment of Glaucoma. *Dtsch. Ärztebl. Int.* **117**, 225–234 (2020).

49. Hood, D. C. Does Retinal Ganglion Cell Loss Precede Visual Field Loss in Glaucoma? *J. Glaucoma* **28**, 945–951 (2019).
50. Waisberg, E. & Micieli, J. A. Neuro-Ophthalmological Optic Nerve Cupping: An Overview. *Eye Brain* **13**, 255–268 (2021).
51. Weinreb, R. N., Aung, T. & Medeiros, F. A. The Pathophysiology and Treatment of Glaucoma: A Review. *JAMA* **311**, 1901 (2014).
52. Levene, R. Z. Low tension glaucoma. Part II. Clinical characteristics and pathogenesis. *Ann. Ophthalmol.* **12**, 1383 (1980).
53. Levene, R. Z. Low tension glaucoma: a critical review and new material. *Surv. Ophthalmol.* **24**, 621–664 (1980).
54. Goel, M., Picciani, R. G., Lee, R. K. & Bhattacharya, S. K. Aqueous Humor Dynamics: A Review. *Open Ophthalmol. J.* **4**, 52–59 (2010).
55. Sunderland, D. K. & Sapra, A. Physiology, Aqueous Humor Circulation. in *StatPearls* (StatPearls Publishing, 2023).
56. Tamm, E. R. & Fuchshofer, R. What Increases Outflow Resistance in Primary Open-angle Glaucoma? *Surv. Ophthalmol.* **52**, S101–S104 (2007).
57. Kwon, Y. H., Fingert, J. H., Kuehn, M. H. & Alward, W. L. M. Primary Open-Angle Glaucoma. *N. Engl. J. Med.* **360**, 1113–1124 (2009).
58. Khazaeni, B. & Khazaeni, L. Acute Closed Angle Glaucoma. in *StatPearls* (StatPearls Publishing, 2023).
59. Zhang, J. *et al.* Leber's hereditary optic neuropathy (LHON)-associated ND5 12338T > C mutation altered the assembly and function of complex I, apoptosis and mitophagy. *Hum. Mol. Genet.* **27**, 1999–2011 (2018).
60. Savontaus, M.-L. mtDNA mutations in Leber's hereditary optic neuropathy. *Biochim. Biophys. Acta BBA - Mol. Basis Dis.* **1271**, 261–263 (1995).
61. van de Wal, M. A. E. *et al.* Ndufs4 knockout mouse models of Leigh syndrome: pathophysiology and intervention. *Brain* **145**, 45–63 (2021).
62. Kruse, S. E. *et al.* Mice with Mitochondrial Complex I Deficiency Develop a Fatal Encephalomyopathy. *Cell Metab.* **7**, 312–320 (2008).
63. Yu, A. K. *et al.* Mitochondrial complex I deficiency leads to inflammation and retinal ganglion cell death in the Ndufs4 mouse. *Hum. Mol. Genet.* **24**, 2848–2860 (2015).
64. Avrutsky, M. I., Lawson, J. M., Smart, J. E., Chen, C. W. & Troy, C. M. Noninvasive Ophthalmic Imaging Measures Retinal Degeneration and Vision Deficits in Ndufs4−/− Mouse Model of Mitochondrial Complex I Deficiency. *Transl. Vis. Sci. Technol.* **11**, 5 (2022).
65. Maghami, M. H., Sodagar, A. M., Lashay, A., Riazi-Esfahani, H. & Riazi-Esfahani, M. Visual Prostheses: The Enabling Technology to Give Sight to the Blind. *J. Ophthalmic Vis. Res.* **9**, 494–505 (2014).
66. Sperry, R. W. Restoration of vision after crossing of optic nerves and after contralateral transplantation of eye. *J. Neurophysiol.* **8**, 15–28 (1945).
67. Harvey, B. M., Baxter, M. & Granato, M. Optic nerve regeneration in larval zebrafish exhibits spontaneous capacity for retinotopic but not tectum specific axon targeting. *PLoS ONE* **14**, e0218667 (2019).
68. Fague, L. & Marsh-Armstrong, N. Dual leucine zipper kinase is necessary for retinal ganglion cell axonal regeneration in Xenopus laevis. *PNAS Nexus* **2**, pgad109 (2023).
69. Calkins, D. J., Pekny, M., Cooper, M. L. & Benowitz, L. The challenge of regenerative therapies for the optic nerve in glaucoma. *Exp. Eye Res.* **157**, 28–33 (2017).
70. He, Z. & Jin, Y. Intrinsic Control of Axon Regeneration. *Neuron* **90**, 437–451 (2016).
71. Goldberg, J. L. *et al.* Retinal ganglion cells do not extend axons by default: promotion by neurotrophic signaling and electrical activity. *Neuron* **33**, 689–702 (2002).

72. Chen, D. F., Jhaveri, S. & Schneider, G. E. Intrinsic changes in developing retinal neurons result in regenerative failure of their axons. *Proc. Natl. Acad. Sci. U. S. A.* **92**, 7287–7291 (1995).
73. Park, K. K. *et al.* Promoting Axon Regeneration in the Adult CNS by Modulation of the PTEN/mTOR Pathway. *Science* **322**, 963–966 (2008).
74. Kurimoto, T. *et al.* Long-Distance Axon Regeneration in the Mature Optic Nerve: Contributions of Oncomodulin, cAMP, and pten Gene Deletion. *J. Neurosci.* **30**, 15654–15663 (2010).
75. Duan, X. *et al.* Subtype-Specific Regeneration of Retinal Ganglion Cells following Axotomy: Effects of Osteopontin and mTOR Signaling. *Neuron* **85**, 1244–1256 (2015).
76. Mak, H. K., Ng, S. H., Ren, T., Ye, C. & Leung, C. K.-S. Impact of PTEN/SOCS3 deletion on amelioration of dendritic shrinkage of retinal ganglion cells after optic nerve injury. *Exp. Eye Res.* **192**, 107938 (2020).
77. Pearson, R. A. *et al.* Restoration of vision after transplantation of photoreceptors. *Nature* **485**, 99–103 (2012).
78. Chao, J. R. *et al.* Transplantation of Human Embryonic Stem Cell-Derived Retinal Cells into the Subretinal Space of a Non-Human Primate. *Transl. Vis. Sci. Technol.* **6**, 4 (2017).
79. Lamba, D. A., Gust, J. & Reh, T. A. Transplantation of Human Embryonic Stem Cell-Derived Photoreceptors Restores Some Visual Function in Crx-Deficient Mice. *Cell Stem Cell* **4**, 73–79 (2009).
80. MacLaren, R. E. *et al.* Retinal repair by transplantation of photoreceptor precursors. *Nature* **444**, 203–207 (2006).
81. Waldron, P. V. *et al.* Transplanted Donor- or Stem Cell-Derived Cone Photoreceptors Can Both Integrate and Undergo Material Transfer in an Environment-Dependent Manner. *Stem Cell Rep.* **10**, 406–421 (2018).
82. Heegaard, S., Jensen, O. A. & Prause, J. U. Structure and composition of the inner limiting membrane of the retina. *Graefes Arch. Clin. Exp. Ophthalmol.* **224**, 355–360 (1986).
83. Peynshaert, K., Devoldere, J., Minnaert, A.-K., De Smedt, S. C. & Remaut, K. Morphology and Composition of the Inner Limiting Membrane: Species-Specific Variations and Relevance toward Drug Delivery Research. *Curr. Eye Res.* **44**, 465–475 (2019).
84. de Vries, Victor. A., Bassil, F. L. & Ramdas, Wishal. D. The effects of intravitreal injections on intraocular pressure and retinal nerve fiber layer: a systematic review and meta-analysis. *Sci. Rep.* **10**, 13248 (2020).
85. Radius, R. L. & de Bruin, J. Anatomy of the retinal nerve fiber layer. *Invest. Ophthalmol. Vis. Sci.* **21**, 745–749 (1981).
86. Hankin, M. H. & Lund, R. D. Directed early axonal outgrowth from retinal transplants into host rat brains. *J. Neurobiol.* **21**, 1202–1218 (1990).
87. Hankin, M. H. & Lund, R. D. Specific target-directed axonal outgrowth from transplanted embryonic rodent retinae into neonatal rat superior colliculus. *Brain Res.* **408**, 344–348 (1987).
88. Hankin, M. H. & Lund, R. D. Role of the target in directing the outgrowth of retinal axons: transplants reveal surface-related and surface-independent cues. *J. Comp. Neurol.* **263**, 455–466 (1987).
89. Baden, T., Euler, T. & Berens, P. Understanding the retinal basis of vision across species. *Nat. Rev. Neurosci.* **21**, 5–20 (2020).
90. Martinez-Morales, J.-R., Cavodeassi, F. & Bovolenta, P. Coordinated Morphogenetic Mechanisms Shape the Vertebrate Eye. *Front. Neurosci.* **11**, 721 (2017).
91. Casey, M. A., Lusk, S. & Kwan, K. M. Eye Morphogenesis in Vertebrates. *Annu. Rev. Vis. Sci.* **9**, null (2023).
92. Tam, P. P. L. & Behringer, R. R. Mouse gastrulation: the formation of a mammalian body plan. *Mech. Dev.* **68**, 3–25 (1997).

93. Diacou, R. *et al.* Cell fate decisions, transcription factors and signaling during early retinal development. *Prog. Retin. Eye Res.* **91**, 101093 (2022).
94. Bosze, B. *et al.* Multiple roles for Pax2 in the embryonic mouse eye. *Dev. Biol.* **472**, 18–29 (2021).
95. Zhang, X., Leavey, P., Appel, H., Makrides, N. & Blackshaw, S. Molecular mechanisms controlling vertebrate retinal patterning, neurogenesis, and cell fate specification. *Trends Genet.* **0**, (2023).
96. Bassett, E. A. & Wallace, V. A. Cell fate determination in the vertebrate retina. *Trends Neurosci.* **35**, 565–573 (2012).
97. Turner, D. L., Snyder, E. Y. & Cepko, C. L. Lineage-independent determination of cell type in the embryonic mouse retina. *Neuron* **4**, 833–845 (1990).
98. Turner, D. L. & Cepko, C. L. A common progenitor for neurons and glia persists in rat retina late in development. *Nature* **328**, 131–136 (1987).
99. Carter-Dawson, L. D. & LaVail, M. M. Rods and cones in the mouse retina. II. Autoradiographic analysis of cell generation using tritiated thymidine. *J. Comp. Neurol.* **188**, 263–272 (1979).
100. Nguyen-Ba-Charvet, K. T. & Rebsam, A. Neurogenesis and Specification of Retinal Ganglion Cells. *Int. J. Mol. Sci.* **21**, 451 (2020).
101. Cepko, C. L., Austin, C. P., Yang, X., Alexiades, M. & Ezzeddine, D. Cell fate determination in the vertebrate retina. *Proc. Natl. Acad. Sci. U. S. A.* **93**, 589–595 (1996).
102. Cayouette, M., Barres, B. A. & Raff, M. Importance of Intrinsic Mechanisms in Cell Fate Decisions in the Developing Rat Retina. *Neuron* **40**, 897–904 (2003).
103. Oliveira-Valença, V. M., Bosco, A., Vetter, M. L. & Silveira, M. S. On the Generation and Regeneration of Retinal Ganglion Cells. *Front. Cell Dev. Biol.* **8**, 581136 (2020).
104. La Torre, A., Georgi, S. & Reh, T. A. Conserved microRNA pathway regulates developmental timing of retinal neurogenesis. *Proc. Natl. Acad. Sci.* **110**, E2362–E2370 (2013).
105. He, J. *et al.* How Variable Clones Build an Invariant Retina. *Neuron* **75**, 786–798 (2012).
106. Gomes, F. L. A. F. *et al.* Reconstruction of rat retinal progenitor cell lineages in vitro reveals a surprising degree of stochasticity in cell fate decisions. *Development* **138**, 227–235 (2011).
107. Prasov, L. & Glaser, T. Dynamic expression of ganglion cell markers in retinal progenitors during the terminal cell cycle. *Mol. Cell. Neurosci.* **50**, 160–168 (2012).
108. Brown, N. L., Patel, S., Brzezinski, J. & Glaser, T. Math5 is required for retinal ganglion cell and optic nerve formation. *Dev. Camb. Engl.* **128**, 2497–2508 (2001).
109. Gan, L. *et al.* POU domain factor Brn-3b is required for the development of a large set of retinal ganglion cells. *Proc. Natl. Acad. Sci. U. S. A.* **93**, 3920–3925 (1996).
110. Wu, F. *et al.* Two transcription factors, Pou4f2 and Isl1, are sufficient to specify the retinal ganglion cell fate. *Proc. Natl. Acad. Sci. U. S. A.* **112**, E1559-1568 (2015).
111. Triplett, J. W. *et al.* Dendritic and axonal targeting patterns of a genetically-specified class of retinal ganglion cells that participate in image-forming circuits. *Neural Develop.* **9**, 2 (2014).
112. Zheng, D. *et al.* Pou4f2-GFP knock-in mouse line: A model for studying retinal ganglion cell development. *Genes. N. Y. N 2000* **54**, 534–541 (2016).
113. Xiang, M. Requirement for Brn-3b in early differentiation of postmitotic retinal ganglion cell precursors. *Dev. Biol.* **197**, 155–169 (1998).
114. Miltner, A. M. *et al.* A Novel Reporter Mouse Uncovers Endogenous Brn3b Expression. *Int. J. Mol. Sci.* **20**, 2903 (2019).
115. Icha, J., Kunath, C., Rocha-Martins, M. & Norden, C. Independent modes of ganglion cell translocation ensure correct lamination of the zebrafish retina. *J. Cell Biol.* **215**, 259–275 (2016).

116. Amini, R., Rocha-Martins, M. & Norden, C. Neuronal Migration and Lamination in the Vertebrate Retina. *Front. Neurosci.* **11**, 742 (2018).
117. Reh, T. A. & Kljavin, I. J. Age of differentiation determines rat retinal germinal cell phenotype: induction of differentiation by dissociation. *J. Neurosci. Off. J. Soc. Neurosci.* **9**, 4179–4189 (1989).
118. Wang, Y., Dakubo, G. D., Thurig, S., Mazerolle, C. J. & Wallace, V. A. Retinal ganglion cell-derived sonic hedgehog locally controls proliferation and the timing of RGC development in the embryonic mouse retina. *Dev. Camb. Engl.* **132**, 5103–5113 (2005).
119. Miesfeld, J. B. *et al.* The Atoh7 remote enhancer provides transcriptional robustness during retinal ganglion cell development. *Proc. Natl. Acad. Sci. U. S. A.* **117**, 21690–21700 (2020).
120. Prasov, L., Nagy, M., Rudolph, D. D. & Glaser, T. Math5 (Atoh7) gene dosage limits retinal ganglion cell genesis: *NeuroReport* **23**, 631–634 (2012).
121. Brown, N. L., Dagenais, S. L., Chen, C.-M. & Glaser, T. Molecular characterization and mapping of ATOH7, a human atonal homolog with a predicted role in retinal ganglion cell development. *Mamm. Genome Off. J. Int. Mamm. Genome Soc.* **13**, 95–101 (2002).
122. Riesenberg, A. N. *et al.* Pax6 regulation of Math5 during mouse retinal neurogenesis. *Genes. N. Y. N 2000* **47**, 175–187 (2009).
123. Vitorino, M. *et al.* Vsx2 in the zebrafish retina: restricted lineages through derepression. *Neural Develop.* **4**, 14 (2009).
124. Lee, H. Y. *et al.* Multiple requirements for Hes1 during early eye formation. *Dev. Biol.* **284**, 464–478 (2005).
125. Hufnagel, R. B., Le, T. T., Riesenberg, A. L. & Brown, N. L. Neurog2 controls the leading edge of neurogenesis in the mammalian retina. *Dev. Biol.* **340**, 490–503 (2010).
126. Zhou, H., Yoshioka, T. & Nathans, J. Retina-derived POU-domain factor-1: a complex POU-domain gene implicated in the development of retinal ganglion and amacrine cells. *J. Neurosci.* **16**, 2261–2274 (1996).
127. Erkman, L. *et al.* Role of transcription factors a Brn-3.1 and Brn-3.2 in auditory and visual system development. *Nature* **381**, 603–606 (1996).
128. Pak, W., Hindges, R., Lim, Y.-S., Pfaff, S. L. & O'Leary, D. D. M. Magnitude of binocular vision controlled by islet-2 repression of a genetic program that specifies laterality of retinal axon pathfinding. *Cell* **119**, 567–578 (2004).
129. Pfaff, S. L., Mendelsohn, M., Stewart, C. L., Edlund, T. & Jessell, T. M. Requirement for LIM homeobox gene Isl1 in motor neuron generation reveals a motor neuron-dependent step in interneuron differentiation. *Cell* **84**, 309–320 (1996).
130. Galli-Resta, L., Resta, G., Tan, S.-S. & Reese, B. E. Mosaics of Islet-1-Expressing Amacrine Cells Assembled by Short-Range Cellular Interactions. *J. Neurosci.* **17**, 7831–7838 (1997).
131. Tsuchida, T. *et al.* Topographic organization of embryonic motor neurons defined by expression of LIM homeobox genes. *Cell* **79**, 957–970 (1994).
132. Brown, A. *et al.* Topographic mapping from the retina to the midbrain is controlled by relative but not absolute levels of EphA receptor signaling. *Cell* **102**, 77–88 (2000).
133. Herrera, E. *et al.* Zic2 patterns binocular vision by specifying the uncrossed retinal projection. *Cell* **114**, 545–557 (2003).
134. Williams, D. R. Imaging single cells in the living retina. *Vision Res.* **51**, 1379–1396 (2011).
135. Miller, D. T., Williams, D. R., Morris, G. M. & Liang, J. Images of cone photoreceptors in the living human eye. *Vision Res.* **36**, 1067–1079 (1996).
136. Elliott, A. D. Confocal Microscopy: Principles and Modern Practices. *Curr. Protoc. Cytom.* **92**, e68 (2020).
137. Fischer, J., Otto, T., Delori, F., Pace, L. & Staurenghi, G. Scanning Laser Ophthalmoscopy (SLO). in *High Resolution Imaging in Microscopy and Ophthalmology: New Frontiers in Biomedical Optics* (ed. Bille, J. F.) (Springer, 2019).

138. Seeliger, M. W. *et al.* In vivo confocal imaging of the retina in animal models using scanning laser ophthalmoscopy. *Vision Res.* **45**, 3512–3519 (2005).
139. Zawadzki, R. J. *et al.* Adaptive-optics SLO imaging combined with widefield OCT and SLO enables precise 3D localization of fluorescent cells in the mouse retina. *Biomed. Opt. Express* **6**, 2191 (2015).
140. Zhang, P. *et al.* In vivo wide-field multispectral scanning laser ophthalmoscopy–optical coherence tomography mouse retinal imager: longitudinal imaging of ganglion cells, microglia, and Müller glia, and mapping of the mouse retinal and choroidal vasculature. *J. Biomed. Opt.* **20**, 126005 (2015).
141. Zhang, P. *et al.* Adaptive optics scanning laser ophthalmoscopy and optical coherence tomography (AO-SLO-OCT) system for in vivo mouse retina imaging. *Biomed. Opt. Express* **14**, 299–314 (2022).
142. Geng, Y. *et al.* Adaptive optics retinal imaging in the living mouse eye. *Biomed. Opt. Express* **3**, 715–734 (2012).
143. Schmucker, C. & Schaeffel, F. A paraxial schematic eye model for the growing C57BL/6 mouse. *Vision Res.* **44**, 1857–1867 (2004).
144. Remtulla, S. & Hallett, P. E. A schematic eye for the mouse, and comparisons with the rat. *Vision Res.* **25**, 21–31 (1985).
145. Geng, Y. *et al.* Optical properties of the mouse eye. *Biomed. Opt. Express* **2**, 717–738 (2011).
146. Huang, D. *et al.* Optical Coherence Tomography. *Science* **254**, 1178–1181 (1991).
147. Aumann, S., Donner, S., Fischer, J. & Müller, F. Optical Coherence Tomography (OCT): Principle and Technical Realization. in *High Resolution Imaging in Microscopy and Ophthalmology: New Frontiers in Biomedical Optics* (ed. Bille, J. F.) (Springer, 2019).
148. Fujimoto, J. G., Pitris, C., Boppart, S. A. & Brezinski, M. E. Optical Coherence Tomography: An Emerging Technology for Biomedical Imaging and Optical Biopsy. *Neoplasia N. Y. N* **2**, 9–25 (2000).
149. Brinkmann, C. K., Wolf, S. & Wolf-Schnurrbusch, U. E. K. Multimodal imaging in macular diagnostics: combined OCT-SLO improves therapeutical monitoring. *Graefes Arch. Clin. Exp. Ophthalmol. Albrecht Von Graefes Arch. Klin. Exp. Ophthalmol.* **246**, 9–16 (2008).
150. Song, W. *et al.* Integrating photoacoustic ophthalmoscopy with scanning laser ophthalmoscopy, optical coherence tomography, and fluorescein angiography for a multimodal retinal imaging platform. *J. Biomed. Opt.* **17**, 061206 (2012).
151. Malone, J. D. *et al.* Simultaneous multimodal ophthalmic imaging using swept-source spectrally encoded scanning laser ophthalmoscopy and optical coherence tomography. *Biomed. Opt. Express* **8**, 193–206 (2017).
152. de Carlo, T. E., Romano, A., Waheed, N. K. & Duker, J. S. A review of optical coherence tomography angiography (OCTA). *Int. J. Retina Vitr.* **1**, 5 (2015).
153. Waddington, C. H. *The Strategy of the Genes*. (Routledge, 2014).
154. Becker, A. J., McCULLOCH, E. A. & Till, J. E. Cytological Demonstration of the Clonal Nature of Spleen Colonies Derived from Transplanted Mouse Marrow Cells. *Nature* **197**, 452–454 (1963).
155. Siminovitch, L., Mcculloch, E. A. & Till, J. E. THE DISTRIBUTION OF COLONY-FORMING CELLS AMONG SPLEEN COLONIES. *J. Cell. Comp. Physiol.* **62**, 327–336 (1963).
156. Takahashi, K. & Yamanaka, S. Induction of Pluripotent Stem Cells from Mouse Embryonic and Adult Fibroblast Cultures by Defined Factors. *Cell* **126**, 663–676 (2006).
157. Briggs, R. & King, T. J. Transplantation of living nuclei from blastula cells into enucleated frogs' eggs *. *Proc. Natl. Acad. Sci.* **38**, 455–463 (1952).
158. Gurdon, J. B. The Developmental Capacity of Nuclei Taken from Differentiating Endoderm Cells of Xenopus Laevis. *Development* **8**, 505–526 (1960).

159. Gurdon, J. B. The Developmental Capacity of Nuclei taken from Intestinal Epithelium Cells of Feeding Tadpoles. *Development* **10**, 622–640 (1962).
160. Liu, C., Oikonomopoulos, A., Sayed, N. & Wu, J. C. Modeling human diseases with induced pluripotent stem cells: from 2D to 3D and beyond. *Development* **145**, dev156166 (2018).
161. de Figueiredo, C. S. *et al.* Insulin-like growth factor-1 stimulates retinal cell proliferation via activation of multiple signaling pathways. *Curr. Res. Neurobiol.* **4**, 100068 (2023).
162. Gill, K. P., Hewitt, A. W., Davidson, K. C., Pébay, A. & Wong, R. C. B. Methods of Retinal Ganglion Cell Differentiation From Pluripotent Stem Cells. *Transl. Vis. Sci. Technol.* **3**, 7 (2014).
163. Eiraku, M. *et al.* Self-organizing optic-cup morphogenesis in three-dimensional culture. *Nature* **472**, 51–56 (2011).
164. Capowski, E. E. *et al.* Reproducibility and staging of 3D human retinal organoids across multiple pluripotent stem cell lines. *Dev. Camb. Engl.* **146**, dev171686 (2019).
165. Spin∞: an updated miniaturized spinning bioreactor design for the generation of human cerebral organoids from pluripotent stem cells | Elsevier Enhanced Reader. https://reader.elsevier.com/reader/sd/pii/S2468067219300422?token=4A7057636B97A9E68CF5178983D79F4F7F99B45EF2E3EF0CD9EAE2558040CAC7B01FB4DF9B494F13CB2802B8F11D277F&originRegion=us-east-1&originCreation=20220119231157 doi:10.1016/j.ohx.2019.e00084.
166. Vergara, M. N. *et al.* Three-dimensional automated reporter quantification (3D-ARQ) technology enables quantitative screening in retinal organoids. *Dev. Camb. Engl.* **144**, 3698–3705 (2017).
167. Eldred, K. C. *et al.* Thyroid hormone signaling specifies cone subtypes in human retinal organoids. *Science* **362**, eaau6348 (2018).
168. VanderWall, K. B. *et al.* Retinal Ganglion Cells With a Glaucoma OPTN(E50K) Mutation Exhibit Neurodegenerative Phenotypes when Derived from Three-Dimensional Retinal Organoids. *Stem Cell Rep.* **15**, 52–66 (2020).
169. Gao, M.-L. *et al.* Patient-Specific Retinal Organoids Recapitulate Disease Features of Late-Onset Retinitis Pigmentosa. *Front. Cell Dev. Biol.* **8**, 128 (2020).
170. Pereiro, X., Miltner, A. M., La Torre, A. & Vecino, E. Effects of Adult Müller Cells and Their Conditioned Media on the Survival of Stem Cell-Derived Retinal Ganglion Cells. *Cells* **9**, 1759 (2020).
171. Rodieck, R. W. *The vertebrate retina: Principles of structure and function*. 1044 (W. H. Freeman, 1973).
172. Rheaume, B. A. *et al.* Single cell transcriptome profiling of retinal ganglion cells identifies cellular subtypes. *Nat. Commun.* **9**, 2759 (2018).
173. Tran, N. M. *et al.* Single-cell profiles of retinal ganglion cells differing in resilience to injury reveal neuroprotective genes. *Neuron* **104**, 1039-1055.e12 (2019).
174. Shekhar, K., Whitney, I. E., Butrus, S., Peng, Y.-R. & Sanes, J. R. Diversification of multipotential postmitotic mouse retinal ganglion cell precursors into discrete types. *eLife* **11**, e73809 (2022).
175. Hahn, J. *et al.* Evolution of neuronal cell classes and types in the vertebrate retina. 2023.04.07.536039 Preprint at https://doi.org/10.1101/2023.04.07.536039 (2023).
176. Curcio, C. A., Sloan, K. R., Kalina, R. E. & Hendrickson, A. E. Human photoreceptor topography. *J. Comp. Neurol.* **292**, 497–523 (1990).
177. Dworak, D. P. & Nichols, J. A review of optic neuropathies. *Dis. Mon.* **60**, 276–281 (2014).
178. Causes of blindness and vision impairment in 2020 and trends over 30 years, and prevalence of avoidable blindness in relation to VISION 2020: the Right to Sight: an analysis for the Global Burden of Disease Study. *Lancet Glob. Health* **9**, e144–e160 (2020).

179. Chen, X. *et al.* Antiapoptotic and Trophic Effects of Dominant-Negative Forms of Dual Leucine Zipper Kinase in Dopamine Neurons of the Substantia Nigra In Vivo. *J. Neurosci.* **28**, 672–680 (2008).
180. Miller, B. R. *et al.* A dual leucine kinase–dependent axon self-destruction program promotes Wallerian degeneration. *Nat. Neurosci.* **12**, 387–389 (2009).
181. Watkins, T. A. *et al.* DLK initiates a transcriptional program that couples apoptotic and regenerative responses to axonal injury. *Proc. Natl. Acad. Sci. U. S. A.* **110**, 4039–4044 (2013).
182. Welsbie, D. S. *et al.* Functional genomic screening identifies dual leucine zipper kinase as a key mediator of retinal ganglion cell death. *Proc. Natl. Acad. Sci.* **110**, 4045–4050 (2013).
183. Pozniak, C. D. *et al.* Dual leucine zipper kinase is required for excitotoxicity-induced neuronal degeneration. *J. Exp. Med.* **210**, 2553–2567 (2013).
184. Welsbie, D. S. *et al.* Targeted disruption of dual leucine zipper kinase and leucine zipper kinase promotes neuronal survival in a model of diffuse traumatic brain injury. *Mol. Neurodegener.* **14**, 44 (2019).
185. Shin, J. E. *et al.* Dual leucine zipper kinase is required for retrograde injury signaling and axonal regeneration. *Neuron* **74**, 1015–1022 (2012).
186. Patel, A. K. *et al.* Inhibition of GCK-IV kinases dissociates cell death and axon regeneration in CNS neurons. *Proc. Natl. Acad. Sci.* **117**, 33597–33607 (2020).
187. Sun, F. *et al.* Sustained axon regeneration induced by co-deletion of PTEN and SOCS3. *Nature* **480**, 372–375 (2011).
188. Almasieh, M., Wilson, A. M., Morquette, B., Cueva Vargas, J. L. & Di Polo, A. The molecular basis of retinal ganglion cell death in glaucoma. *Prog. Retin. Eye Res.* **31**, 152–181 (2012).
189. Anderson, D. R. & Normal Tension Glaucoma Study. Collaborative normal tension glaucoma study. *Curr. Opin. Ophthalmol.* **14**, 86–90 (2003).
190. Wareham, L. K. *et al.* Solving neurodegeneration: common mechanisms and strategies for new treatments. *Mol. Neurodegener.* **17**, 23 (2022).
191. Miltner, A. M. & La Torre, A. Retinal Ganglion Cell Replacement: Current Status and Challenges Ahead: Retinal Ganglion Cell Replacement. *Dev. Dyn.* **248**, 118–128 (2019).
192. Oswald, J., Kegeles, E., Minelli, T., Volchkov, P. & Baranov, P. Transplantation of miPSC/mESC-derived retinal ganglion cells into healthy and glaucomatous retinas. *Mol. Ther. Methods Clin. Dev.* **21**, 180–198 (2021).
193. Hertz, J. *et al.* Survival and Integration of Developing and Progenitor-Derived Retinal Ganglion Cells following Transplantation. *Cell Transplant.* **23**, 855–872 (2014).
194. Venugopalan, P. *et al.* Transplanted neurons integrate into adult retinas and respond to light. *Nat. Commun.* **7**, 10472 (2016).
195. Wu, Y.-R. *et al.* Transplanted Mouse Embryonic Stem Cell–Derived Retinal Ganglion Cells Integrate and Form Synapses in a Retinal Ganglion Cell-Depleted Mouse Model. *Invest. Ophthalmol. Vis. Sci.* **62**, 26 (2021).
196. Johnson, T. V., Bull, N. D. & Martin, K. R. Identification of Barriers to Retinal Engraftment of Transplanted Stem Cells. *Investig. Opthalmology Vis. Sci.* **51**, 960 (2010).
197. Kramer, J., Chirco, K. R. & Lamba, D. A. Immunological Considerations for Retinal Stem Cell Therapy. in *Pluripotent Stem Cells in Eye Disease Therapy* (ed. Bharti, K.) 99–119 (Springer International Publishing, 2019). doi:10.1007/978-3-030-28471-8_4.
198. Norte-Muñoz, M. *et al.* Immune recognition of syngeneic, allogeneic and xenogeneic stromal cell transplants in healthy retinas. *Stem Cell Res. Ther.* **13**, 430 (2022).
199. Jager, R. D., Aiello, L. P., Patel, S. C. & Cunningham, E. T. J. RISKS OF INTRAVITREOUS INJECTION: A COMPREHENSIVE REVIEW. *RETINA* **24**, 676 (2004).
200. Aiello, L. P. *et al.* EVOLVING GUIDELINES FOR INTRAVITREOUS INJECTIONS. *RETINA* **24**, S3 (2004).

201. Chen, G. Y. & Nuñez, G. Sterile inflammation: sensing and reacting to damage. *Nat. Rev. Immunol.* **10**, 826–837 (2010).
202. Amor, S. *et al.* Inflammation in neurodegenerative diseases – an update. *Immunology* **142**, 151–166 (2014).
203. Russo, R. *et al.* Retinal ganglion cell death in glaucoma: Exploring the role of neuroinflammation. *Eur. J. Pharmacol.* **787**, 134–142 (2016).
204. Benhar, Inbal, London, A. & Schwartz, M. The privileged immunity of immune privileged organs: the case of the eye. *Front. Immunol.* **3**, (2012).
205. Medawar, P. B. Immunity to Homologous Grafted Skin. III. The Fate of Skin Homographs Transplanted to the Brain, to Subcutaneous Tissue, and to the Anterior Chamber of the Eye. *Br. J. Exp. Pathol.* **29**, 58–69 (1948).
206. Niederkorn, J. Y. The immunopathology of intraocular tumour rejection. *Eye* **5**, 186–192 (1991).
207. Streilein, J. W. Ocular immune privilege: therapeutic opportunities from an experiment of nature. *Nat. Rev. Immunol.* **3**, 879–889 (2003).
208. Murakami, Y., Ishikawa, K., Nakao, S. & Sonoda, K.-H. Innate immune response in retinal homeostasis and inflammatory disorders. *Prog. Retin. Eye Res.* **74**, 100778 (2020).
209. Nimmerjahn, A., Kirchhoff, F. & Helmchen, F. Resting Microglial Cells Are Highly Dynamic Surveillants of Brain Parenchyma in Vivo. *Science* **308**, 1314–1318 (2005).
210. Karlstetter, M. *et al.* Retinal microglia: Just bystander or target for therapy? *Prog. Retin. Eye Res.* **45**, 30–57 (2015).
211. Hanisch, U.-K. & Kettenmann, H. Microglia: active sensor and versatile effector cells in the normal and pathologic brain. *Nat. Neurosci.* **10**, 1387–1394 (2007).
212. Rashid, K., Akhtar-Schaefer, I. & Langmann, T. Microglia in Retinal Degeneration. *Front. Immunol.* **10**, (2019).
213. Szepesi, Z., Manouchehrian, O., Bachiller, S. & Deierborg, T. Bidirectional Microglia–Neuron Communication in Health and Disease. *Front. Cell. Neurosci.* **12**, 323 (2018).
214. Wolf, Y., Yona, S., Kim, K.-W. & Jung, S. Microglia, seen from the CX3CR1 angle. *Front. Cell. Neurosci.* **7**, (2013).
215. Jung, S. *et al.* Analysis of Fractalkine Receptor CX_3 CR1 Function by Targeted Deletion and Green Fluorescent Protein Reporter Gene Insertion. *Mol. Cell. Biol.* **20**, 4106–4114 (2000).
216. Zabel, M. K. *et al.* Microglial phagocytosis and activation underlying photoreceptor degeneration is regulated by CX3CL1-CX3CR1 signaling in a mouse model of retinitis pigmentosa. *Glia* **64**, 1479–1491 (2016).
217. Huang, L., Xu, W. & Xu, G. Transplantation of CX3CL1-expressing mesenchymal stem cells provides neuroprotective and immunomodulatory effects in a rat model of retinal degeneration. *Ocul. Immunol. Inflamm.* **21**, 276–285 (2013).
218. Márquez-Ropero, M., Benito, E., Plaza-Zabala, A. & Sierra, A. Microglial Corpse Clearance: Lessons From Macrophages. *Front. Immunol.* **11**, (2020).
219. Wei, X., Cho, K.-S., Thee, E. F., Jager, M. J. & Chen, D. F. Neuroimmflammation and microglia in glaucoma – time for a paradigm shift. *J. Neurosci. Res.* **97**, 70–76 (2019).
220. Bellver-Landete, V. *et al.* Microglia are an essential component of the neuroprotective scar that forms after spinal cord injury. *Nat. Commun.* **10**, 518 (2019).
221. Kwon, H. S. & Koh, S.-H. Neuroinflammation in neurodegenerative disorders: the roles of microglia and astrocytes. *Transl. Neurodegener.* **9**, 42 (2020).
222. Campbell, M. & Humphries, P. The Blood-Retina Barrier. in *Biology and Regulation of Blood-Tissue Barriers* (ed. Cheng, C. Y.) 70–84 (Springer, 2013). doi:10.1007/978-1-4614-4711-5_3.

223. Jin, N., Gao, L., Fan, X. & Xu, H. Friend or Foe? Resident Microglia vs Bone Marrow-Derived Microglia and Their Roles in the Retinal Degeneration. *Mol. Neurobiol.* **54**, 4094–4112 (2017).
224. Ronning, K. E., Karlen, S. J., Miller, E. B. & Burns, M. E. Molecular profiling of resident and infiltrating mononuclear phagocytes during rapid adult retinal degeneration using single-cell RNA sequencing. *Sci. Rep.* **9**, 4858 (2019).
225. Ronning, K. E., Karlen, S. J. & Burns, M. E. Structural and functional distinctions of co-resident microglia and monocyte-derived macrophages after retinal degeneration. *J. Neuroinflammation* **19**, 299 (2022).
226. Karlen, S. J. *et al.* Monocyte infiltration rather than microglia proliferation dominates the early immune response to rapid photoreceptor degeneration. *J. Neuroinflammation* **15**, 344 (2018).
227. Jiang, S., Kametani, M. & Chen, D. F. Adaptive Immunity: New Aspects of Pathogenesis Underlying Neurodegeneration in Glaucoma and Optic Neuropathy. *Front. Immunol.* **11**, (2020).
228. Ma, W. *et al.* Monocyte infiltration and proliferation reestablish myeloid cell homeostasis in the mouse retina following retinal pigment epithelial cell injury. *Sci. Rep.* **7**, 8433 (2017).
229. Torres-Costa, S. *et al.* Incidence of endophthalmitis after intravitreal injection with and without topical antibiotic prophylaxis. *Eur. J. Ophthalmol.* **31**, 600–606 (2021).
230. Ail, D. *et al.* Systemic and local immune responses to intraocular AAV vector administration in non-human primates. *Mol. Ther. Methods Clin. Dev.* **24**, 306–316 (2022).
231. Cox, J. T., Eliott, D. & Sobrin, L. Inflammatory Complications of Intravitreal Anti-VEGF Injections. *J. Clin. Med.* **10**, 981 (2021).
232. Grzybowski, A. *et al.* 2018 Update on Intravitreal Injections: Euretina Expert Consensus Recommendations. *Ophthalmol. J. Int. Ophtalmol. Int. J. Ophthalmol. Z. Augenheilkd.* **239**, 181–193 (2018).
233. Anderson, W. J. *et al.* Mechanisms of sterile inflammation after intravitreal injection of antiangiogenic drugs: a narrative review. *Int. J. Retina Vitr.* **7**, 37 (2021).
234. Sato, T., Takeuchi, M., Karasawa, Y., Enoki, T. & Ito, M. Intraocular inflammatory cytokines in patients with neovascular age-related macular degeneration before and after initiation of intravitreal injection of anti-VEGF inhibitor. *Sci. Rep.* **8**, 1098 (2018).
235. Bouquet, C. *et al.* Immune Response and Intraocular Inflammation in Patients With Leber Hereditary Optic Neuropathy Treated With Intravitreal Injection of Recombinant Adeno-Associated Virus 2 Carrying the ND4 Gene: A Secondary Analysis of a Phase 1/2 Clinical Trial. *JAMA Ophthalmol.* **137**, 399–406 (2019).
236. Jiang, L. Q., Jorquera, M. & Streilein, J. W. Subretinal space and vitreous cavity as immunologically privileged sites for retinal allografts. *Invest. Ophthalmol. Vis. Sci.* **34**, 3347–3354 (1993).
237. Tassoni, A., Gutteridge, A., Barber, A. C., Osborne, A. & Martin, K. R. Molecular Mechanisms Mediating Retinal Reactive Gliosis Following Bone Marrow Mesenchymal Stem Cell Transplantation. *Stem Cells Dayt. Ohio* **33**, 3006–3016 (2015).
238. Vernon-Roberts, B. The effects of steroid hormones on macrophage activity. *Int. Rev. Cytol.* **25**, 131–159 (1969).
239. Clements, R., Turk, R., Campbell, K. P. & Wright, K. M. Dystroglycan Maintains Inner Limiting Membrane Integrity to Coordinate Retinal Development. *J. Neurosci.* **37**, 8559–8574 (2017).
240. Zhang, K. Y. & Johnson, T. V. The internal limiting membrane: roles in retinal development and implications for emerging ocular therapies. *Exp. Eye Res.* **206**, 108545 (2021).
241. Halfter, W., Dong, S., Dong, A., Eller, A. W. & Nischt, R. Origin and turnover of ECM proteins from the inner limiting membrane and vitreous body. *Eye* **22**, 1207–1213 (2008).

242. Candiello, J., Cole, G. J. & Halfter, W. Age-dependent changes in the structure, composition and biophysical properties of a human basement membrane. *Matrix Biol.* **29**, 402–410 (2010).
243. Chan, F. L., Inoue, S. & Leblond, C. P. The basement membranes of cryofixed or aldehyde-fixed, freeze-substituted tissues are composed of a lamina densa and do not contain a lamina lucida. *Cell Tissue Res.* **273**, 41–52 (1993).
244. Chan, F. L. & Inoue, S. Lamina lucida of basement membrane: an artefact. *Microsc. Res. Tech.* **28**, 48–59 (1994).
245. Zhang, K. Y. *et al.* Role of the Internal Limiting Membrane in Structural Engraftment and Topographic Spacing of Transplanted Human Stem Cell-Derived Retinal Ganglion Cells. *Stem Cell Rep.* **16**, 149–167 (2021).
246. A, C. *et al.* Swelling of the arcuate nerve fiber layer after internal limiting membrane peeling. *Retina Phila. Pa* **32**, (2012).
247. Burda, J. E. & Sofroniew, M. V. Reactive gliosis and the multicellular response to CNS damage and disease. *Neuron* **81**, 229–248 (2014).
248. Jäkel, S. & Dimou, L. Glial Cells and Their Function in the Adult Brain: A Journey through the History of Their Ablation. *Front. Cell. Neurosci.* **11**, (2017).
249. Eng, L. F., Ghirnikar, R. S. & Lee, Y. L. Glial fibrillary acidic protein: GFAP-thirty-one years (1969-2000). *Neurochem. Res.* **25**, 1439–1451 (2000).
250. Yang, Z. & Wang, K. K. W. Glial Fibrillary acidic protein: From intermediate filament assembly and gliosis to neurobiomarker. *Trends Neurosci.* **38**, 364–374 (2015).
251. Potokar, M., Morita, M., Wiche, G. & Jorgačevski, J. The Diversity of Intermediate Filaments in Astrocytes. *Cells* **9**, 1604 (2020).
252. Eddleston, M. & Mucke, L. Molecular profile of reactive astrocytes—Implications for their role in neurologic disease. *Neuroscience* **54**, 15–36 (1993).
253. Chen, K.-Z. *et al.* Vimentin as a potential target for diverse nervous system diseases. *Neural Regen. Res.* **18**, 969 (2023).
254. Pekny, M. *et al.* Abnormal Reaction to Central Nervous System Injury in Mice Lacking Glial Fibrillary Acidic Protein and Vimentin. *J. Cell Biol.* **145**, 503–514 (1999).
255. Menet, V., Prieto, M., Privat, A. & Ribotta, M. G. y. Axonal plasticity and functional recovery after spinal cord injury in mice deficient in both glial fibrillary acidic protein and vimentin genes. *Proc. Natl. Acad. Sci. U. S. A.* **100**, 8999–9004 (2003).
256. Triolo, D. *et al.* Loss of glial fibrillary acidic protein (GFAP) impairs Schwann cell proliferation and delays nerve regeneration after damage. *J. Cell Sci.* **119**, 3981–3993 (2006).
257. Pekny, M. & Pekna, M. Astrocyte intermediate filaments in CNS pathologies and regeneration. *J. Pathol.* **204**, 428–437 (2004).
258. Nakazawa, T. *et al.* Attenuated Glial Reactions and Photoreceptor Degeneration after Retinal Detachment in Mice Deficient in Glial Fibrillary Acidic Protein and Vimentin. *Invest. Ophthalmol. Vis. Sci.* **48**, 2760–2768 (2007).
259. Liu, Z. *et al.* Beneficial Effects of GFAP/Vimentin Reactive Astrocytes for Axonal Remodeling and Motor Behavioral Recovery in Mice after Stroke. *Glia* **62**, 2022–2033 (2014).
260. Kinouchi, R. *et al.* Robust neural integration from retinal transplants in mice deficient in GFAP and vimentin. *Nat. Neurosci.* **6**, 863–868 (2003).
261. Widestrand, Å. *et al.* Increased Neurogenesis and Astrogenesis from Neural Progenitor Cells Grafted in the Hippocampus of GFAP−/−Vim−/− Mice. *Stem Cells* **25**, 2619–2627 (2007).
262. Allison, K., Patel, D. & Alabi, O. Epidemiology of Glaucoma: The Past, Present, and Predictions for the Future. *Cureus* **12**, e11686.

263. Vrathasha, V. *et al.* Transplanted human induced pluripotent stem cells- derived retinal ganglion cells embed within mouse retinas and are electrophysiologically functional. *iScience* **25**, (2022).
264. Luo, Z. *et al.* Directly induced human retinal ganglion cells mimic fetal RGCs and are neuroprotective after transplantation in vivo. *Stem Cell Rep.* (2022) doi:10.1016/j.stemcr.2022.10.011.
265. Wang, S.-T. *et al.* Transplantation of Retinal Progenitor Cells from Optic Cup-Like Structures Differentiated from Human Embryonic Stem Cells In Vitro and In Vivo Generation of Retinal Ganglion-Like Cells. *Stem Cells Dev.* **28**, 258–267 (2019).
266. Watson, A. B. A formula for human retinal ganglion cell receptive field density as a function of visual field location. *J. Vis.* **14**, 15 (2014).
267. Liu, Z., Kurokawa, K., Zhang, F., Lee, J. J. & Miller, D. T. Imaging and quantifying ganglion cells and other transparent neurons in the living human retina. *Proc. Natl. Acad. Sci. U. S. A.* **114**, 12803–12808 (2017).
268. Data - OPTN. *Organ Procurement & Transplantation Network* https://optn.transplant.hrsa.gov/data/.
269. Martin, G. R. Isolation of a pluripotent cell line from early mouse embryos cultured in medium conditioned by teratocarcinoma stem cells. *Proc. Natl. Acad. Sci. U. S. A.* **78**, 7634–7638 (1981).
270. Thomson, J. A. *et al.* Embryonic stem cell lines derived from human blastocysts. *Science* **282**, 1145–1147 (1998).
271. Takahashi, K. *et al.* Induction of Pluripotent Stem Cells from Adult Human Fibroblasts by Defined Factors. *Cell* **131**, 861–872 (2007).
272. Yu, J. *et al.* Induced Pluripotent Stem Cell Lines Derived from Human Somatic Cells. **318**, 5 (2007).
273. Lamba, D. A., Karl, M. O., Ware, C. B. & Reh, T. A. Efficient generation of retinal progenitor cells from human embryonic stem cells. *Proc. Natl. Acad. Sci. U. S. A.* **103**, 12769–12774 (2006).
274. Meyer, J. S. *et al.* Modeling early retinal development with human embryonic and induced pluripotent stem cells. *Proc. Natl. Acad. Sci. U. S. A.* **106**, 16698–16703 (2009).
275. Wahlin, K. J. *et al.* Photoreceptor Outer Segment-like Structures in Long-Term 3D Retinas from Human Pluripotent Stem Cells. *Sci. Rep.* **7**, 766 (2017).
276. Brooks, M. J. *et al.* Improved Retinal Organoid Differentiation by Modulating Signaling Pathways Revealed by Comparative Transcriptome Analyses with Development In Vivo. *Stem Cell Rep.* **13**, 891–905 (2019).
277. Li, X., Zhang, L., Tang, F. & Wei, X. Retinal Organoids: Cultivation, Differentiation, and Transplantation. *Front. Cell. Neurosci.* **15**, (2021).
278. Le Pichon, C. E. *et al.* Loss of dual leucine zipper kinase signaling is protective in animal models of neurodegenerative disease. *Sci. Transl. Med.* **9**, eaag0394 (2017).
279. Welsbie, D. S. *et al.* Enhanced Functional Genomic Screening Identifies Novel Mediators of Dual Leucine Zipper Kinase-Dependent Injury Signaling in Neurons. *Neuron* **94**, 1142-1154.e6 (2017).
280. Chen, M. *et al.* Leucine Zipper-bearing Kinase promotes axon growth in mammalian central nervous system neurons. *Sci. Rep.* **6**, 31482 (2016).
281. Fague, L., Liu, Y. A. & Marsh-Armstrong, N. The basic science of optic nerve regeneration. *Ann. Transl. Med.* **9**, 1276 (2021).
282. Fernandes, K. A., Harder, J. M., Kim, J. & Libby, R. T. JUN regulates early transcriptional responses to axonal injury in retinal ganglion cells. *Exp. Eye Res.* **112**, 106–117 (2013).
283. Raivich, G. *et al.* The AP-1 transcription factor c-Jun is required for efficient axonal regeneration. *Neuron* **43**, 57–67 (2004).

284. Gordon, T. Nerve regeneration in the peripheral and central nervous systems. *J. Physiol.* **594**, 3517–3520 (2016).
285. Perry, R. B.-T. *et al.* Subcellular Knockout of Importin β1 Perturbs Axonal Retrograde Signaling. *Neuron* **75**, 294–305 (2012).
286. Leibinger, M., Andreadaki, A., Diekmann, H. & Fischer, D. Neuronal STAT3 activation is essential for CNTF- and inflammatory stimulation-induced CNS axon regeneration. *Cell Death Dis.* **4**, e805–e805 (2013).
287. Trakhtenberg, E. F. *et al.* Zinc chelation and Klf9 knockdown cooperatively promote axon regeneration after optic nerve injury. *Exp. Neurol.* **300**, 22–29 (2018).
288. Moore, D. L. *et al.* KLF family members regulate intrinsic axon regeneration ability. *Science* **326**, 298–301 (2009).
289. Larhammar, M., Huntwork-Rodriguez, S., Rudhard, Y., Sengupta-Ghosh, A. & Lewcock, J. W. The Ste20 Family Kinases MAP4K4, MINK1, and TNIK Converge to Regulate Stress-Induced JNK Signaling in Neurons. *J. Neurosci. Off. J. Soc. Neurosci.* **37**, 11074–11084 (2017).
290. Triplett, J. W. *et al.* Dendritic and axonal targeting patterns of a genetically-specified class of retinal ganglion cells that participate in image-forming circuits. *Neural Develop.* **9**, 2 (2014).
291. Brzezinski, J. A., Prasov, L. & Glaser, T. Math5 defines the ganglion cell competence state in a subpopulation of retinal progenitor cells exiting the cell cycle. *Dev. Biol.* **365**, 395–413 (2012).
292. Wang, S. W. *et al.* Requirement for math5 in the development of retinal ganglion cells. *Genes Dev.* **15**, 24–29 (2001).
293. Martín-Partido, G. & Francisco-Morcillo, J. The role of Islet-1 in cell specification, differentiation, and maintenance of phenotypes in the vertebrate neural retina. *Neural Regen. Res.* **10**, 1951–1952 (2015).
294. Baas, D. *et al.* The subcellular localization of Otx2 is cell-type specific and developmentally regulated in the mouse retina. *Brain Res. Mol. Brain Res.* **78**, 26–37 (2000).
295. Shekhar, K. *et al.* Comprehensive Classification of Retinal Bipolar Neurons by Single-Cell Transcriptomics. *Cell* **166**, 1308-1323.e30 (2016).
296. Ammirati, M. *et al.* Discovery of an in Vivo Tool to Establish Proof-of-Concept for MAP4K4-Based Antidiabetic Treatment. *ACS Med. Chem. Lett.* **6**, 1128–1133 (2015).
297. VanderWall, K. B. *et al.* Differential susceptibility of retinal ganglion cell subtypes in acute and chronic models of injury and disease. *Sci. Rep.* **10**, 17359 (2020).
298. Zhao, M. *et al.* Osteopontin drives retinal ganglion cell resiliency in glaucomatous optic neuropathy. *Cell Rep.* **42**, 113038 (2023).
299. Zhao, X. *et al.* Review on the Vascularization of Organoids and Organoids-on-a-Chip. *Front. Bioeng. Biotechnol.* **9**, (2021).
300. Winzeler, A. & Wang, J. T. Purification and Culture of Retinal Ganglion Cells from Rodents. *Cold Spring Harb. Protoc.* **2013**, pdb.prot074906 (2013).
301. Robles, E. & Gomez, T. M. Focal adhesion kinase signaling at sites of integrin-mediated adhesion controls axon pathfinding. *Nat. Neurosci.* **9**, 1274–1283 (2006).
302. Yue, J. *et al.* Microtubules Regulate Focal Adhesion Dynamics through MAP4K4. *Dev. Cell* **31**, 572–585 (2014).
303. Kerrigan–Baumrind, L. A., Quigley, H. A., Pease, M. E., Kerrigan, D. F. & Mitchell, R. S. Number of Ganglion Cells in Glaucoma Eyes Compared with Threshold Visual Field Tests in the Same Persons. *Invest. Ophthalmol. Vis. Sci.* **41**, 741–748 (2000).
304. Medeiros, F. A. *et al.* Estimating the Rate of Retinal Ganglion Cell Loss in Glaucoma. *Am. J. Ophthalmol.* **154**, 814-824.e1 (2012).
305. Susanna, R., De Moraes, C. G., Cioffi, G. A. & Ritch, R. Why Do People (Still) Go Blind from Glaucoma? *Transl. Vis. Sci. Technol.* **4**, 1 (2015).

306. West, E. L. *et al.* Pharmacological disruption of the outer limiting membrane leads to increased retinal integration of transplanted photoreceptor precursors. *Exp. Eye Res.* **86**, 601–611 (2008).
307. West, E. L. *et al.* Long-Term Survival of Photoreceptors Transplanted into the Adult Murine Neural Retina Requires Immune Modulation. *STEM CELLS* **28**, 1997–2007 (2010).
308. Kalargyrou, A. A. *et al.* Nanotube-like processes facilitate material transfer between photoreceptors. *EMBO Rep.* (2021) doi:10.15252/embr.202153732.
309. Ortin-Martinez, A. *et al.* Photoreceptor nanotubes mediate the *in vivo* exchange of intracellular material. *EMBO J.* (2021) doi:10.15252/embj.2020107264.
310. Ortin-Martinez, A. *et al.* A Reinterpretation of Cell Transplantation: GFP Transfer From Donor to Host Photoreceptors. *Stem Cells Dayt. Ohio* **35**, 932–939 (2017).
311. Pearson, R. A. *et al.* Donor and host photoreceptors engage in material transfer following transplantation of post-mitotic photoreceptor precursors. *Nat. Commun.* **7**, 13029 (2016).
312. Boia, R. *et al.* Neuroprotective Strategies for Retinal Ganglion Cell Degeneration: Current Status and Challenges Ahead. *Int. J. Mol. Sci.* **21**, 2262 (2020).
313. Huebner, E. A. & Strittmatter, S. M. Axon Regeneration in the Peripheral and Central Nervous Systems. *Results Probl. Cell Differ.* **48**, 339–351 (2009).
314. Pennesi, M. E. *et al.* Long-Term Characterization of Retinal Degeneration in rd1 and rd10 Mice Using Spectral Domain Optical Coherence Tomography. *Invest. Ophthalmol. Vis. Sci.* **53**, 4644–4656 (2012).
315. Chen, J. *et al.* Comparative Analysis of Induced vs. Spontaneous Models of Autoimmune Uveitis Targeting the Interphotoreceptor Retinoid Binding Protein. *PLoS ONE* **8**, e72161 (2013).
316. Chen, J., Qian, H., Horai, R., Chan, C.-C. & Caspi, R. R. Use of Optical Coherence Tomography and Electroretinography to Evaluate Retinal Pathology in a Mouse Model of Autoimmune Uveitis. *PLOS ONE* **8**, e63904 (2013).
317. Chu, C. J. *et al.* Multimodal analysis of ocular inflammation using the endotoxin-induced uveitis mouse model. *Dis. Model. Mech.* **9**, 473–481 (2016).
318. Maurice, D. M. Flow of water between aqueous and vitreous compartments in the rabbit eye. *Am. J. Physiol.* **252**, F104-108 (1987).
319. Steel, D. Retinal detachment. *BMJ Clin. Evid.* **2014**, 0710 (2014).
320. Secondi, R., Kong, J., Blonska, A. M., Staurenghi, G. & Sparrow, J. R. Fundus Autofluorescence Findings in a Mouse Model of Retinal Detachment. *Invest. Ophthalmol. Vis. Sci.* **53**, 5190–5197 (2012).
321. Li, Q. *et al.* Noninvasive Imaging by Optical Coherence Tomography to Monitor Retinal Degeneration in the Mouse. *Invest. Ophthalmol. Vis. Sci.* **42**, 2981–2989 (2001).
322. Invernizzi, A., Cozzi, M. & Staurenghi, G. Optical coherence tomography and optical coherence tomography angiography in uveitis: A review. *Clin. Experiment. Ophthalmol.* **47**, 357–371 (2019).
323. Li, J. *et al.* Quantitative Characterization of Autoimmune Uveoretinitis in an Experimental Mouse Model. *Invest. Ophthalmol. Vis. Sci.* **58**, 4193–4200 (2017).
324. Zhang, P. *et al. In vivo* wide-field multispectral scanning laser ophthalmoscopy–optical coherence tomography mouse retinal imager: longitudinal imaging of ganglion cells, microglia, and Müller glia, and mapping of the mouse retinal and choroidal vasculature. *J. Biomed. Opt.* **20**, 126005 (2015).
325. Thévenaz, P., Ruttimann, U. E. & Unser, M. A pyramid approach to subpixel registration based on intensity. *IEEE Trans. Image Process. Publ. IEEE Signal Process. Soc.* **7**, 27–41 (1998).
326. Rabesandratana, O. *et al.* Generation of a Transplantable Population of Human iPSC-Derived Retinal Ganglion Cells. *Front. Cell Dev. Biol.* **8**, (2020).

327. Divya, M. S. *et al.* Intraocular Injection of ES Cell-Derived Neural Progenitors Improve Visual Function in Retinal Ganglion Cell-Depleted Mouse Models. *Front. Cell. Neurosci.* **11**, 295 (2017).
328. Cho, J.-H., Mao, C.-A. & Klein, W. H. Adult mice transplanted with embryonic retinal progenitor cells: New approach for repairing damaged optic nerves. *Mol. Vis.* **18**, 2658–2672 (2012).
329. Herz, J., Filiano, A. J., Wiltbank, A. T., Yogev, N. & Kipnis, J. Myeloid Cells in the Central Nervous System. *Immunity* **46**, 943–956 (2017).
330. Ousman, S. S. & Kubes, P. Immune surveillance in the central nervous system. *Nat. Neurosci.* **15**, 1096–1101 (2012).
331. Crapser, J. D., Arreola, M. A., Tsourmas, K. I. & Green, K. N. Microglia as hackers of the matrix: sculpting synapses and the extracellular space. *Cell. Mol. Immunol.* **18**, 2472–2488 (2021).
332. Perez, V. L. & Caspi, R. R. Immune Mechanisms in Inflammatory and Degenerative Eye Disease. *Trends Immunol.* **36**, 354–363 (2015).
333. Miller, E. B., Zhang, P., Ching, K., Pugh, E. N. & Burns, M. E. In vivo imaging reveals transient microglia recruitment and functional recovery of photoreceptor signaling after injury. *Proc. Natl. Acad. Sci. U. S. A.* **116**, 16603–16612 (2019).
334. Ferreira, T. A. *et al.* Neuronal morphometry directly from bitmap images. *Nat. Methods* **11**, 982–984 (2014).
335. Justiz Vaillant, A. A., Misra, S. & Fitzgerald, B. M. Acute Transplantation Rejection. in *StatPearls* (StatPearls Publishing, 2023).
336. Vendomèle, J., Khebizi, Q. & Fisson, S. Cellular and Molecular Mechanisms of Anterior Chamber-Associated Immune Deviation (ACAID): What We Have Learned from Knockout Mice. *Front. Immunol.* **8**, 1686 (2017).
337. Mahar, M. & Cavalli, V. Intrinsic mechanisms of neuronal axon regeneration. *Nat. Rev. Neurosci.* **19**, 323–337 (2018).
338. Oliveira-Valença, V. M., Bosco, A., Vetter, M. L. & Silveira, M. S. On the Generation and Regeneration of Retinal Ganglion Cells. *Front. Cell Dev. Biol.* **8**, (2020).
339. Xu, H., Chen, M. & Forrester, J. V. Para-inflammation in the aging retina. *Prog. Retin. Eye Res.* **28**, 348–368 (2009).
340. Gupta, N. *et al.* Recent progress in therapeutic strategies for microglia-mediated neuroinflammation in neuropathologies. *Expert Opin. Ther. Targets* **22**, 765–781 (2018).
341. Ashhurst, T. M., Vreden, C. van, Niewold, P. & King, N. J. C. The plasticity of inflammatory monocyte responses to the inflamed central nervous system. *Cell. Immunol.* **291**, 49–57 (2014).
342. Guillonneau, X. *et al.* On phagocytes and macular degeneration. *Prog. Retin. Eye Res.* **61**, 98–128 (2017).
343. Paschalis, E. I. *et al.* Permanent neuroglial remodeling of the retina following infiltration of CSF1R inhibition-resistant peripheral monocytes. *Proc. Natl. Acad. Sci.* **115**, E11359–E11368 (2018).
344. Kumar, A., Pandey, R. K., Miller, L. J., Singh, P. K. & Kanwar, M. Müller Glia in Retinal Innate Immunity: A perspective on their roles in endophthalmitis. *Crit. Rev. Immunol.* **33**, 119–135 (2013).
345. Huang, C.-Y., Mikowski, M. & Wu, L. Pneumatic retinopexy: an update. *Graefes Arch. Clin. Exp. Ophthalmol. Albrecht Von Graefes Arch. Klin. Exp. Ophthalmol.* **260**, 711–722 (2022).
346. Pearson, R. A. *et al.* Restoration of vision after transplantation of photoreceptors. *Nature* **485**, 99–103 (2012).
347. Nguyen-Ba-Charvet, K. T. & Rebsam, A. Neurogenesis and Specification of Retinal Ganglion Cells. *Int. J. Mol. Sci.* **21**, 451 (2020).

348. Wong, K. A. & Benowitz, L. I. Retinal Ganglion Cell Survival and Axon Regeneration after Optic Nerve Injury: Role of Inflammation and Other Factors. *Int. J. Mol. Sci.* **23**, 10179 (2022).
349. Rodríguez, A. M., Rodríguez, J. & Giambartolomei, G. H. Microglia at the Crossroads of Pathogen-Induced Neuroinflammation. *ASN Neuro* **14**, 17590914221104566 (2022).
350. Mariani, M. M. & Kielian, T. Microglia in Infectious Diseases of the Central Nervous System. *J. Neuroimmune Pharmacol. Off. J. Soc. NeuroImmune Pharmacol.* **4**, 448–461 (2009).